Article I: Reaction of NH^+, NH_2^+, and NH_3^+ ions with H_2 at low temperatures-The pathway to ammonia production in the interstellar medium

Rednyk, S., Roučka, Š., Kovalenko, A., Tran, T. D., Dohnal, P., Plašil, R., & Glosík, J.

2019

Reaction of NH$^+$, NH$_2^+$, and NH$_3^+$ ions with H$_2$ at low temperatures

The pathway to ammonia production in the interstellar medium

S. Rednyk, Š. Roučka, A. Kovalenko, T. D. Tran, P. Dohnal, R. Plašil, and J. Glosík

Department of Surface and Plasma Science, Faculty of Mathematics and Physics, Charles University, V Holešovičkách 2, 180 00 Prague, Czech Republic
e-mail: stepan.roucka@mff.cuni.cz

ABSTRACT

Aims. We present an experimental investigation of the exothermic reactions of NH$^+$, NH$_2^+$, and NH$_3^+$ ions with H$_2$ at temperatures relevant for interstellar clouds.
Methods. The reactions were studied using a variable-temperature 22-pole radio frequency ion trap instrument.
Results. The temperature dependences of rate coefficients of these reactions have been obtained at temperatures from 15 up to 300 K. The reaction of NH$^+$ with H$_2$ has two channels, which lead to NH$_2^+$ (∼97%) and H$_3^+$ (∼3%) with nearly constant reaction rate coefficients ($k_{NH^+}^a(17\,K) = 1.0 \times 10^{-9}\,cm^3\,s^{-1}$ and $k_{NH^+}^b(17\,K) = 4.0 \times 10^{-11}\,cm^3\,s^{-1}$, respectively). The reaction of NH$_2^+$ with H$_2$ produces only NH$_3^+$ ions. The measured rate coefficient monotonically decreases with increasing temperature from $k_{NH_2^+}(17\,K) = 6 \times 10^{-10}\,cm^3\,s^{-1}$ to $k_{NH_2^+}(300\,K) = 2 \times 10^{-10}\,cm^3\,s^{-1}$. The measured rate coefficient of the reaction of NH$_3^+$ with H$_2$, producing NH$_4^+$, increases with decreasing temperature from 80 K down to 15 K, confirming that the reaction proceeds by tunnelling through a potential barrier.

Key words. astrochemistry – molecular data – molecular processes – methods: laboratory: molecular – ISM: molecules

1. Introduction

Nitrogen is among the six most abundant elements in the Universe. Owing to the dominance of hydrogen in the Universe, it is not surprising that nitrogen hydrides are present in the interstellar medium (ISM). Ammonia was the first polyatomic molecule discovered in interstellar space (Cheung et al. 1968). Later, other nitrogen hydrides were detected: NH by Meyer & Roth (1991), NH$_2$ by van Dishoeck et al. (1993), and NH$_3$D$^+$ by Cernicharo et al. (2013). Atomic and molecular nitrogen were also observed in the ISM (Nieva & Przybilla 2012; Knauth et al. 2004). For information on recent observations of nitrogen hydrides, see the results from the *Herschel*/HIFI instrument (Persson et al. 2010, 2012; Caselli et al. 2017), and from the SOFIA instrument (Wyrowski et al. 2016). For a detailed description of interstellar chemistry of nitrogen hydrides, see for example Rist et al. (2013) and Harju et al. (2017) and the reviews by Le Gal et al. (2014), Gerin et al. (2016), and Acharyya & Herbst (2015). Despite some differences between observed values and the modelled predictions of populations of nitrogen hydrides (see e.g. Le Gal et al. 2014; Persson et al. 2012; Novotný et al. 2014 and references therein), it is generally accepted that the main pathway to gas-phase formation of ammonia in the ISM is a chain of hydrogen abstraction reactions followed by the dissociative recombination of NH$_4^+$ (Herbst & Klemperer 1973; Le Gal et al. 2014; Gerin et al. 2016). The suggested pathway of the gas-phase formation of the NH$_4^+$ in the ISM starting from N$^+$ is (Le Gal et al. 2014)

$$N^+ \xrightarrow{+H_2} NH^+ \xrightarrow{+H_2} NH_2^+ \xrightarrow{+H_2} NH_3^+ \xrightarrow{+H_2} NH_4^+. \tag{1}$$

In current understanding of nitrogen chemistry, the production of N$^+$ in the low-temperature (10 K) dark clouds results from dissociative ionization of N$_2$ in reaction with He$^+$ (Hily-Blant et al. 2013; Le Gal et al. 2014). Alternatively, the chain may also be initiated by N + H$_3^+$ → NH$_2^+$ + H, although this reaction has a high activation energy (Herbst et al. 1987; Scott et al. 1997; Le Gal et al. 2014). It is expected that neutral NH$_3$ molecules are consequently formed in the dissociative recombination of NH$_4^+$ ions with electrons. Other hydrides can also be formed by the recombination of ions from this sequence with electrons (Florescu-Mitchell & Mitchell 2006). To model the production of ammonia in the ISM it is important to know the rate coefficients of all the reactions in the chain (1) for temperatures down to 10 K.

The first binary ion-molecule reaction of the chain is

$$N^+ + H_2 \xrightarrow{k_{N^+}} NH^+ + H \quad E_a = 16.5\,meV \tag{2}$$
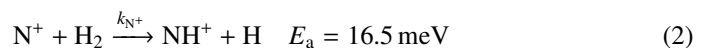
with a corresponding reaction rate coefficient denoted as k_{N^+}. Since the enthalpy of this reaction is not yet known with sufficient precision, we provide the activation energy E_a obtained by Zymak et al. (2013). The enthalpies of the other hydrogen abstraction reactions were taken from Rist et al. (2013). This endothermic reaction of the N$^+$ ion with molecular hydrogen has been studied using several well-established experimental techniques (e.g. Adams & Smith 1985; SIFDT, Marquette et al. 1988; CRESU, and Gerlich 1993; 22-pole ion trap). It has also been studied in our laboratory using the 22-pole ion trap instrument with consideration of para- and ortho-spin configurations of the reacting hydrogen molecule (Zymak et al. 2013; Plašil et al. 2014).

The next reaction of the chain (1) is

$$NH^+ + H_2 \begin{array}{c} \xrightarrow{k^a_{NH^+}} NH_2^+ + H \qquad \Delta H^0 = -1.9\,eV \qquad (3a) \\ \xrightarrow{k^b_{NH^+}} H_3^+ + N \qquad \Delta H^0 = -0.8\,eV, \qquad (3b) \end{array}$$

where $k^a_{NH^+}$ and $k^b_{NH^+}$ are reaction rate coefficients of channels with production of NH_2^+ and H_3^+, respectively. We also define the overall rate coefficient of the reaction of NH^+ ion with H_2 as $k_{NH^+} = (k^a_{NH^+} + k^b_{NH^+})$. The enthalpy of the proton transfer channel (3b) was calculated from the corresponding proton affinities (Hunter & Lias 1998). Reaction (3) was studied at 300 K by Fehsenfeld et al. (1967; FA), Kim et al. (1975; ICR), and Adams et al. (1980; SIFT). At 15 K, it was studied by Gerlich (1993; ion trap). The production of H_3^+ ion (reaction (3b)) was only reported by Adams et al. (1980).

The produced NH_2^+ ion further reacts with H_2 in reaction

$$NH_2^+ + H_2 \xrightarrow{k_{NH_2^+}} NH_3^+ + H \quad \Delta H^0 = -1.1\,eV \qquad (4)$$
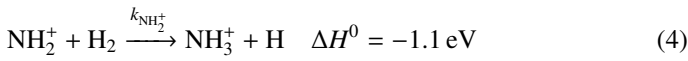
with a reaction rate coefficient $k_{NH_2^+}$. This reaction was studied by Fehsenfeld et al. (1967; FA), Kim et al. (1975; ICR), and Adams et al. (1980; SIFT) at 300 K. Using an ion trap instrument, the rate coefficient of the reaction (4) was measured at 15 K by Gerlich (1993).

The final reaction of chain (1) is

$$NH_3^+ + H_2 \xrightarrow{k_{NH_3^+}} NH_4^+ + H \quad \Delta H^0 = -1.0\,eV \qquad (5)$$
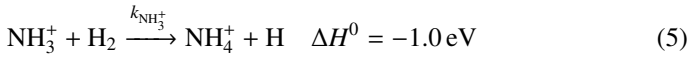
with a rate coefficient $k_{NH_3^+}$. This reaction was studied experimentally over broad range of temperatures by Fehsenfeld et al. (1975), Kim et al. (1975), Smith & Adams (1981), Luine & Dunn (1985), Böhringer (1985), Barlow & Dunn (1987), Adams & Smith (1984), and Gerlich (1993). It was also studied theoretically by Herbst et al. (1991) and recently by Álvarez-Barcia et al. (2016). At temperatures above 300 K, the measured temperature dependence of the rate coefficient of the exothermic reaction (5) exhibits dependence typical for endoergic reactions. If the temperature dependence of $k_{NH_3^+}$ measured at temperatures above 300 K is extrapolated towards lower temperatures relevant for interstellar clouds using Arrhenius dependence (Fehsenfeld et al. 1975), then the values will be far too low to explain the observed NH_3 abundances. This problem was solved when measurements at temperatures below 100 K indicated that the temperature dependence of the reaction rate coefficient has a local minimum, and then slowly increases with temperature decreasing below 50 K. These temperature dependences of rate coefficients of ion-molecule reactions with minimum have been observed several times (e.g. Smith & Adams 1981) and they are typical of exothermic reactions proceeding by tunnelling through a potential barrier (Ng et al. 1994). The observed increase in the reaction rate coefficient $k_{NH_3^+}$ at low temperatures due to the tunnelling is sufficient for reaction (5) to play an important role in interstellar chemistry.

The recent observations of nitrogen hydrides in many areas of the ISM have led to the modelling of their production and destruction in the corresponding environments. This requires the knowledge of the rate coefficients of reactions playing a role in the production and destruction of nitrogen hydrides at temperatures down to 10 K. The present contribution reports the results of the studies of the reactions of ions NH^+, NH_2^+, and NH_3^+ with H_2 at temperatures from 15 to 300 K using a 22-pole radio frequency (RF) ion trap. After a brief description of the instrument and typical measuring procedures, new data including measured temperature dependences of the reaction rate coefficients ($k^a_{NH^+}$, $k^b_{NH^+}$, $k_{NH_2^+}$, and $k_{NH_3^+}$) are presented. The new results are compared with values from previous experiments and with available theoretical predictions.

2. Experiment and data analysis

The experiments were carried out by means of a linear RF 22-pole ion trap instrument operating at temperatures (T_{22PT}) from 10 to 300 K. The basics of storing ions in RF fields have been described thoroughly by Gerlich (1992, 1995). Only a very short description of the apparatus and its operation are given here (for details, see e.g. Gerlich 1992; Gerlich et al. 2011; Plašil et al. 2011; Zymak et al. 2013). The ion trap is surrounded by a copper box, which is mounted onto a cold head of a closed-cycle helium refrigerator. Helium and hydrogen are introduced into the trap via leak valves and optionally in short pulses (∼10 ms) via a piezo valve (Gerlich 2008).

The primary reactant ions are produced by electron bombardment of the precursor gas in a storage ion source (SIS). In the present experiments, a mixture of N_2 and H_2 was used as a source gas. The produced ions were periodically extracted from the ion source and mass selected with a quadrupole mass filter. The mass-selected (primary) ions were transferred into the 22-pole ion trap, filled with a mixture of He buffer gas and H_2 reactant gas. The helium number density used in the experiments was in the range of $10^{13}-10^{14}\,cm^{-3}$ during the measurements and it was temporarily increased to $10^{15}\,cm^{-3}$ during the injection of ions into the trap by adding He via the piezo valve. In the present experiments, normal hydrogen was used as a reactant gas with number densities in the trap varying from 10^{10} up to $10^{12}\,cm^{-3}$. In normal H_2, the para/ortho ratio is 1/3, corresponding to the thermal equilibrium at 300 K (for discussion, see Zymak et al. 2013; Hejduk et al. 2012). As the rotational excitation in hydrogen gas is thermalized only within para and ortho manifolds, H_2 gas flowing through the gas inlet system into the trap volume is not thermalized at trap temperatures below 200 K (Zymak et al. 2013; Hejduk et al. 2015). The gas number density inside the ion trap is determined using a spinning rotor gauge and a calibrated ionization gauge with estimated uncertainty of 20%. This constant systematic uncertainty is not included in the error bars of our figures, which indicate the relative uncertainties.

At the number densities of He buffer gas and H_2 reactant gas in the present experiment, the kinetic energy of the injected ion was cooled by hundreds of collisions with He atoms prior to colliding with H_2. After various trapping times, the ions were extracted from the trap and after passing through a second quadrupole mass filter, they were detected with an MCP detector. The standard measuring procedure is based on filling the ion trap at a fixed frequency with a well-defined number of primary ions and by analysing the content of the ions in the ion trap after different trapping (reaction) times. The data are analysed under the assumption that the numbers of detected ions are proportional to the numbers of ions in the ion trap. In the following text these relative numbers of different ions of particular mass detected (counted) after trapping time t are denoted $n_x(t)$, where the index x refers to the various ions in the ion trap. For easier comparison of the experimental results, the data plotted in the figures were normalized by dividing by the total number of detected ions $n_{\Sigma 0} = \sum n_x(t_0)$, where t_0 is the shortest trapping time. The symbol $\Sigma(t)$ in the figures indicates the normalized total number of ions in the trap, $\Sigma(t) = \sum n_x(t)/n_{\Sigma 0}$. The mass discrimination of the detection system is considered in the
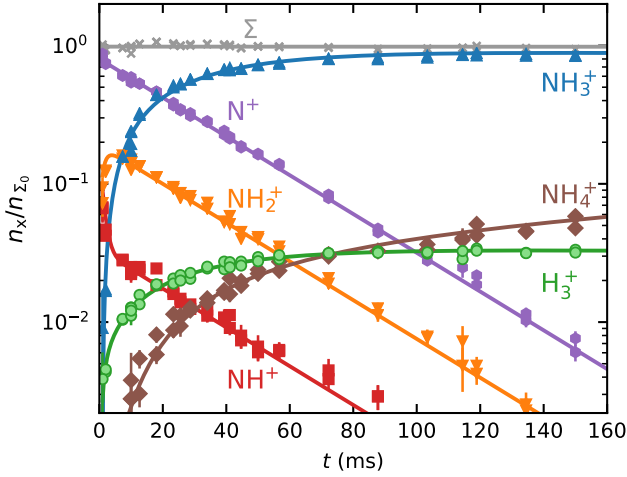
Fig. 1. Measured time evolutions of normalized numbers ($n_x(t)/n_{\Sigma 0}$) of N^+, NH^+, NH_2^+, NH_3^+, NH_4^+, and H_3^+ ions in the trap filed with He/H_2 gas mixture after the injection of N^+ ions from the SIS. The collisional temperature is $T = 16\,K$, hydrogen number density is $[H_2] = 5.7 \times 10^{10}\,cm^{-3}$ and helium number density is $[He] = 5.6 \times 10^{13}\,cm^{-3}$. The fitted solution of the corresponding system of rate equations is indicated with the solid lines. The crosses (x) indicate the sum of the normalized numbers ($\Sigma(t)$) of all ions in the ion trap.

data analysis (see e.g. Kovalenko et al. 2018, for details) and for some ions (H_3^+ in comparison with NH^+), it was calibrated using a suitable chemical reaction (see Sect. 3.1).

In recent experiments with our apparatus (Zymak et al. 2013; Plašil et al. 2012; Roučka et al. 2018) and in other 22-pole ion trap experiments (Hauser et al. 2015; Endres et al. 2017) it has been confirmed that the collisional temperature (here denoted simply T) is slightly higher than the temperature of the copper box surrounding the ion trap (nominal ion trap temperature, T_{22PT}). At the present experimental conditions, we can safely assume that the collisional temperature in the interaction of ions with H_2 does not exceed the ion trap temperature by more than $10\,K$. For simplicity of presentation, we define the collisional temperature as $T = T_{22PT} + 5\,K$ with an uncertainty of $\pm 5\,K$.

To illustrate the character of the results from the ion trap experiment, the typical data measured in an experiment with injection of N^+ ions into the ion trap filled with He buffer gas and H_2 reactant gas are shown in Fig. 1. Plotted are the time evolutions of normalized numbers ($n_x(t)/n_{\Sigma 0}$) of N^+, NH^+, NH_2^+, NH_3^+, NH_4^+, and H_3^+ ions in the ion trap. The mass discriminations for particular ions are considered in the evaluation of the measured data. Owing to the large differences between the values of the rate coefficients of the reactions in chain (1), the data were collected in small time steps over a broad time interval. The dominant process after the injection of N^+ ions is their reaction with H_2 in which the NH^+ ions are formed. The NH^+ ions further react with H_2, producing NH_2^+ and H_3^+. The NH_2^+ ions consequently react with H_2 to produce NH_3^+. Finally, the NH_4^+ ions are produced in slow reactions of NH_3^+ with H_2. From the time evolution of the normalized number of H_3^+ ions it can be seen that at very long trapping times H_3^+ ions are slowly removed by reactions with N_2 (see e.g. Marquette et al. 1989) that penetrates into the trap volume from the ion source:

$$H_3^+ + N_2 \xrightarrow{k_{H_3^+}} N_2H^+ + H_2 \quad \Delta H^0 = -0.7\,eV. \tag{6}$$
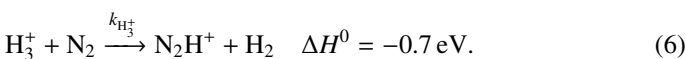
At low temperatures ($\lesssim 40\,K$), this process becomes negligible because the number density of N_2 in the trap is reduced by condensation on the walls of the trap.

The time evolution of the numbers of ions in the ion trap after injection of N^+ ions can be described by the following set of differential balance equations, which can be derived from the chemical Eqs. (2)–(6):

$$\frac{dn_{N^+}}{dt} = -r_{N^+} n_{N^+} \tag{7}$$

$$\frac{dn_{NH^+}}{dt} = r_{N^+} n_{N^+} - n_{NH^+} \left(r_{NH^+}^a + r_{NH^+}^b \right) \tag{8}$$

$$\frac{dn_{H_3^+}}{dt} = r_{NH^+}^b n_{NH^+} - r_{H_3^+} n_{H_3^+} \tag{9}$$

$$\frac{dn_{NH_2^+}}{dt} = r_{NH^+}^a n_{NH^+} - r_{NH_2^+} n_{NH_2^+} \tag{10}$$

$$\frac{dn_{NH_3^+}}{dt} = r_{NH_2^+} n_{NH_2^+} - r_{NH_3^+} n_{NH_3^+} \tag{11}$$

$$\frac{dn_{NH_4^+}}{dt} = r_{NH_3^+} n_{NH_3^+}. \tag{12}$$

The reactions are parametrized by the reaction rates r_x, which are proportional to the reaction rate coefficients and the number densities of the neutral reactants, i.e. $r_x = k_x[H_2]$ in the case of reactions with H_2 and $r_{H_3^+} = k_{H_3^+}[N_2]$ in Eq. (9). The rate coefficients of the reactions (2)–(6) can therefore be determined by fitting the solution of the corresponding set of differential rate equations to the experimental data with the reaction rates and initial numbers of ions as free parameters. From the fitted rates r_x at given hydrogen density $[H_2]$, we calculate the corresponding reaction rate coefficients as $k_x = r_x/[H_2]$. An example of a fitted solution is also shown in Fig. 1.

In measurements with NH^+ and NH_2^+ primary ions, the system can be simplified by setting n_{N^+} and (n_{N^+}, n_{NH^+}, $n_{H_3^+}$) to zero, respectively. Special attention should be paid to the possible excitation of the intermediate ions produced in the sequence of reactions in trap. Details concerning the studies of specific reactions are discussed in Sect. 3.

To confirm that the observed reaction rates are indeed caused by binary reactions with H_2 and to evaluate the possible loss of ions due to other (background) processes, we measured the time evolutions of the relative numbers of the ions at several number densities of hydrogen in the ion trap. In these particular experiments, N^+ ions were injected into the ion trap (see example in Fig. 1). The examples of the dependences of the reaction loss rates (r_x) on $[H_2]$ for the reactions (2)–(5) measured at $T = 18\,K$ are shown in Fig. 2. The values of $r_{NH_3^+}$ were obtained from the fits of the measured time evolutions of relative number of ions at long trapping times, i.e. from evolutions of $n_{NH_3^+}$ and $n_{NH_4^+}$ (not shown in Fig. 1; see Fig. 9 below). The linearity of the dependences plotted in Fig. 2 confirms that the time evolutions of the relative numbers of particular ions in the ion trap are controlled by binary ion-molecule reactions with H_2. The measured loss rates can be expressed by the formula, $r_x = k_x[H_2] + r_{xbg}$, where r_{xbg} is the background loss rate for particular ions. The corresponding binary reaction rate coefficients k_{N^+}, k_{NH^+}, $k_{NH_2^+}$, and $k_{NH_3^+}$ are given by the slope of the plotted dependences. The value of $k_{N^+}(18\,K) = (1.0 \pm 0.4) \times 10^{-10}\,cm^3\,s^{-1}$ obtained from the data plotted in Fig. 2 is in very good agreement with the values obtained in previous studies (Zymak et al. 2013). The values of the other reaction rate coefficients obtained from the data in Fig. 2 are discussed below.
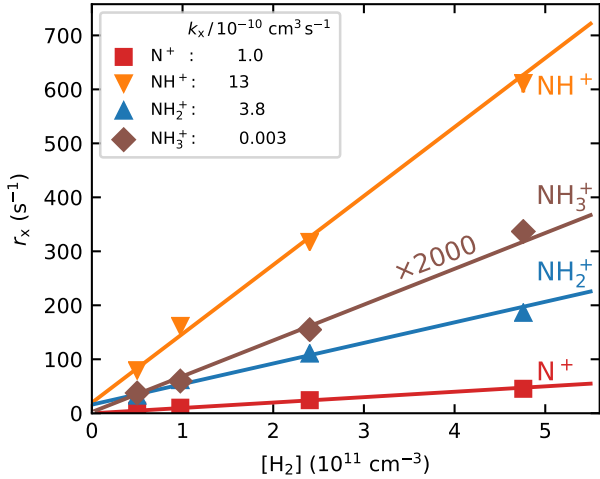
Fig. 2. Measured reaction loss rates r_{N^+}, r_{NH^+}, $r_{NH_2^+}$, and $r_{NH_3^+}$ of N^+, NH^+, NH_2^+, and NH_3^+ ions, respectively, as a function of H_2 number density. The primary N^+ ions are injected into the ion trap from the SIS. The collisional temperature is $T = 18$ K and helium number density is $[He] = 8 \times 10^{13}$ cm^{-3}. For the relatively slow reaction of NH_3^+ ions, the plotted values of $r_{NH_3^+}$ are multiplied by a factor of 2000. The corresponding binary reaction rate coefficients k_{N^+}, k_{NH^+}, $k_{NH_2^+}$, and $k_{NH_3^+}$ given by the slope of the plotted dependences are indicated in the legend.

In order to increase the accuracy of the measured reaction rate coefficients for reactions of particular ions, these ions are produced in the SIS and injected into the ion trap. The corresponding reaction rate coefficient can then be calculated from the decay (time evolution) of the relative number of this particular ion. The obvious advantage of the determination of the rate coefficient from the decrease in the relative number of the studied ion is that the decrease in the relative number of the injected ions is influenced only by the reaction of particular ions with the reactant gas.

3. Results and discussion

3.1. Reaction $NH^+ + H_2$

We measured the rate coefficients for the atom abstraction reaction (3a) and for the proton transfer reaction (3b) at the ion trap temperatures from 10 up to 130 K. In these experiments, NH^+ ions were produced by electron bombardment of the mixture of H_2 and N_2 gases in the SIS and injected into the trap. The typical time evolutions of the normalized numbers of primary and product ions are shown in Fig. 3.

Since the mass filters in our instrument cannot resolve between $^{14}NH^+$ and the $^{15}N^+$ isotope, we also injected a small fraction of $^{15}N^+$. This mixture of $^{14}NH^+$ and $^{15}N^+$ ions (mass 15 Da) is denoted A^+(15 Da). The relative populations of $^{14}NH^+$ and $^{15}N^+$ ions injected to the ion trap are influenced by the natural abundance of ^{15}N in N_2 and by kinetics in the ion source at particular conditions (partial pressures of gases, electron energy, and storage time in the SIS). The decrease in the normalized number of A^+(15 Da) is exponential (dash-dotted straight line in semi-log plot) with a leveling at $\sim$0.025 (dotted line indicated as $^{15}N^+$). This leveling of the A^+(15 Da) numbers was not observed when $^{14}NH^+$ ions were produced directly in the trap in the reaction of H_2 with $^{14}N^+$ ions (with well-known isotopic composition; see the example in Fig. 1). This confirms that the slowly reacting ions are $^{15}N^+$ ions. The presence of $^{15}N^+$ is considered
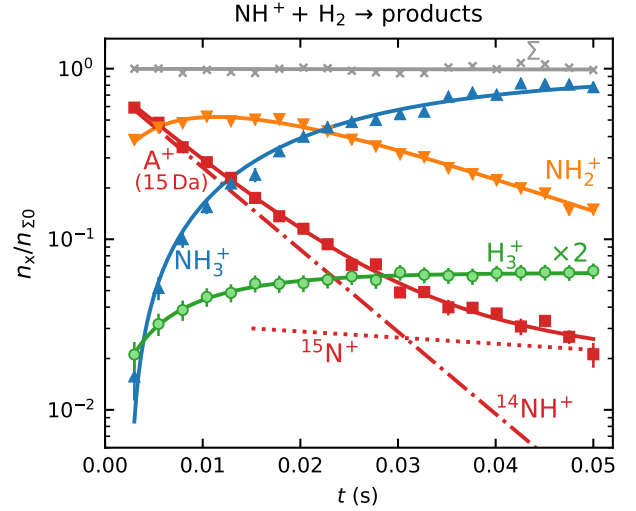

Fig. 3. Measured time evolutions of the normalized numbers $(n_x(t)/n_{\Sigma 0})$ of indicated ions in the trap. A^+(15 Da) indicates a normalized number of ions with mass 15 Da (mixture of $^{14}NH^+$ and $^{15}N^+$ ions). The measurements were performed at $T = 34$ K, $[H_2] = 6.2 \times 10^{10}$ cm^{-3}, and $[He] \approx 10^{14}$ cm^{-3}. The solid lines are least-squares fits, which were used to determine the reaction rate coefficients. The dash-dotted straight line indicates the decrease in the normalized numbers of $^{14}NH^+$ ions and the dotted line indicates the normalized numbers of $^{15}N^+$ ions. The crosses ($\times$) indicate the sum of the normalized numbers of all ions in the ion trap, $\Sigma(t)$. The normalized numbers of H_3^+ ions are increased by a factor of 2.

in the data analysis. Owing to its small rate coefficient, the reaction of $^{15}N^+$ with H_2 does not influence the evaluation of the rate coefficient k_{NH^+}. Nevertheless, we take it into account, assuming that it has the same rate coefficient as the $^{14}N^+ + H_2$ reaction (Zymak et al. 2013).

From the data plotted in Fig. 3, we can see the decrease in the relative number of NH^+ ions and the production of NH_2^+ and H_3^+ ions. To obtain the branching ratio for the reactions (3a) and (3b), the ion detection system had to be calibrated. We obtained the discrimination of the detection system between ions of mass 3 Da and 16 Da by measuring the discrimination between mass 3 Da and 17 Da using a calibration reaction of $H_3^+ + CH_4 \rightarrow CH_5^+ + H_2$ (Bohme et al. 1980) and by taking into account the discrimination between mass 16 Da and 17 Da known from the present experiment with reaction $NH_2^+ + H_2 \rightarrow NH_3^+ + H$.

We verified the binary character of the reactions (3a) and (3b) at the present experimental conditions by measuring the dependences of the reaction rates $r_{NH^+}^a$ and $r_{NH^+}^b$ on hydrogen number density. The examples of the dependences measured at temperature $T = 20$ K are shown in Fig. 4. The number density of H_2 leaking from the ion source has also been measured and is accounted for in our figures.

By fitting the measured time evolutions of the relative numbers of ions in the ion trap, the reaction rate coefficients $k_{NH^+}^a$ and $k_{NH^+}^b$ for the reaction channel (3a) and (3b) were obtained. The temperature dependences of the reaction rate coefficients $k_{NH^+}^a$ and $k_{NH^+}^b$ are shown in Fig. 5. Also plotted is the value of k_{NH^+} measured at 300 K by Kim et al. (1975). There is just one value of the reaction rate coefficient k_{NH^+} measured in the ion trap experiment at 15 K by Gerlich (1993). In the ion trap experiment, Gerlich measured the overall reaction rate coefficient k_{NH^+} (see Fig. 5). Production of H_3^+ ions was observed only in the selected ion flow tube (SIFT) studies of Adams et al. (1980). At 300 K, they observed 85% of NH_2^+ and 15% of H_3^+
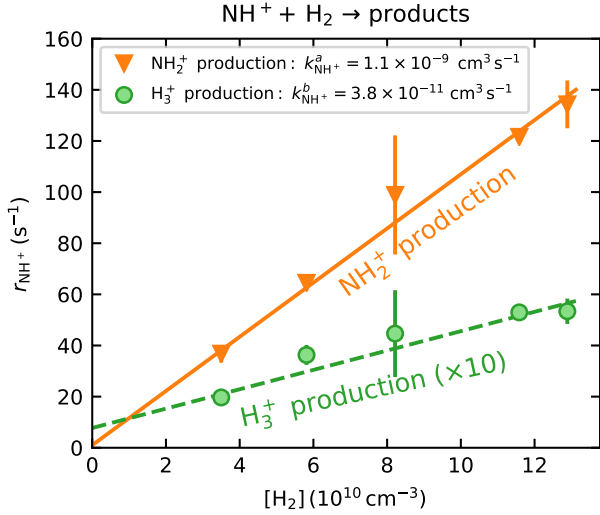
Fig. 4. Measured dependences of the reaction rates $r_{NH^+}^a$ and $r_{NH^+}^b$, corresponding to the production of NH$_2^+$ and H$_3^+$ ions, on H$_2$ number density. The plotted values of $r_{NH^+}^b$ (corresponding to H$_3^+$ production) are increased by a factor of 10. The mean helium number density was of the order of 10^{14} cm^{-3}. The collisional temperature is $T = 20$ K. In these experiments, the primary NH$^+$ ions were produced in the SIS and injected into the ion trap. The values of the binary reaction rate coefficients $k_{NH^+}^a$ and $k_{NH^+}^b$ obtained from the slopes of the corresponding dependences are shown in the legend.

Fig. 5. Measured temperature dependences of the reaction rate coefficients $k_{NH^+}^a$ and $k_{NH^+}^b$ of the reactions (3a) and (3b), respectively. The data were binned and averaged for presentation. The raw data without binning are indicated with the smaller points. The stars (at 20 K) indicate the reaction rate coefficients obtained from the dependences of $r_{NH^+}^a$ and $r_{NH^+}^b$ on [H$_2$] (Fig. 4). The horizontal solid line (k_L) indicates the value of the Langevin collisional rate coefficient. Results of Kim et al. (1975), Adams et al. (1980), and Gerlich (1993) are indicated with the open symbols. The values taken from the KIDA (Wakelam et al. 2012) and UMIST (McElroy et al. 2013) databases are also plotted.

products. The corresponding values of $k_{NH^+}^a$ and $k_{NH^+}^b$ are plotted in Fig. 5. If we extrapolate our data from 130 K towards 300 K as a constant, then there is good agreement with the previously obtained values of k_{NH^+} by Kim et al. (1975) and $k_{NH^+}^a$ by Adams et al. (1980). However, the value of $k_{NH^+}^b$ for the production of H$_3^+$, measured by Adams et al. (1980) is almost a factor of 4 higher than the present value at 130 K. Values recommended by the Kinetic Database for Astrochemistry (KIDA, Wakelam et al. 2012) and by the University of Manchester Institute of Science and Technology (UMIST) Database for Astrochemistry (McElroy et al. 2013) are also included in Fig. 5.

There have been several previous studies of reaction of NH$^+$ with H$_2$; however, this is the first study giving the temperature dependences of the reaction rate coefficients $k_{NH^+}^a$ and $k_{NH^+}^b$ from 15 up to 130 K, i.e. for astrophysically relevant temperatures.

3.2. Reaction NH$_2^+$ + H$_2$

As mentioned above, in the experiments where N$^+$ ions were injected into the ion trap and NH$_2^+$ ions were produced in the chain of reactions with H$_2$, we observed the dependence of the measured reaction rate coefficient $k_{NH_2^+}$ on partial pressures of gases in the ion trap and on the trapping time. This is presumably connected with internal excitation of NH$_2^+$ ions formed in exothermic reactions, which did not encounter enough collisions with He and H$_2$ for collisional de-excitation prior to the hydrogen abstraction reaction. To avoid uncertainties, the NH$_2^+$ ions were produced in the SIS and injected into the ion trap. The primary NH$_2^+$ ions were produced by electron bombardment of the mixture of N$_2$ and H$_2$ with number density ratio [N$_2$]:[H$_2$] $\approx$ 10:3. In these experiments, the temperature of the ion trap was varied from 10 K to 300 K. An example of measured time evolutions of the normalized numbers of primary NH$_2^+$ and produced NH$_3^+$ ions is shown in Fig. 6. The exponential decrease in the normalized numbers of NH$_2^+$ ions over two
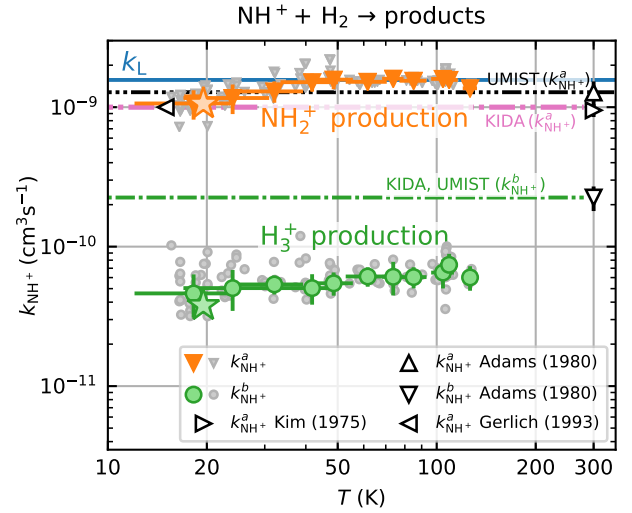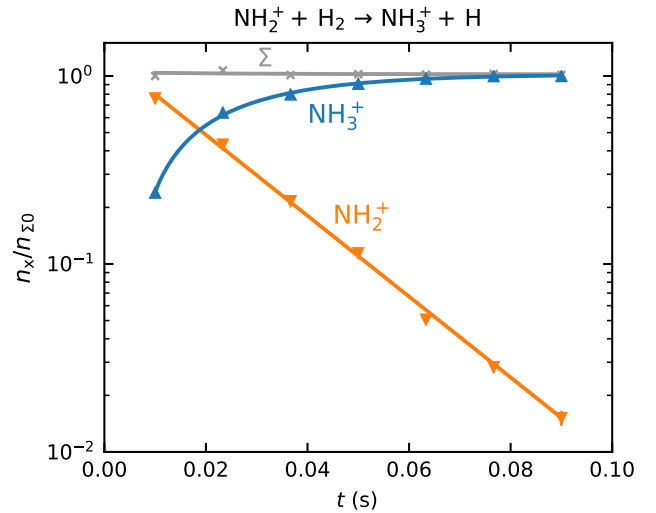

Fig. 6. Measured time evolutions of the normalized numbers ($n_x(t)/n_{\Sigma 0}$) of the primary NH$_2^+$ ions and of the produced NH$_3^+$ ions. The measurements were performed at the collisional temperature $T = 39$ K, hydrogen number density [H$_2$] $= 6.2 \times 10^{10}$ cm^{-3}, and helium number density [He] $\sim 10^{14}$ cm^{-3}. The solid lines are fits of the measured data. The crosses (x) indicate the sum of the normalized numbers of all ions in the ion trap, $\Sigma(t)$.

orders of magnitude indicates a reaction with a constant reaction rate coefficient.

Two examples of dependences of the reaction rates $r_{NH_2^+}$ on [H$_2$] for reaction (4) measured at $T = 18$ K and $T = 24$ K are shown in Fig. 7. The linearity of the obtained dependences confirms that the time evolution of the relative numbers of NH$_2^+$ ions in the ion trap is controlled by a binary reaction with H$_2$. The slope of the obtained linear dependence is given by the rate coefficient $k_{NH_2^+}$ for the corresponding binary reaction.

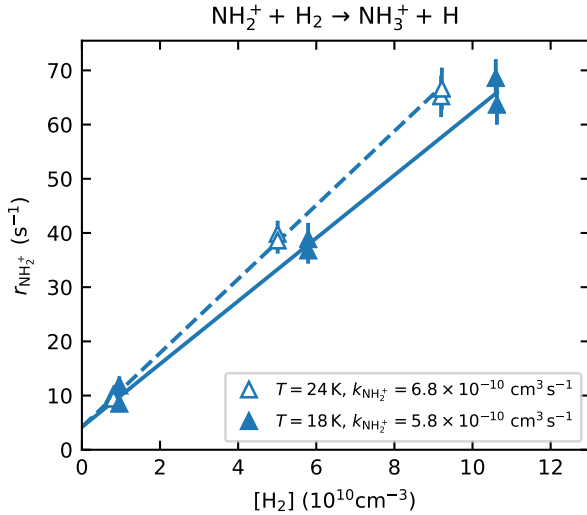**Fig. 7.** Measured dependence of the reaction rate $r_{NH_2 f}$ of NH_2^+ ions on H_2 number density. The helium number density is $[He] \sim 1.1 \times 10^{14}$ cm^{-3}. The collisional temperatures are $T = 18$ K and 24 K. The corresponding values of the binary reaction rate coefficient $k_{NH_2^+}$ are given by the slope of the plotted dependences. The primary NH_2^+ ions were produced in the SIS and injected into the ion trap.

The measured temperature dependence of the rate coefficient $k_{NH_2^+}$ between 15 and 300 K is shown in Fig. 8. Also plotted are the results of previous studies at 300 K (Kim et al. 1975; Adams et al. 1980), which are in agreement (within experimental accuracy) with the present value of $k_{NH_2^+}$(300 K). Gerlich (1993) measured the rate coefficient $k_{NH_2^+}$ of reaction (4) at 15 K using a 22-pole ion trap with injection of N^+ ions. From time evolutions of the number of ions in the trap filled with mixture of He and H_2, he obtained the reaction rate coefficient $k_{NH_2^+}$(15 K) $= 2.5 \times 10^{-10}$ cm^3 s^{-1} (point G in Fig. 8). At similar conditions in present experiments using the injection of N^+ ions into the ion trap, we obtained $k_{NH_2^+}$(16 K) $= (3.4 \pm 1.3) \times 10^{-10}$ cm^3 s^{-1} (point A, the value obtained from the data shown in Fig. 1) and $k_{NH_2^+}$(18 K) $= (3.8 \pm 1.6) \times 10^{-10}$ cm^3 s^{-1} (point B, the value obtained from the data shown in Fig. 2). The present results (point A and B) and the value from Gerlich (1993) (point G) are in rather good agreement, but we note again, that they were measured with short relaxation time, i.e. at conditions without sufficient relaxation of reacting ions (see also discussion in Gerlich 1993). The values of $k_{NH_2^+}$ recommended by KIDA (Wakelam et al. 2012) and UMIST (McElroy et al. 2013) are also indicated in Fig. 8. KIDA and UMIST only use values measured at 300 K, and the differences in the measured temperature dependences are obvious.

In the experiments with injection of N^+ or NH^+ ions, we observed that at temperatures below ~ 100 K the measured values of $k_{NH_2^+}$ are dependent on processes of formation of NH_2^+ ions. The detailed investigation of this phenomenon, including dependence on para/ortho population of H_2, will be a subject of further studies in our laboratory and are not discussed here.

3.3. Reaction $NH_3^+ + H_2$

The exothermic reaction (5) of NH_3^+ ion with H_2 has been studied many times owing to fundamental interest and to its predicted role in the formation of NH_3 in interstellar clouds (Herbst & Klemperer 1973; Le Gal et al. 2014; Gerin et al. 2016). Recent theoretical calculations of the temperature
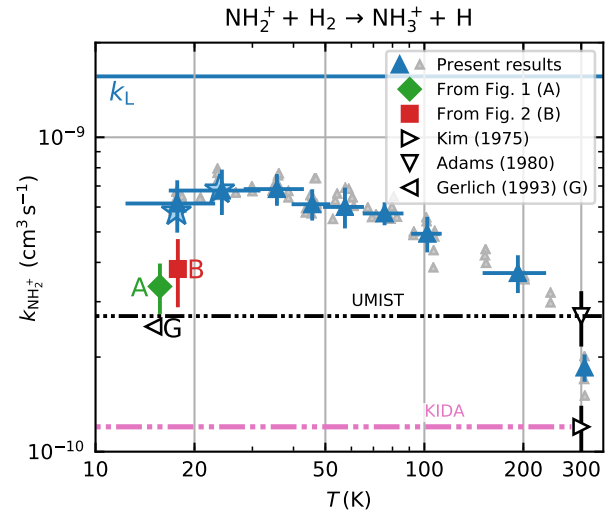

Fig. 8. Temperature dependence of the rate coefficient $k_{NH_2^+}$ of the reaction (4). The upward pointing triangles indicate the binned values measured in the present experiments with the injection of NH_2^+ ions into the ion trap. The raw data without binning are indicated with the smaller points. The stars indicate the reaction rate coefficients obtained from the $[H_2]$ dependences (see Fig. 7). The horizontal straight line (k_L) indicates the value of the Langevin collisional rate coefficient. The values of $k_{NH_2^+}$ measured in previous experiments at 300 K by Kim et al. (1975; ICR) and by Adams et al. (1980; SIFT) are indicated with the open triangles. The labels A and B indicate values of $k_{NH_2^+}$ obtained in the present experiments with the injection of N^+ ions into the trap at 16 and 18 K, respectively. The label G indicates the value of $k_{NH_2^+}$ measured in similar conditions in ion trap at 15 K by Gerlich (1993).

dependence of the reaction rate coefficient $k_{NH_3^+}$ for temperatures down to 20 K (Álvarez-Barcia et al. 2016) are in qualitative agreement with the experiments; nevertheless, at temperatures between 30 and 100 K the calculated reaction rate coefficient is smaller than the available experimental values. To provide further experimental evidence, we measured the reaction rate coefficients at temperatures ranging from 15 to 100 K. In these experiments, N^+ ions were injected into the ion trap and in a sequence of hydrogen abstraction reactions, NH_3^+ ions were formed there (see example in Fig. 1). Since reaction (5) is slow in the temperature range covered, the NH_3^+ ions formed in the ion trap have thousands of collisions with He and H_2 prior to the reaction. We can expect that in these collisions NH_3^+ ions are thermalized. To see the eventual influence of excitation/de-excitation of NH_3^+ ions in collisions with H_2 the data were collected using a broad range of hydrogen densities (see the example of the data plotted in Fig. 2). The example of the measured time evolutions of the normalized numbers $(n_x(t)/n_{\Sigma 0})$ of the primary NH_3^+ ions and of the produced NH_4^+ ions measured at long storage time is shown in Fig. 9. The data plotted in Fig. 9 were measured at identical experimental conditions as data plotted in Fig. 1, the only difference is in the time scale. We also monitored the time evolution of the normalized numbers of H_3^+, N^+, NH^+, and NH_2^+ ions in the trap (see the example plotted in Fig. 1), but in Fig. 9 these data are not included. As we can see from the data plotted in Fig. 1, the ions N^+, NH^+, and NH_2^+ are within 0.2 s removed from the trap in the sequence of fast reactions with H_2.

The values of $k_{NH_3^+}$ obtained from the fits of measured time evolutions of $n_x(t)$ at long trapping times (i.e. with long relaxation times) at temperatures from 15 up to 100 K are plotted in Fig. 10. We can see the agreement of the present results with the previous experimental results over the
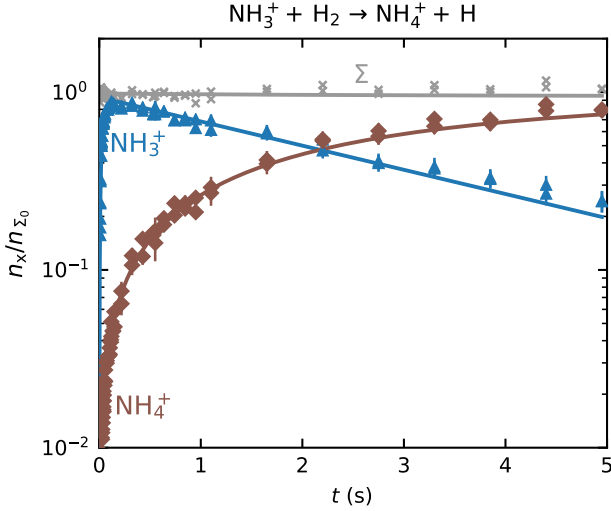
Fig. 9. Measured time evolutions of normalized numbers ($n_x(t)/n_{\Sigma 0}$) of NH_3^+ and NH_4^+ ions in the trap filed with He/H_2 gas mixture after the injection of N^+ ions from the SIS and fast formation of NH_3^+ ions. The collisional temperature is T = 16 K, hydrogen number density is [H_2] = 5.7×10^{10} cm^3 s^{-1} and helium number density is [He] = 5.6×10^{13} cm^3 s^{-1}. The fitted solution of the corresponding system of rate equations is indicated with the solid lines. The crosses (×) indicate the sum of the normalized numbers of all ions in the ion trap ($\Sigma(t)$).

covered range of temperatures; in other words, our experiment confirms that the recently calculated reaction rate coefficient by Álvarez-Barcia et al. (2016) is systematically lower than the experimental data at low temperatures.

When the trapping time was short ($\lesssim$100 ms) and the time for the relaxation of produced NH_3^+ ions was not long enough, we observed a substantial increase in the reaction rate coefficient $k_{NH_3^+}$ in comparison with values obtained in experiments using long trapping time. An example of a value of $k_{NH_3^+}$ obtained from the fit of time evolutions of $n_x(t)$ at a short trapping time (i.e. with a short relaxation time) is plotted in Fig. 10, labelled A (non-thermalized $k_{NH_3^+}^*$(17 K) = 4.0×10^{-12} cm^3 s^{-1}). A similar increase in the reaction rate coefficient at short trapping time was observed by Gerlich with his ion trap experiment at 15 K (Gerlich 1993). His results obtained at short and long trapping times are labelled G1 and G2 in Fig. 10. At He pressures used in the ion trap in the present experiments (with NH_3^+) we did not observe any effect of a ternary reaction. The temperature dependences of $k_{NH_3^+}$ recommended by KIDA (Wakelam et al. 2012) and by UMIST (McElroy et al. 2013) are also plotted in Fig. 10.

4. Summary

Following our previous studies of the reaction of N^+ ions with molecular hydrogen, we studied the chain of hydrogen abstraction reactions of NH^+, NH_2^+, and NH_3^+ ions with molecular hydrogen leading to the formation of NH_4^+ ions at temperatures relevant for interstellar clouds. Using the 22-pole ion trap apparatus, we measured the temperature dependences of the rate coefficients of the reactions of NH^+, NH_2^+, and NH_3^+ ions with H_2 at temperatures down to 15 K.

In the reactions of NH^+ ions, we observed two products: NH_2^+ ($\sim$97%) and H_3^+ ($\sim$3%) (see Figs. 3–5). There have been several previous studies of the reaction of NH^+ with H_2, but this is the first study giving the temperature dependences of the reaction rate coefficients $k_{NH^+}^a$ and $k_{NH^+}^b$ at astrophysically

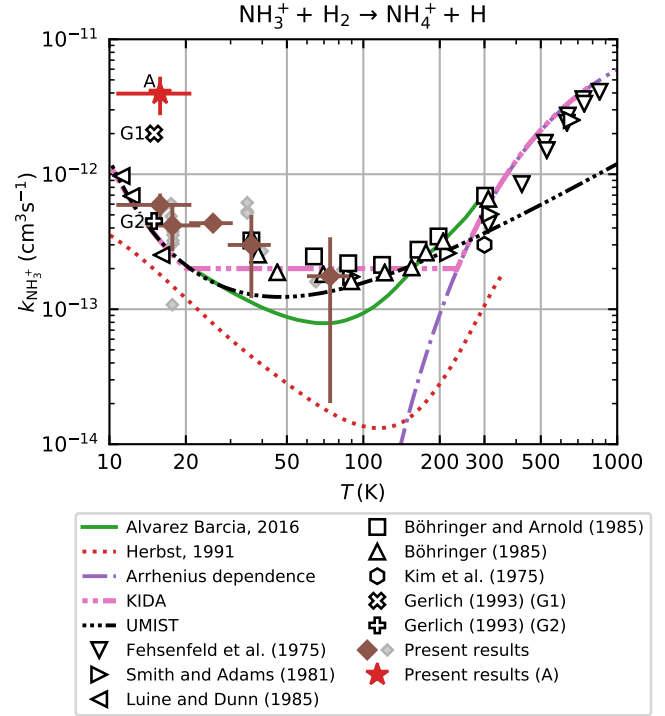**Fig. 10.** The temperature dependence of the reaction rate coefficient $k_{NH_3^+}$. The binned present data measured with long trapping times are indicated with the full diamonds. The raw data without binning are indicated with the smaller points. Present data measured with short trapping time are indicated with a red star (label A). The points labelled as G1 and G2 are the values measured by Gerlich (1993) using short and long trapping time, respectively. Previous experimentally determined binary rate coefficient are taken from Fehsenfeld et al. (1975), Kim et al. (1975), Smith & Adams (1981), Adams & Smith (1984), Luine & Dunn (1985), Böhringer & Arnold (1985), Böhringer (1985), Barlow & Dunn (1987). The plotted theoretical temperature dependences were calculated by Herbst et al. (1991) (dashed line) and by Álvarez-Barcia et al. (2016) (solid line). The dash dotted line indicates the Arrhenius dependence obtained by the fit of the data measured at temperatures above 300 K (Fehsenfeld et al. 1975). Included are also the temperature dependences recommended by KIDA (Wakelam et al. 2012) and by UMIST (McElroy et al. 2013).

relevant temperatures. In the covered temperature range, from 15 to 130 K, both reaction rate coefficients are approximately constant (see Fig. 5). The value of $k_{NH^+}^b$ obtained in our experiment at 130 K, $k_{NH^+}^b$ = $(6.0 \pm 2.4) \times 10^{-11}$ cm^3 s^{-1} is approximately 4 times lower than the only previously available value, which was obtained at 300 K (Adams et al. 1980, $k_{NH^+}^b$ = $(23 \pm 5) \times 10^{-11}$ cm^3 s^{-1}). Although these values are not directly comparable due to the difference in temperatures, it is unlikely that the reaction rate coefficient, which is constant below 130 K, would change by a factor of 4 between 130 K and 300 K. There are several systematic effects that can specifically affect the measurement of such a minor reaction channel. We are not able to discuss the possible sources of error in the experiment of Adams et al. (1980), such as different detection efficiencies and diffusion rates for H_3^+ and NH_2^+. In our study, the detection efficiency was calibrated in experiments with H_3^+ and CH_4 (see Sect. 3.1) at otherwise identical conditions to the NH^+ experiments. The standard deviation of the detection efficiency was smaller than 10% at given experimental conditions, although it can vary by tens of percentage points with change of potentials in the extraction and detection system. The other systematic effect is related to

the kinetic energy release of the reaction. Although we do not know what fraction of the 0.8 eV reaction exothermicity is converted to kinetic energy of the products, it is possible that the H_3^+ ion gains sufficient energy to escape from the trap. However, we did not observe any variation in the branching ratio with trap RF amplitude or He pressure, which would indicate this effect.

The temperature dependence of the rate coefficient of the reaction of NH_2^+ ion with H_2 was measured for temperatures from 15 to 300 K (see Fig. 8). The only observed product of the reaction was the NH_3^+ ion. The rate coefficient of this reaction drops monotonically from $k_{NH_2^+}(17\,\mathrm{K}) = 6.0 \times 10^{-10}\,\mathrm{cm^3\,s^{-1}}$ to $k_{NH_2^+}(300\,\mathrm{K}) = 2.0 \times 10^{-10}\,\mathrm{cm^3\,s^{-1}}$. At 300 K, our value of $k_{NH_2^+}$ is in agreement with the results of both previous studies (Kim et al. 1975; Adams et al. 1980). At 15 K, our value is significantly higher than that of Gerlich (1993). Our tests indicate that this might be due to insufficient relaxation of the NH_2^+ ions in the experimental procedure of Gerlich (1993). Our experiments were carried out with an injection of NH_2^+ ions from the SIS to the ion trap, and the decay of the number of primary ions was observed over long trapping times to exclude the influence of the process of formation and relaxation of NH_2^+. The time dependence of the NH_2^+ ion formation process and its relaxation in He or H_2 collisions is discussed. The detailed investigation of this phenomenon, including dependence on para/ortho population of H_2, will be a subject of further studies in our laboratory and is not discussed here. This is the first study giving the temperature dependence of the reaction rate coefficient $k_{NH_2^+}$ from 15 K to 300 K.

Due to the astrophysical significance, the temperature dependence of the rate coefficient of the reaction of NH_3^+ with H_2, producing NH_4^+, was also studied. The measured temperature dependence of the reaction rate coefficient has a minimum at temperatures around 70 K ($k_{NH_3^+}(70\,\mathrm{K}) = 1.0 \times 10^{-13}\,\mathrm{cm^3\,s^{-1}}$). At lower temperatures the value of $k_{NH_3^+}$ slowly increases with decreasing temperature. The presented data for the reaction of NH_3^+ ions with H_2 are in agreement with previous experimental values. The recently calculated reaction rate coefficient of Álvarez-Barcia et al. (2016) is systematically lower than all the experimental data at temperatures below 150 K, although the discrepancy is close to the experimental error.

Studies of the reactions of NH^+, NH_2^+, and NH_3^+ ions with D_2, HD, and para-H_2 are in preparation.

References

Acharyya, K., & Herbst, E. 2015, ApJ, 812, 142
Adams, N., & Smith, D. 1984, IJMSI, 61, 133
Adams, N., & Smith, D. 1985, CPL, 117, 67
Adams, N. G., Smith, D., & Paulson, J. F. 1980, JChP, 72, 288
Álvarez-Barcia, S., Russ, M.-S., Meisner, J., & Kästner, J. 2016, FaDi, 195, 69
Barlow, S. E., & Dunn, G. H. 1987, IJMSI, 80, 227
Bohme, D. K., Mackay, G. I., & Schiff, H. I. 1980, JChP, 73, 4976
Böhringer, H. 1985, CPL, 122, 185
Böhringer, H., & Arnold, F. 1985, Molecular Astrophysics, NATO ASI Series (Dordrecht: Springer), 639
Caselli, P., Bizzocchi, L., Keto, E., et al. 2017, A&A, 603, L1
Cernicharo, J., Tercero, B., Fuente, A., et al. 2013, ApJ, 771, L10
Cheung, A. C., Rank, D. M., Townes, C. H., Thornton, D. D., & Welch, W. J. 1968, PhRvL, 21, 1701
Endres, E., Egger, G., Lee, S., et al. 2017, JMoSp, 332, 134
Fehsenfeld, F. C., Schmeltekopf, A. L., & Ferguson, E. E. 1967, JChP, 46, 2802
Fehsenfeld, F. C., Lindinger, W., Schmeltekopf, A. L., Albritton, D. L., & Ferguson, E. E. 1975, JChP, 62, 2001
Florescu-Mitchell, A. I., & Mitchell, J. B. A. 2006, PhR, 430, 277
Gerin, M., Neufeld, D. A., & Goicoechea, J. R. 2016, ARA&A, 54, 181
Gerlich, D. 1992, AdChP, 82, 1
Gerlich, D. 1993, FaTr, 89, 2199
Gerlich, D. 1995, PhyS, 1995, 256
Gerlich, D. 2008, Low Temperatures and Cold Molecules (Imperial College Press), 121
Gerlich, D., Borodi, G., Luca, A., Mogo, C., & Smith, M. A. 2011, ZPC, 225, 5
Harju, J., Daniel, F., Sipilä, O., et al. 2017, A&A, 600, A61
Hauser, D., Lee, S., Carelli, F., et al. 2015, NatPh, 11, 467
Hejduk, M., Dohnal, P., Varju, J., et al. 2012, PSST, 21, 024002
Hejduk, M., Dohnal, P., Rubovič, P., et al. 2015, JChP, 143, 044303
Herbst, E., & Klemperer, W. 1973, ApJ, 185, 505
Herbst, E., Defrees, D. J., & McLean, A. D. 1987, ApJ, 321, 898
Herbst, E., DeFrees, D. J., Talbi, D., et al. 1991, JChP, 94, 7842
Hily-Blant, P., Pineau des Forêts, G., Faure, A., Le Gal, R., & Padovani, M. 2013, A&A, 557, A65
Hunter, E. P. L., & Lias, S. G. 1998, JPCRD, 27, 413
Kim, J. K., Theard, L. P., & Huntress, W. T. 1975, JChP, 62, 45
Knauth, D. C., Andersson, B. G., McCandliss, S. R., & Warren Moos, H. 2004, Nature, 429, 636
Kovalenko, A., Tran, T., Rednyk, S., et al. 2018, ApJ, 856, 100
Le Gal, R., Hily-Blant, P., Faure, A., et al. 2014, A&A, 562, A83
Luine, J. A., & Dunn, G. H. 1985, ApJ, 299, L67
Marquette, J. B., Rebrion, C., & Rowe, B. R. 1988, JChP, 89, 2041
Marquette, J. B., Rebrion, C., & Rowe, B. R. 1989, A&A, 213, L29
McElroy, D., Walsh, C., Markwick, A. J., et al. 2013, A&A, 550, A36
Meyer, D. M., & Roth, K. C. 1991, ApJ, 376, L49
Ng, C., Baer, T., & Powis, I. 1994, Unimolecular and Bimolecular Ion-Molecule Reaction Dynamics, Wiley Series In Ion Chemistry and Physics (Wiley)
Nieva, M.-F., & Przybilla, N. 2012, A&A, 539, A143
Novotný, O., Berg, M., Bing, D., et al. 2014, ApJ, 792, 132
Persson, C. M., Black, J. H., Cernicharo, J., et al. 2010, A&A, 521, L45
Persson, C., Luca, M., Mookerjea, B., et al. 2012, A&A, 543, A145
Plašil, R., Mehner, T., Dohnal, P., et al. 2011, ApJ, 737, 60
Plašil, R., Zymak, I., Jusko, P., et al. 2012, RSPTA, 370, 5066
Plašil, R., Zymak, I., Hejduk, M., et al. 2014, J. Phys. Conf. Ser., 488, 122003
Rist, C., Faure, A., Hily-Blant, P., & Le Gal, R. 2013, JPCA, 117, 9800
Roučka, S., Rednyk, S., Kovalenko, A., et al. 2018, A&A, 615, L6
Scott, G. B. I., Freeman, C. G., & McEwan, M. J. 1997, MNRAS, 290, 636
Smith, D., & Adams, N. G. 1981, MNRAS, 197, 377
van Dishoeck, E. F., Jansen, D. J., Schilke, P., & Phillips, T. G. 1993, ApJ, 416, L83
Wakelam, V., Herbst, E., Loison, J.-C., et al. 2012, ApJS, 199, 21
Wyrowski, F., Güsten, R., Menten, K. M., et al. 2016, A&A, 585, A149
Zymak, I., Hejduk, M., Mulin, D., et al. 2013, ApJ, 768, 86

Article II: OH$^+$ Formation in the Low-temperature O$^+$(4S) + H$_2$ Reaction

Kovalenko, A., Tran, T. D., Rednyk, S., Roučka, Š., Dohnal, P., Plašil, R., Gerlich, J., Glosík, J.

CrossMark

OH$^+$ Formation in the Low-temperature O$^+$(^{4}S) + H$_2$ Reaction

Artem Kovalenko [ORCID], Thuy Dung Tran [ORCID], Serhiy Rednyk [ORCID], Štěpán Roučka [ORCID], Petr Dohnal [ORCID], Radek Plašil [ORCID], Dieter Gerlich [ORCID], and Juraj Glosík [ORCID]

Department of Surface and Plasma Science, Faculty of Mathematics and Physics, Charles University, Prague, Czech Republic; radek.plasil@mff.cuni.cz

Received 2017 December 18; revised 2018 February 7; accepted 2018 February 18; published 2018 March 28

Abstract

Formation of OH$^+$ in collisions of ground-state O$^+$(^{4}S) ions with normal H$_2$ has been studied using a variable temperature 22-pole RF ion trap. From 300 to 30 K the measured reaction rate coefficient is temperature-independent, with a small decrease toward 15 K. The recent wave packet calculation predicts a slightly steeper temperature dependence. The rate coefficients at 300 and 15 K are almost the same, $(1.4 \pm 0.3) \times 10^{-9}$ cm^3 s^{-1} and $(1.3 \pm 0.3) \times 10^{-9}$ cm^3 s^{-1}, respectively. The influence of traces of the two metastable ions, O$^+$(^{2}D) and O$^+$(^{2}P), has been examined by monitoring the H$^+$ products of their reactions with H$_2$, as well as by chemically probing them with N$_2$ reactant gas.

Key words: astrochemistry – ISM: molecules – molecular data – molecular processes

1. Introduction

Oxygen, the third most abundant element in the universe, plays an important role in the chemistry of many environments. In the interstellar medium, the formation of OH$^+$ ions in reactions of O$^+$ with H$_2$ is a key process in the synthesis of water molecules (Gerin et al. 2016). Subsequent reactions of OH$^+$ with H$_2$ lead to H$_2$O$^+$ and H$_3$O$^+$ formation, which, following dissociative recombination with electrons, produce H$_2$O (Jensen et al. 2000; Neau et al. 2000). The vital importance of H$_2$O in interstellar space has recently been discussed by Hollenbach et al. (2012). New ground- and space-based observations (e.g., Pilbratt et al. 2010; Wyrowski et al. 2010; Hollenbach et al. 2012; Gómez-Carrasco et al. 2014; Indriolo et al. 2015; Muller et al. 2016; Neufeld & Wolfire 2016, 2017) that focused on the role of OH$_n^+$ in the interstellar medium indicate that in H$_2$-dominated regions, there are two main routes to form OH$^+$ (Hollenbach et al. 2009, 2012; Gerin et al. 2016). In the first one, cosmic rays (CR) ionize H$_2$. The H$_2^+$ reacts with H$_2$ to H$_3^+$, which transfers a proton to O (de Ruette et al. 2016). In the second one, CR first forms protons. Electron transfer from O to H$^+$ leads to O$^+$ and OH$^+$ is formed by the title reaction. The importance of these reactions and many other competing processes depends on the conditions prevailing in the different regions of space. To understand the astronomical observations, more theoretical and experimental studies of the formation and destruction of OH$^+$ ions are needed (Indriolo et al. 2015), especially at the low temperatures of dense interstellar clouds.

In the present study, we focus predominantly on the temperature dependence of the exoergic reaction of ground-state O$^+$(^{4}S) ion with H$_2$ molecule:

$$\text{O}^+(^4\text{S}) + \text{H}_2 \xrightarrow{k_{\text{O+}}} \text{OH}^+ + \text{H}; \quad \Delta H = -0.54 \text{ eV}. \quad (1)$$
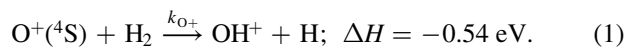
The rate coefficient is denoted $k_{\text{O+}}$. The reaction enthalpy ΔH at 0 K was calculated from tabulated enthalpies of formation, ionization potentials, and dissociation energies (Wiedmann et al. 1992; Chase 1998; Sansonetti & Martin 2005; Liu et al. 2009). The estimated errors do not exceed 1 on the last digit of all enthalpies given in this paper.

As thoroughly reviewed in previous papers (Bulut et al. 2015, for instance) and summarized below in Section 4, the reaction (1) has been studied often, both experimentally and theoretically. Nonetheless, there are no reports of measurements below 300 K in the literature so far, although an understanding of the title reaction at low temperatures is required for the astronomical modeling. Therefore, we decided to extend the temperature range of measurements of the title reaction from room temperature down to 15 K.

In the following, we first briefly describe the present experiments. In Section 3 the new experimental results for the title reaction are presented. The new data are compared with those from previous experiments and with recent theoretical predictions.

2. Experimental

2.1. 22PT Instrument

The cryogenic 22-pole RF ion trap instrument used in the present study has been described previously (see, e.g., Gerlich et al. 2011, 2012, 2013; Zymak et al. 2011, 2013; Plašil et al. 2012; Mulin et al. 2015). Therefore, only a brief description is given here. Atomic oxygen ions, O$^+$, are produced in the storage ion source by bombarding N$_2$O with electrons of energies E_e. For most experiments, $E_e = 50$ eV has been used. To vary the fraction of metastable O$^+$ ions (O$^+$(^{2}D) and O$^+$(^{2}P)), the electron energy has been varied between 21 and 145 eV. The formed ions are extracted from the ion source, selected according to their mass-to-charge ratio, and injected into the ion trap. Typically, one filling of the trap consists of a few hundred primary reactant ions. The kinetic energy of the ions is cooled in collisions with helium atoms of the buffer gas, while a small admixture of H$_2$ leads to reaction ([He]/[H$_2$] $\approx$ 100). After a preselected trapping time (t, here up to 500 ms), all ions are extracted, their mass is analyzed with a quadrupole mass spectrometer, and they are counted using a micro channel plate detector.

2.2. Gas Number Density

The number density of buffer and reactant gases inside the trap is determined using a spinning rotor gauge connected

directly to the trap. In addition, an ion gauge mounted onto the vacuum chamber containing the trap is used to monitor the gas flow. It is calibrated from time to time using the spinning rotor gauge. The uncertainty of the reactant number density is estimated conservatively to be 20%.

2.3. Ortho- and Para-H_2

In the present study we used normal hydrogen, composed of $\frac{1}{4}$ para-H$_2$ and $\frac{3}{4}$ ortho-H$_2$. It has been checked (Zymak et al. 2013) that there is no ortho-para conversion in the gas inlet system or in the trap at low temperatures. Previous experimental studies of the title reaction O$^+$ + H$_2$ (by FA, SIFT, SIFDT, GIB, and ICR experiments, the details and the references are given below) were carried out with hydrogen at 300 K, i.e., with normal hydrogen.

2.4. Collision Temperature

In most radiofrequency (RF) ion traps, the translational temperature of the thermalized ions is slightly higher than that of the trap (T_{22PT}), as discussed in the literature (Gerlich & Horning 1992; Gerlich 2008; Asvany & Schlemmer 2009; Chakrabarty et al. 2013; Endres et al. 2017). Due to the favorable ionic and molecular mass ratio 16:2 in reaction (1), the collisional temperature, denoted here simply by T, is mainly determined by the cold H$_2$. Note that T is the mass-weighted mean value of the temperature of the two reactants. We estimate that in our trap $T < T_{22PT} + 10$ K and for simplicity we define it as $T = T_{22PT} + (5 \pm 5)$ K. For more details and discussions see Plašil et al. (2012), Zymak et al. (2013), Mulin et al. (2015), and Tran et al. (2018).

2.5. Internal Excitation of O$^+$ Ions

Depending on the electron energy and the number density, the O$^+$ ions from the storage ion source are either in the ground-state ^{4}S or in one of two excited metastable states (^{2}D or ^{2}P). Quenching the excited O$^+$ in the trap via collisions with He atoms is inefficient. See, e.g., confirmation in a helium-buffered SIFT experiment (Glosík et al. 1978). The radiative life-times of these metastables are larger than 5.6×10^3 s and 4.9 s, respectively (Zeippen 1987; Godefroid & Fischer 1984), which are long in comparison with the length of typical storage time used in the present experiments (<0.5 s).

To determine the population of trapped O$^+$ ions in the ^{2}D and ^{2}P states, we studied their interaction with N$_2$ in the trap. Note that for the O$^+$(^{4}S) ground-state ions the charge transfer reaction is endoergic by 1.96 eV. In analyses of the experimental data we have used the results of previous experimental studies in which a very slow reaction of O$^+$(^{4}S) with N$_2$ producing NO$^+$ and a very efficient charge transfer reaction of excited O$^+$(^{2}D, ^{2}P) ions with N$_2$ producing N$_2^+$ were observed (Glosík et al. 1978; Smith et al. 1978; Johnsen & Biondi 1980; Hierl et al. 1997; Le Garrec et al. 2003). Thus, by monitoring the production of NO$^+$ and N$_2^+$, it is possible to determine the relative populations of the ground-state O$^+$(^{4}S) ions and of the excited O$^+$(^{2}D, ^{2}P) ions in the ion trap.

The measured data are in good agreement with results of previous studies (Glosík et al. 1978; Hierl et al. 1997; Le Garrec et al. 2003). An example of data obtained at collision temperature $T = 72$ K, [N$_2$] $= 3.9 \times 10^{11}$ cm^{-3}, [He] $= 5.7 \times 10^{13}$ cm^{-3}, and electron energy $E_e = 75$ eV is shown in Figure 1. We observed that only 5% of the injected

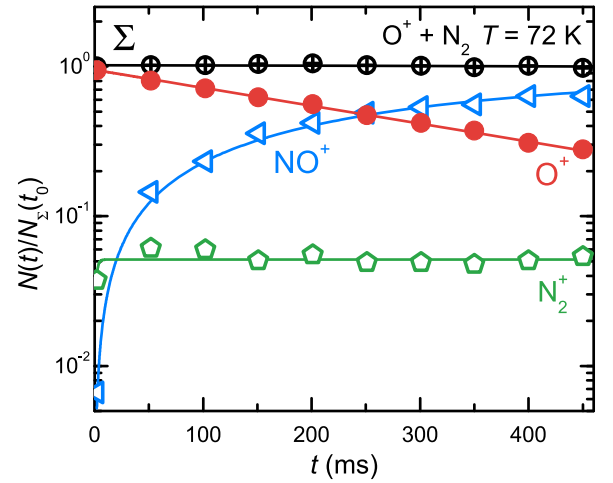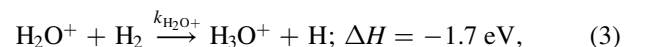**Figure 1.** Time evolutions of the numbers of trapped O$^+$, N$_2^+$, and NO$^+$ ions. The time dependence of the total number of ions (Σ) is also indicated. The data were measured at a temperature $T = 72$ K, the number densities in the trap [N$_2$] $= 3.9 \times 10^{11}$ cm^{-3}, [He] $= 5.7 \times 10^{13}$ cm^{-3}, and the energy of ionizing electrons $E_e = 75$ eV.

O$^+$ were converted into N$_2^+$ ions. The rate coefficient obtained for the reaction O$^+$(^{4}S) + N$_2$ is equal to $(6.6 \pm 0.1) \times 10^{-12}$ cm^3 s^{-1}. This value agrees within a few percent with the CRESU results measured at the same temperature (Le Garrec et al. 2003). On the base of these studies we can safely conclude that over 90% of the trapped O$^+$ ions are in the ^{4}S ground state when using the energy of ionizing electrons $E_e < 75$ eV. In the experiments where the rate coefficients k_{O+} of reaction (1) were measured as a function of collision temperature, the energy of ionizing electrons $E_e = 50$ eV was used.

3. Results

A typical result for trapping of O$^+$ ions in a He/H$_2$ mixture is shown in the upper panel of Figure 2. The number of different ions counted after storage times t is denoted as $N_X(t)$, where the index X refers to the various ions in the trap, e.g., $N_{O+}(t)$ is the number of O$^+$ ions. The total number of detected ions at time t is $N_\Sigma(t) = \sum N_X(t)$. For a better comparison of the results from different experiments, we divide the ion counts by the total number of ions measured at the shortest trapping time t_0, i.e., we plot normalized values $N_X(t)/N_\Sigma(t_0)$. The plotted numbers of H$^+$ are corrected for the difference in detection efficiency relative to O$^+$, which was obtained using a separate calibration reaction (H$^+$ + CH$_4$ producing CH$_3^+$ and CH$_4^+$). The decrease of $\Sigma = N_\Sigma(t)/N_\Sigma(t_0)$ (crossed open circles in Figure 2) with time indicates smaller detection efficiencies for OH$^+$, H$_2$O$^+$, and H$_3$O$^+$ relative to O$^+$. The detection efficiencies of these heavier ions are not accounted for in the plots; however, they are treated as free parameters in the fits.

Inspection of the upper panel of Figure 2 reveals that O$^+$ ions react to produce OH$^+$, followed by a sequence of additional exothermic reactions with H$_2$:

$$\text{OH} + \text{H}_2 \xrightarrow{k_{OH+}} \text{H}_2\text{O}^+ + \text{H}; \quad \Delta H = -1.02 \text{ eV}, \quad (2)$$

$$\text{H}_2\text{O}^+ + \text{H}_2 \xrightarrow{k_{H2O+}} \text{H}_3\text{O}^+ + \text{H}; \quad \Delta H = -1.7 \text{ eV}, \quad (3)$$

with the rate coefficients denoted as k_{OH+} and k_{H2O+}. The final product ion is protonated water. The given 0 K enthalpy

Figure 3. Loss rates r_{O+}, r_{OH+}, and r_{H2O+} of O^+, OH^+, and H_2O^+ ions as a function of H_2 number density. The collisional temperature $T = 259$ K. The corresponding binary reaction rate coefficients k_{O+}, k_{OH+}, and k_{H2O+} are given by the slope of the plotted dependencies (see the text).
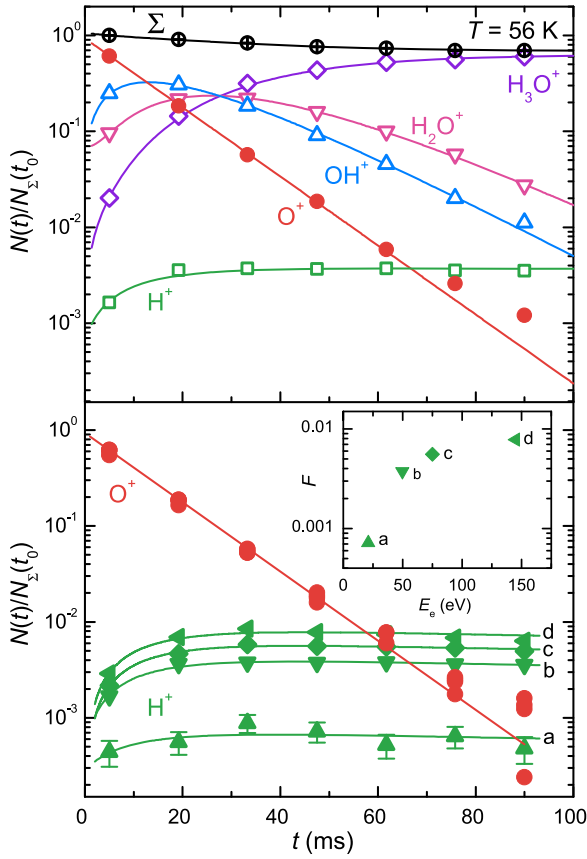
Figure 2. Time dependence of the normalized numbers of the indicated ions after injecting O^+ ions into the trap. The measurements were performed at $T = 56$ K, $[H_2] = 5.4 \times 10^{10}$ cm^{-3}, and $[He] = 5.5 \times 10^{12}$ cm^{-3}. All lines indicate the results from the fits (see the explanation in the text). Upper panel: electron energy $E_e = 50$ eV. Note that almost all injected O^+ ions are finally converted into H_3O^+ ions via sequential reactions with H_2. The small amount of H^+ ions produced (growing to $\approx 0.5\%$) is indicative of the relative population of metastable $O^+(^2D, ^2P)$ ions. Lower panel: electron energies $E_e = 21$, 50, 75, and 145 eV. The inset in the lower panel reveals that the fraction of H^+ products, F, increases with E_e.

changes given in eV were calculated from the relevant heats of formation (Haney & Franklin 1969; Chase 1998), ionization potentials (Wiedmann et al. 1992; Lauzin et al. 2015), and dissociation energies (Liu et al. 2009).

The observed H^+ ions are not due to $O^+(^4S) + H_2$, since this reaction is not only endoergic by 0.06 eV but also spin-forbidden (Flesch & Ng 1991; Li et al. 1997). These protons are produced in reactions of electronically excited metastable $O^+(^2D)$ and $O^+(^2P)$ ions with H_2

$$O^+(^2D, ^2P) + H_2 \rightarrow H^+ + OH, \qquad (4)$$
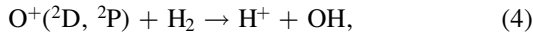
where $O^+(^2D, ^2P)$ indicates an unspecified mixture of $O^+(^2D)$ and $O^+(^2P)$ ions, with respective reaction enthalpies $\Delta H(^2D) = -3.27$ eV, $\Delta H(^2P) = -4.96$ eV.

The low fraction of H^+ products in comparison with the population of $O^+(^2D, ^2P)$ obtained in experiments with N_2 indicates that OH^+ is also produced in reactions of $O^+(^2D, ^2P)$. Based on reactions (1)–(4), the time variations of the primary ions and all product ions were fitted using a kinetic model. Free parameters are the rate coefficients, the initial numbers of all ions, as well as the detection efficiencies, as mentioned above. The overall agreement of the fits (solid lines) and the data
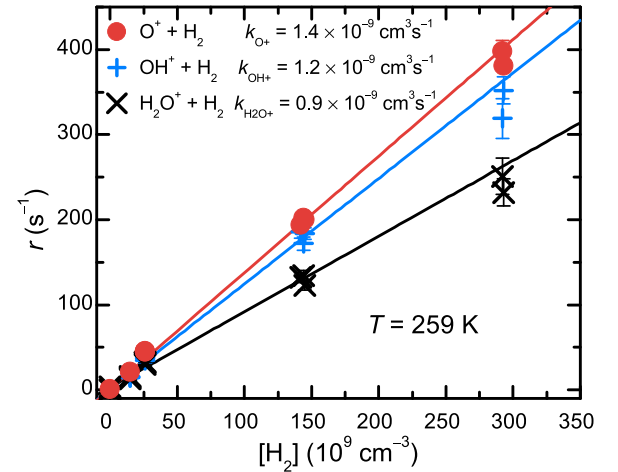
points is very good. The number of O^+ is well-described by a mono-exponential decay over almost 3 orders of magnitude.

The lower panel of Figure 2 illustrates the increase of the fraction of metastable O^+ ions with energy of the ionizing electrons E_e increasing from 21 to 145 eV. The fraction of H^+ ions produced via reaction (4), which is proportional to the population of $O^+(^2D, ^2P)$ ions in the trap, reaches up to 1% (see inset). This is consistent with the results of probing with N_2, which revealed that over 90% of trapped O^+ ions are in ground-state $O^+(^4S)$ for $E_e < 75$ eV (see Section 2.5).

The reaction rate coefficient obtained for OH^+ production, $k_{O+}(56 \pm 5$ K$) = (1.5 \pm 0.3) \times 10^{-9}$ cm^3 s^{-1}, is within the uncertainty of our data constant for all electron energies, which confirms that the measured values of k_{O+} are not influenced by the presence of metastable $O^+(^2D, ^2P)$ ions. This is because the fraction of $O^+(^2D, ^2P)$ is low (below 0.1) and the rate coefficient for the reaction of $O^+(^4S)$ is nearly collisional, i.e., the contribution from $O^+(^2D, ^2P)$ ions to the decay rate of $N_{O+}(t)$ can be on the order of few percent. To minimize the influence of $O^+(^2D, ^2P)$ ions, the electron energy was kept at $E_e = 50$ eV in all measurements of k_{O+} and the production of H^+ ions was monitored.

Another experimental test carried out was the dependence of the reaction rate r_{O+} on the reactant gas number density $[H_2]$ measured at $T = 259$ K, which is shown in Figure 3. The linearity of the dependencies obtained confirms that the decrease of the number of primaries in the trap is due to a binary ion-molecule reaction with H_2, i.e., the rate can be expressed by the formula, $r_{O+} = k_{O+}[H_2] + r_{bg}$. The level of the background loss rate (r_{bg}) measured in the experiment with pure He without H_2 is $r_{bg} = 0.9$ s^{-1}. At lower temperatures, cryopumping is more efficient in reducing the residual background gas (mostly N_2O, H_2O from the ion source). Figure 3 also includes reaction rates r_{OH+} and r_{H2O+} obtained from the fits of the same set of the data. The reaction rate coefficients obtained from the linear fits of the data in Figure 3 are: $k_{O+}(259$ K$) = (1.4 \pm 0.3) \times 10^{-9}$ cm^3 s^{-1}, $k_{OH+}(259$ K$) = (1.2 \pm 0.2) \times 10^{-9}$ cm^3 s^{-1}, and $k_{H2O+}(259$ K$) = (0.90 \pm 0.18) \times 10^{-9}$ cm^3 s^{-1}. These values are in good agreement with results from previous experiments at 300 K (see, e.g., ref. SIFT (Jones et al. 1981), FA (Fehsenfeld
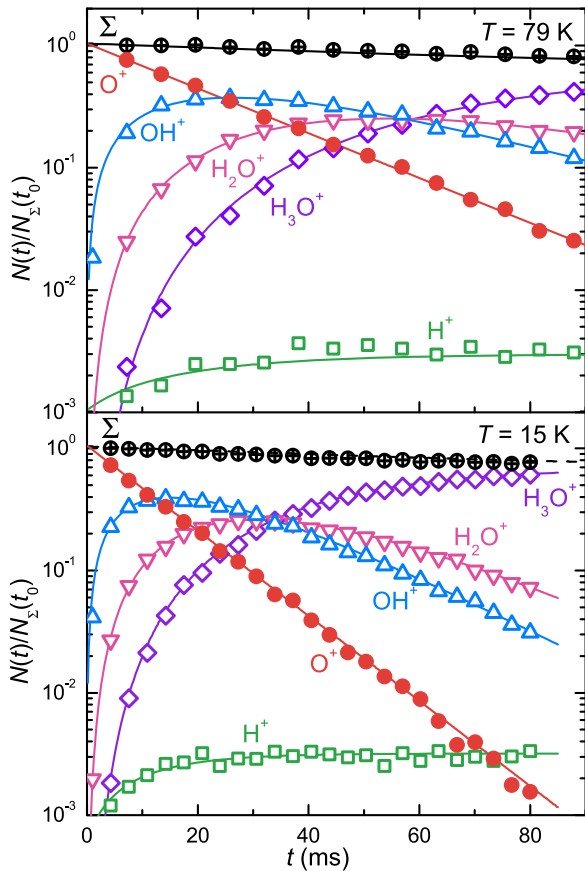
Figure 4. Time dependence of the normalized number of indicated ions in the trap after injection of O^+ ions. The open circles indicate the normalized total number of ions (Σ). Upper panel: $T = 79$ K, $[H_2] = 2.7 \times 10^{10}$ cm^{-3}, $[He] = 6.7 \times 10^{12}$ cm^{-3}. Lower panel: $T = 15$ K, $[H_2] = 6.0 \times 10^{10}$ cm^{-3}, $[He] = 1.5 \times 10^{14}$ cm^{-3}. The experimental data are fitted by a kinetic model (solid lines) resulting in the rate coefficients for reactions (1)–(3).

et al. 1967), ICR (Kim et al. 1975), and VT-SIFT (Martinez et al. 2015)).

No dependence of the measured reaction rate coefficients on the helium number density was observed in the range of $5 \times 10^{12} - 5 \times 10^{13}$ cm^{-3}.

The change of the ion composition with increasing storage time at collisional temperatures $T = 15$ and 79 K is shown in Figure 4 together with the results from fits. Similar to Figure 2, sequential addition of hydrogen atoms to O^+ leads finally to H_3O^+ and less than one percent of H^+ ions are formed. The decay rate of the number of O^+ ions has been studied at several collisional temperatures, ranging from 15 K to 300 K.

The temperature dependence obtained for the rate coefficient k_{O+} of the title reaction is plotted in Figure 5. The spread of the data is indicative of the reproducibility of our measurements. Plotted is also a collection of results from previous experiments and theories. All these results will be discussed below.

4. Discussion

4.1. The Role of Metastable O^+

As is illustrated in the lower part of Figure 2, the variation of electron energy, used in the ion source for production of O^+ from N_2O, results in different populations of the ^4S ground state and of the metastable excited states, ^2D and ^2P. By monitoring the production of N_2^+ ions in the reaction of trapped O^+ ions
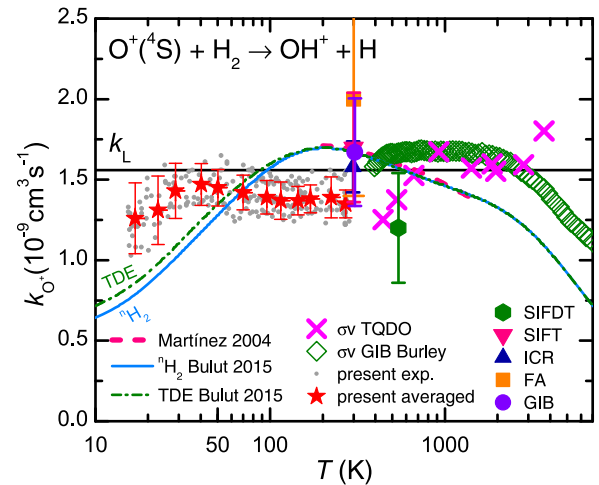

Figure 5. Dependence of the rate coefficient k_{O+} for the reaction of the ground-state $O^+(^4S)$ ions with normal H_2 on the collision temperature. The dots are the present data, as measured and explained in the text, while the filled stars are weighted averages over logarithmically spaced bins in temperature. The error bars indicate the sum of statistical uncertainties and the influence of temperature uncertainty. The horizontal straight line (k_L) indicates the value of the Langevin collisional rate coefficient. The filled symbols at 300 and 500 K are the results measured with the methods indicated (see the text). The points extending above 1000 K are effective rate coefficients measured by the guided ion beam technique (GIB; Burley et al. 1987) and TQDO (Li et al. 1997). The solid and dashed–dotted lines are reaction rate coefficients for normal H_2 and for H_2 with a thermal population of nuclear spin states, respectively, based on theoretical cross sections of Bulut et al. (2015). The theoretical rate coefficients of Martínez et al. (2004) are indicated by the dashed line.

with N_2 we have found operating conditions where the population of the excited metastable ions is $\approx 5\%$. Under these conditions ($E_e < 50$ eV), the influence of metastable O^+ ions on the determination of k_{O+} is negligible (see the lower panel of Figure 2 and related text). This is because 5% of $O^+(^2D, ^2P)$ can add to a measured value of the rate coefficient by at most 5% of the value of collisional rate coefficient ($\approx 0.08 \times 10^{-9}$ cm^3 s^{-1}).

4.2. Temperature Dependence

At first sight, Figure 5 shows a typical temperature dependence expected for an exothermic ion-molecule reaction: the measured rate coefficients, k_{O+}, are close to the Langevin rate coefficient k_L (horizontal straight line). The two sets of data above room temperature have been measured by guiding an ion beam through a 300 K target gas cell in experiments GIB (Burley et al. 1987) and TQDO (Li et al. 1997). Their agreement with k_L below and deviations from k_L above 0.3 eV are discussed in the relevant papers and in Bulut et al. (2015). Note that the plotted points are effective rate coefficients, as derived from the measured effective cross sections just by multiplying them with the mean relative velocity. Additionally, we have corrected the center of mass energy of Li et al. (1997) for the thermal motion of the neutral target with temperature $T_{GAS} \approx 300$ K by adding a term $(3/2)k_B T_{GAS} m_{O+}/(m_{O+} + m_{H2})$, where m_{O+} and m_{H2} are the O^+ and H_2 masses, respectively. The large filled points around 300 K summarize 50 years of ion-molecule reaction studies using well-established techniques such as flowing afterglow (FA) (Fehsenfeld et al. 1967), ion cyclotron resonance (ICR) ion trap (Kim et al. 1975), and selected ion flow tube (SIFT) (Smith et al. 1978). The selected ion flow-drift tube (SIFDT) value was measured at a mean relative kinetic energy of 0.07 eV (Federer et al. 1984).

We do not know of any previous experimental data for the studied reaction measured below room temperature. Taking into account only the indicated statistical errors, our ion trap data are slightly below k_L. On one side this may indicate that a fraction of the collision complexes decays back to the reactants. On the other side, this may be due to a systematic error, which is estimated to be up to 20% for the trapping experiments. From 300 to 30 K the measured reaction rate coefficient is temperature-independent. Below there may be a weak temperature dependence, as also indicated by theoretical results, shown as a solid line (Bulut et al. 2015).

Bulut et al. (2015) used time-dependent wave packet calculations (TDWP) to determine the integral cross sections for reactive collisions of O^+ with $H_2(j)$ at collision energies from 1 eV down to 1 meV and for $j = 0$, 1, and 2 (Bulut et al. 2015). They used a global potential energy surface (PES) calculated for the ground electronic state $1^4A'$ of H_2O^+ by Martínez et al. (2004). On this surface, reactants can progress to the $OH^+ + H$ product channel without a barrier. In accordance with this, the cross sections they obtained are in very good agreement with the predictions of the Langevin model for a 300 K population of the rotational states (see Bulut et al. 2015, Figure 8). Important for our low-temperature results is that the theoretical cross sections level off below 10 meV. Thermal rate coefficients have been calculated using these results and accounting for the T-dependent j-population of the normal H_2 and of H_2 with thermal population of nuclear spin states. The results are indicated by the solid and dashed–dotted lines in Figure 5, respectively. The difference between the rate coefficients at low temperatures is caused by a small ($\approx 10\%$) but significant decrease of the cross sections, with j increasing from 0 to 2.

It is too early to speculate whether the rate coefficients for reaction (1) really decrease at low temperatures and why. The authors of Bulut et al. (2015) also do not yet know why the TDWP cross sections depart from the Langevin model below 10 meV. They provide thermal rate coefficients only above 200 K and suspect that the leveling off may be due to errors in the theoretical treatment or due to incorrect long-range behavior of the PES.

5. Conclusion and Outlook

The temperature range of experimentally determined rate coefficients for the title reaction has been extended down to a nominal trap temperature of $T_{22PT} = 10$ K, corresponding to a collisional temperature of 15 K. Overall, the hydrogen abstraction reaction follows the behavior of many exothermic ion-molecule reactions, as described by the Langevin capture model. The values obtained at 300 K are in relatively good agreement with the results of previous experimental studies. Nevertheless, we have to keep in mind that in those previous experiments, the internal excitation of reacting O^+ ions was not specified, with the exception of the TQDO study of Li et al. (1997) and of the GIB study of Burley et al. (1987).

There are some indications that the rate coefficient for the title reaction decreases slightly below 30 K in accordance with the TDWP cross sections, which level off below 10 meV (Bulut et al. 2015). However, to test this, more experiments are needed and the theory also has to be re-examined for collision energies relevant to 10 K. Measurements with para-H_2 may reveal additional changes at low temperatures. Also, an extension of

the collision energy below 10 K is within the reach of modern cryogenic traps.

We also obtained rate coefficients for the reactions (2) and (3), leading finally to H_3O^+. The values obtained at room temperature are in good agreement with previous results from SIFT (Jones et al. 1981), FA (Fehsenfeld et al. 1967), ICR (Kim et al. 1975), and VT-SIFT (Martinez et al. 2015) experiments. The results derived from the fits at low temperatures indicate that there are no surprising changes in this reaction rate coefficient. The results of our detailed studies of reactions (2) and (3) with directly injected and cooled OH^+ and H_2O^+ ions have been published (Tran et al. 2018).

ORCID iDs

Artem Kovalenko ⬤ https://orcid.org/0000-0001-9521-6821
Thuy Dung Tran ⬤ https://orcid.org/0000-0002-9894-1647
Serhiy Rednyk ⬤ https://orcid.org/0000-0002-0408-0170
Štěpán Roučka ⬤ https://orcid.org/0000-0002-2419-946X
Petr Dohnal ⬤ https://orcid.org/0000-0003-0341-0382
Radek Plašil ⬤ https://orcid.org/0000-0001-8520-8983
Dieter Gerlich ⬤ https://orcid.org/0000-0002-3550-305X
Juraj Glosík ⬤ https://orcid.org/0000-0002-2638-9435

References

Asvany, O., & Schlemmer, S. 2009, IJMSp, 279, 147
Bulut, N., Castillo, J. F., Jambrina, P. G., et al. 2015, JPCA, 119, 11951
Burley, J. D., Ervin, K. M., & Armentrout, P. B. 1987, IJMIP, 80, 153
Chakrabarty, S., Holz, M., Campbell, E. K., et al. 2013, JPCL, 4, 4051
Chase, M. W. 1998, NIST-JANAF Thermochemical Tables (4th ed.; New York: AIP)
de Ruette, N., Miller, K. A., O'Connor, A. P., et al. 2016, ApJ, 816, 31
Endres, E. S., Egger, G., Lee, S., et al. 2017, JMoSp, 332, 134
Federer, W., Villinger, H., Howorka, F., et al. 1984, PhRvL, 52, 2084
Fehsenfeld, F. C., Schmeltekopf, A. L., & Ferguson, E. E. 1967, JChPh, 46, 2802
Flesch, G. D., & Ng, C. Y. 1991, JChPh, 94, 2372
Gerin, M., Neufeld, D. A., & Goicoechea, J. R. 2016, ARA&A, 54, 181
Gerlich, D. 2008, Low Temperatures and Cold Molecules (Singapore: Imperial College Press), 121
Gerlich, D., Borodi, G., Luca, A., Mogo, C., & Smith, M. A. 2011, ZPC, 225, 475
Gerlich, D., & Horning, S. 1992, ChRv, 92, 1509
Gerlich, D., Jusko, P., Roučka, Š, et al. 2012, ApJ, 749, 22
Gerlich, D., Plašil, R., Zymak, I., et al. 2013, JPCA, 117, 10068
Glosík, J., Rakshit, A. B., Twiddy, N. D., Adams, N. G., & Smith, D. 1978, JPhB, 11, 3365
Godefroid, M., & Fischer, C. F. 1984, JPhB, 17, 681
Gómez-Carrasco, S., Godard, B., Lique, F., et al. 2014, ApJ, 794, 33
Haney, M. A., & Franklin, J. L. 1969, JChPh, 50, 2028
Hierl, P. M., Dotan, I., Seeley, J. V., et al. 1997, JChPh, 106, 3540
Hollenbach, D., Kaufman, M. J., Bergin, E. A., & Melnick, G. J. 2009, ApJ, 690, 1497
Hollenbach, D., Kaufman, M. J., Neufeld, D., Wolfire, M., & Goicoechea, J. R. 2012, ApJ, 754, 105
Indriolo, N., Neufeld, D. A., Gerin, M., et al. 2015, ApJ, 800, 40
Jensen, M. J., Bilodeau, R. C., Safvan, C. P., et al. 2000, ApJ, 543, 764
Johnsen, R., & Biondi, M. A. 1980, JChPh, 73, 190

Jones, J. D. C., Birkinshaw, K., & Twiddy, N. D. 1981, CPL, 77, 484
Kim, J. K., Theard, L. P., & Huntress, W. T. 1975, JChPh, 62, 45
Lauzin, C., Jacovella, U., & Merkt, F. 2015, MolPh, 113, 3918
Le Garrec, J.-L., Carles, S., Speck, T., et al. 2003, CPL, 372, 485
Li, X., Huang, Y.-L., Flesch, G. D., & Ng, C. Y. 1997, JChPh, 106, 564
Liu, J., Salumbides, E. J., Hollenstein, U., et al. 2009, JChPh, 130, 174306
Martinez, O., Ard, S. G., Li, A., et al. 2015, JChPh, 143, 114310
Martínez, R., Millán, J., & González, M. 2004, JChPh, 120, 4705
Mulin, D., Roučka, Š, Jusko, P., et al. 2015, PCCP, 17, 8732
Muller, S., Müller, H. S. P., Black, J. H., et al. 2016, A&A, 595, A128
Neau, A., Al Khalili, A., Rosén, S., et al. 2000, JChPh, 113, 1762
Neufeld, D. A., & Wolfire, M. G. 2016, ApJ, 826, 183
Neufeld, D. A., & Wolfire, M. G. 2017, ApJ, 845, 163
Pilbratt, G. L., Riedinger, J. R., Passvogel, T., et al. 2010, A&A, 518, L1
Plašil, R., Zymak, I., Jusko, P., et al. 2012, RSPTA, 370, 5066
Sansonetti, J. E., & Martin, W. C. 2005, JPCRD, 34, 1559
Smith, D., Adams, N. G., & Miller, T. M. 1978, JChPh, 69, 308
Tran, T. D., Rednyk, S., Kovalenko, A., et al. 2018, ApJ, 854, 25
Wiedmann, R. T., Tonkyn, R. G., White, M. G., Wang, K., & McKoy, V. 1992, JChPh, 97, 768
Wyrowski, F., van der Tak, F., Herpin, F., et al. 2010, A&A, 521, L34
Zeippen, C. J. 1987, A&A, 173, 410
Zymak, I., Hejduk, M., Mulin, D., et al. 2013, ApJ, 768, 86
Zymak, I., Jusko, P., Roučka, Š, et al. 2011, EPJAP, 56, 24010

Article III: Formation of H_2O^+ and H_3O^+ Cations in Reactions of OH^+ and H_2O^+ with H_2: Experimental Studies of the Reaction Rate Coefficients from $T = 15$ to 300 K

Tran, T. D., Rednyk, S., Kovalenko, A., Roučka, Š., Dohnal, P., Plašil, R., Gerlich, J., Glosík, J.

2018

CrossMark

Formation of H_2O^+ and H_3O^+ Cations in Reactions of OH^+ and H_2O^+ with H_2: Experimental Studies of the Reaction Rate Coefficients from $T = 15$ to $300\,K$

Thuy Dung Tran (ORCID), Serhiy Rednyk (ORCID), Artem Kovalenko (ORCID), Štěpán Roučka (ORCID), Petr Dohnal (ORCID), Radek Plašil (ORCID),
Dieter Gerlich (ORCID), and Juraj Glosík (ORCID)
Department of Surface and Plasma Science, Faculty of Mathematics and Physics, Charles University, V Holešovičkách 2,
Prague, 180 00, Czech Republic; stepan.roucka@mff.cuni.cz

Abstract

OH^+ and H_2O^+ cations play a significant role in the chemistry of the cold interstellar medium and hence their hydrogen abstraction reactions with H_2 have to be included in ion chemical models. The reactions lead directly or indirectly to H_3O^+ ions that subsequently recombine with electrons and dissociate into H atoms and H_2O. The experiments described in this paper provide rate coefficients (k_{OH^+} and $k_{H_2O^+}$) for the reactions of OH^+ and H_2O^+ with H_2 over a wide temperature range (from 15 to 300 K). A cryogenic 22-pole RF ion trap instrument was employed for this purpose. It was found that k_{OH^+} increases from $(0.76 \pm 0.30) \times 10^{-9}\,cm^3\,s^{-1}$ at 17 K to $(1.24 \pm 0.25) \times 10^{-9}\,cm^3\,s^{-1}$ at 263 K while $k_{H_2O^+}$ is nearly constant, varying from $(0.93 \pm 0.35) \times 10^{-9}\,cm^3\,s^{-1}$ at 17 K to $(1.00 \pm 0.25) \times 10^{-9}\,cm^3\,s^{-1}$ at 218 K.

Key words: astrochemistry – ISM: molecules – methods: laboratory: molecular – molecular data – molecular processes

1. Introduction

Hydrides, molecules containing a heavy atom and one or more hydrogen atoms, were among the first molecules observed in interstellar space, oxygen hydrides being one of the key species (see recent reviews of Hollenbach et al. 2009; van Dishoeck et al. 2013, 2014; Gerin et al. 2016 and references therein). Major progress in the astronomical studies of oxygen hydrides recently has been made in connection with the Herschel space observatory, the Atacama Large Millimeter/submillimeter Array, the Atacama Pathfinder Experiment, and other observatories. Of particular interest is the detection of OH, OH^+, H_2O, H_2O^+, and H_3O^+ in diffuse and dense Galactic interstellar media (Gerin et al. 2010; Ossenkopf et al. 2010; Pilbratt et al. 2010; Wyrowski et al. 2010; Hollenbach et al. 2012; Gómez-Carrasco et al. 2014; Muller et al. 2016; Neufeld & Wolfire 2016). Hence, the formation of neutral and ionized oxygen hydrides under conditions of the interstellar medium has become an important problem in contemporary laboratory astrophysics (Gerin et al. 2016) and has motivated theoretical studies of these reactions (Ard et al. 2014; Bulut et al. 2015; Martinez et al. 2015; Song et al. 2016a, 2016b, 2017). The results also impact determinations of cosmic ray (CR) ionization rates (Hollenbach et al. 2012; Indriolo et al. 2015; Neufeld & Wolfire 2016, 2017).

The dissociative recombination of H_3O^+ ions with electrons is an important source of H_2O molecules (see Larsson & Orel 2008 and references therein). The formation of OH^+, H_2O^+, and H_3O^+ has been discussed in detail by Hollenbach et al. (2009, 2012). In the hydrogen-rich environment, there are two routes that lead to H_3O^+ ions (see also Hollenbach et al. 2009, 2012; van Dishoeck et al. 2014; Gerin et al. 2016). If the H atom concentration is high, H^+ ions are generated by CR ionization. In a next step, O^+ ions are formed from O atoms in the slightly endothermic electron transfer to H^+. A series of further reactions with H_2 leads to OH^+, H_2O^+, and finally to H_3O^+. The overall simplified scheme is

$$H \xrightarrow{CR} H^+ \xrightarrow{O} O^+ \xrightarrow{H_2} OH^+ \xrightarrow{H_2} H_2O^+ \xrightarrow{H_2} H_3O^+. \quad (1)$$
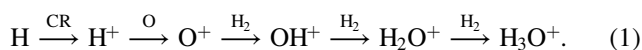
The second reaction chain to H_3O^+ starts with the formation of H_2^+ by the CR ionization of H_2 followed by the formation of H_3^+ via a reaction with H_2. The H_3^+ ion can eventually recombine with an electron (Glosík et al. 2010; Hejduk et al. 2015) or react by proton transfer with a less abundant O atom. Subsequently, the OH^+ ions react with H_2 and a sequence of hydrogen atom abstraction reactions leads to the formation of H_3O^+ (Hollenbach et al. 2012; Indriolo & McCall 2013; van Dishoeck et al. 2013):

$$H_2 \xrightarrow{CR} H_2^+ \xrightarrow{H_2} H_3^+ \xrightarrow{O} OH^+ \xrightarrow{H_2} H_2O^+ \xrightarrow{H_2} H_3O^+. \quad (2)$$
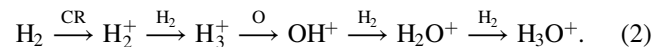
The formation of OH^+ and other oxygen hydrides in various astrophysical environments has been investigated by many authors (see, e.g., van Dishoeck et al. 2013, 2014; Indriolo et al. 2015; Muller et al. 2016; Neufeld & Wolfire 2017, and a recent review of Gerin et al. 2016).
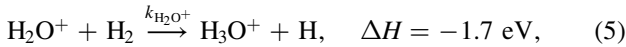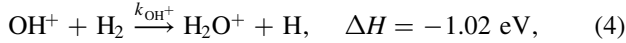
The measurements reported here build on our previous studies in which we used the cryogenic 22-pole RF ion trap apparatus to determine the rate coefficient (k_{O^+}) of the reaction of ground state $O^+(^4S)$ ions with H_2,

$$O^+ + H_2 \xrightarrow{k_{O^+}} OH^+ + H, \quad \Delta H = -0.54\,eV, \quad (3)$$

in the temperature range of 15–300 K. The results and experimental procedures required to obtain the ground state $O^+(^4S)$ ions are described in a separate publication (A. Kovalenko et al. 2017, in preparation). The reaction enthalpy ΔH at 0 K was calculated using tabulated enthalpies of formation, dissociation energies, and ionization potentials (Wiedmann et al. 1992; Chase 1998; Sansonetti & Martin 2005; Liu et al. 2009). Further theoretical and experimental studies of this reaction would be highly desirable to understand the observed data and also for chemical modeling of the interstellar medium (Indriolo et al. 2015; Markus et al. 2016). The rate coefficient k_{O^+} measured by A. Kovalenko et al. (2017, in preparation) is nearly constant in the studied

temperature range with values of k_{O^+} (15 K) = $(1.3 \pm 0.3) \times 10^{-9}$ cm^3 s^{-1} and k_{O^+} (300 K) = $(1.4 \pm 0.3) \times 10^{-9}$ cm^3 s^{-1} at 15 K and 300 K, respectively. The results are in rather good agreement with flowing-afterglow (FA) data at 300 K (Fehsenfeld et al. 1967), the ion cyclotron resonance (ICR) ion trap data of Kim et al. (1975), as well as the selected ion flow tube (SIFT) data of Smith et al. (1978). The cross-sections measured at collision energies from 0.02 to 7 eV (Li et al. 1997) and the theoretical results (Bulut et al. 2015) are also in good agreement.

The present experimental study is focused on the temperature dependence of the two reactions

$$OH^+ + H_2 \xrightarrow{k_{OH^+}} H_2O^+ + H, \quad \Delta H = -1.02 \text{ eV}, \quad (4)$$

$$H_2O^+ + H_2 \xrightarrow{k_{H_2O^+}} H_3O^+ + H, \quad \Delta H = -1.7 \text{ eV}, \quad (5)$$

where the reaction enthalpies were calculated from the heats of formation (Haney & Franklin 1969; Chase 1998), dissociation energies (Liu et al. 2009), and ionization potentials (Wiedmann et al. 1992; Lauzin et al. 2015). Reaction (4) has been studied several times using various experiments including FA (Fehsenfeld et al. 1967), SIFT (Jones et al. 1981; Shul et al. 1988), and ICR (Kim et al. 1975). Reaction (5) has also been studied experimentally using FA (Fehsenfeld et al. 1967), ICR (Kim et al. 1975), drift tube (DT) (Rakshit & Warneck 1980, 1981), flow-drift tube (FDT) (Dotan et al. 1980), and SIFT (Jones et al. 1981). However, these studies were performed at 300 K with the exception of the FDT experiment that covered relative kinetic energies from 0.04 up to 0.3 eV. More recently the temperature dependencies of k_{OH^+} from 200 to 600 K and $k_{H_2O^+}$ from 100 to 600 K have been measured using a variable temperature VT-SIFT experiment (Ard et al. 2014; Martinez et al. 2015). Reactions (4) and (5) have been studied theoretically, including rotational and isotopic effects, for higher collision energies (in the range 0.02–2 eV; Song et al. 2016a, 2016b, 2017).

To our knowledge, there are no experimental studies of the rate coefficients of Reactions (4) and (5) for temperatures below 200 K and 100 K, respectively. The wide range of astrophysical conditions, temperatures in particular, for which the formation and the destruction of the oxygen hydrides are relevant (Hollenbach et al. 2012; van Dishoeck et al. 2014; Indriolo et al. 2015; Gerin et al. 2016; Muller et al. 2016) and the scarcity of experimental data for the temperatures below 300 K are the main motivation for our present study.

In the following text, we shortly describe the experimental arrangement and parameters. The results are presented and discussed in Section 3. They are compared with values from previous experiments and with available theoretical predictions.

2. Experiment

The experiments were carried out using a cryogenic 22-pole RF ion trap (AB-22PT instrument). This apparatus allows us to study the interaction of a neutral reactant gas with a cold thermal ensemble of ions confined in a radiofrequency electric field. It has been described in detail many times (see e.g., Gerlich et al. 2011, 2012, 2013; Zymak et al. 2011, 2013; Plašil et al. 2012; Mulin et al. 2015). The body of the 22-pole ion trap is connected to a cold head, which can reach nominal

temperatures (T_{22PT}) as low as 10 K. It can be safely assumed on the basis of our previous tests (Plašil et al. 2012; Zymak et al. 2013; Mulin et al. 2015; Š. Roučka et al. 2017, in preparation) that the temperature of the buffer and reactant gases (He and H$_2$) in the volume of the trap does not exceed the measured trap temperature by more than 10 K, hence the gas temperature is taken as $T_{GAS} = T_{22PT} + (5 \pm 5)$ K. Likewise, the collisional temperature (T) of collisions between studied ions and H$_2$ is taken as $T = T_{22PT} + (5 \pm 5)$ K. The uncertainties in the temperatures are taken into account when evaluating the gas number densities and consequently also the rate coefficients. For more details and discussion see Paul et al. (1995), Chakrabarty et al. (2013), Jusko et al. (2014), and Endres et al. (2017).

The primary reactants O$^+$, OH$^+$, and H$_2$O$^+$ are generated by electron impact in a storage ion source using a mixture of N$_2$O and H$_2$ gases. We are using N$_2$O because it is safer to handle than O$_2$ and it has higher vapor pressure than, e.g., H$_2$O or H$_2$O$_2$. The ions are stored for typically 100 ms in the ion source before extraction. Once the source is opened, the ions pass through a mass filter and they are injected into the ion trap filled with a mixture of He and H$_2$. The injected ions are cooled in collisions with He atoms. Since the He density is typically 100 times higher than the hydrogen density, the kinetic energy of almost all of the ions is thermalized to T_{GAS} prior to a collision with a molecule of H$_2$. The uncertainty of the reactant gas pressure in the trap is less than 20%.

After the storage time period, varied in the present studies between 5 and 100 ms, the remaining ions are extracted from the trap, their mass is selected by passing through a quadrupole mass spectrometer, and they are counted by a microchannel plate detector. The number of detected ions is proportional to the number of ions of a particular mass in the trap at the moment of opening. The detection efficiency depends on the mass of the ions. However, in the majority of the present experiments we detect O$^+$, OH$^+$, H$_2$O$^+$, and H$_3$O$^+$ ions, whose masses are similar and therefore in the first approximation, the effect of the mass discrimination can be neglected. Furthermore, reaction rates are inferred mainly from the decay of the number of primary ions, so the resulting rate coefficients are not affected by the mass discrimination. Nevertheless, we always monitor the mass discrimination by comparing the observed rate of disappearance of reactant ions with the rate of formation of product ions.

We used normal hydrogen, which is a 300 K statistical mixture of nuclear spin states containing one-fourth of para-H$_2$ and three-fourths of ortho-H$_2$ with total nuclear spins of $I = 0$ and $I = 1$, respectively. If hydrogen is cooled down from 300 K without a catalyst, the para to ortho ratio stays constant, as confirmed by chemical probing with N$^+$ ions in the present experimental setup (Zymak et al. 2013).

In principle, the reaction rate coefficients k_{O^+}, k_{OH^+}, and $k_{H_2O^+}$ can all be determined by injecting O$^+$ ions into the trap and observing the whole chain of hydrogen abstraction reactions at once. Such data are shown in Figure 1 for illustration. In this experiment, a small fraction of O$^+$ was in excited metastable states O$^+$(^{2}D) and O$^+$(^{2}P) and these ions produced H$^+$ in reactions with H$_2$ (see our related publication concerning this reaction for details; A. Kovalenko et al. 2017, in preparation). Figure 1 also shows the total number of ions in the trap ($N_\Sigma(t)$). The slight decrease of the sum over time, which is partly due to loss of H$^+$ from the trap and partly due to
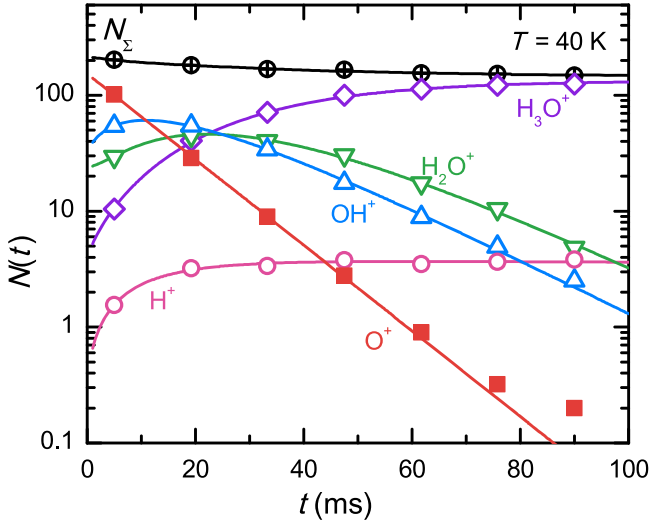
Figure 1. Measured decay of the number of the primary O^+ ions and the time evolutions of the numbers of the H^+, OH^+, H_2O^+, and H_3O^+ product ions. $N_\Sigma(t)$ is the sum of the numbers of all of the ions in the trap. The experiment was carried out under the following conditions: collisional temperature $T = 40 \pm 5$ K, gas number densities $[H_2] = 6.4 \times 10^{10}$ cm^{-3}, and $[He] = 6.5 \times 10^{12}$ cm^{-3}. The lines are computed solutions of the adequate rate equations, using the fitted rate coefficients. The rate coefficients and their overall uncertainties are k_{O^+} (40 K) = $(1.33 \pm 0.34) \times 10^{-9}$ cm^3 s^{-1}, k_{OH^+} (40 K) = $(8.8 \pm 2.3) \times 10^{-10}$ cm^3 s^{-1}, and $k_{H_2O^+}$ (40 K) = $(9.5 \pm 2.5) \times 10^{-10}$ cm^3 s^{-1}.

Figure 2. Measured time evolution of the normalized numbers of the primary OH^+ and product H_2O^+ and H_3O^+ ions. The lines indicate solutions to the set of rate equations. The open circles indicate the sum (Σ) of the normalized numbers of the ions in the trap. The experimental parameters are $T = 44 \pm 5$ K, $[H_2] = 6.4 \times 10^{10}$ cm^{-3}, and $[He] = 1.8 \times 10^{13}$ cm^{-3}. The fitted reaction rate coefficients and their overall uncertainties are k_{OH^+} (44 K) = $(8.7 \pm 2.2) \times 10^{-10}$ cm^3 s^{-1} and $k_{H_2O^+}$ (44 K) = $(9.4 \pm 2.4) \times 10^{-10}$ cm^3 s^{-1}.

mass discrimination, is taken into account in the data analysis. Minor parasitic reactions due to impurities are observed when only pure He is admitted into the trap. This background loss rate is less than 2% of the reaction loss rate and it is subtracted in the data analysis.

The rate coefficients of Reactions (4) and (5) can be measured directly by producing these ions in the ion source and injecting them into the trap. This is more accurate because we do not have two or more simultaneous processes influencing the number of a particular ion in the trap and, furthermore, the intermediate products OH^+ and H_2O^+ in the reaction chain can be produced with internal excitation, which can influence their reaction rates. In the data graphs, the numbers of ions are divided by the total number of trapped ions measured at time t_0 (time of the first measurements after injection).

3. Results and Discussion

Typical examples of the time evolutions of the normalized numbers of the primary OH^+ ions, the product H_2O^+ ions, and the secondary product H_3O^+ ions measured at the collisional temperature $T = 44$ K are shown in Figure 2. Also plotted is the sum $\Sigma(t)$ of the normalized numbers of ions in the trap. Its nearly constant value indicates low losses of ions in the trap due to their reaction with residual gases and gases penetrating from the ion source. Note the mono-exponential decay of the number of OH^+ ions in the trap due to the reaction with H_2, which indicates good thermalization of the ions. The reaction rate coefficients k_{OH^+} and $k_{H_2O^+}$ were obtained simultaneously from the fit of the data.

The rate coefficient $k_{H_2O^+}$ for the reaction of H_2O^+ with H_2 was also obtained in the simpler and more accurate way, which consists of generating H_2O^+ ions in the ion source. Figure 3 shows the mono-exponential decay of H_2O^+ ions obtained in this type of experiment.
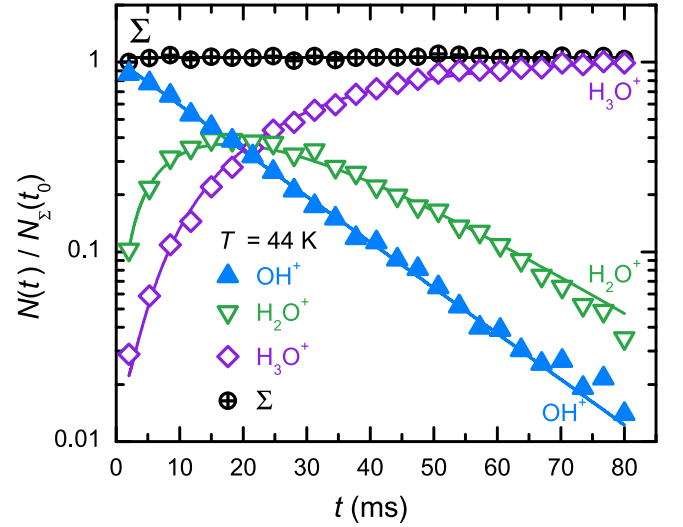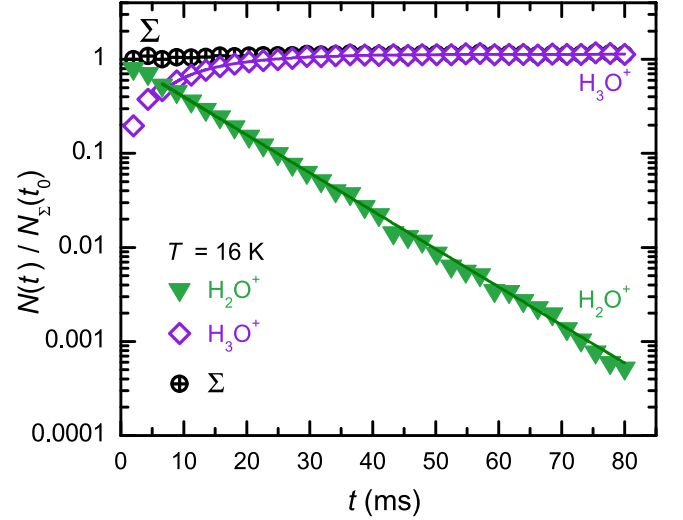

Figure 3. Time evolution of the normalized relative numbers of the primary H_2O^+ and secondary H_3O^+ ions. The lines indicate solutions to the set of rate equations. The open circles indicate the sum (Σ) of the normalized numbers of ions in the trap. The experimental parameters are: $T = 16 \pm 5$ K, $[H_2] = 1.0 \times 10^{11}$ cm^{-3}, and $[He] = 2.9 \times 10^{13}$ cm^{-3}. The obtained reaction rate coefficient is $k_{H_2O^+}$ (16 K) = $(9.2 \pm 3.2) \times 10^{-10}$ cm^3 s^{-1}.

The binary character of the studied reactions was confirmed by measuring the dependencies of the reaction rates on the reactant gas number density $[H_2]$. The linearity of the measured dependencies confirmed that the loss of OH^+ (and H_2O^+) ions in the trap was caused by a binary ion–molecule reaction with H_2.

The measured temperature dependence of the rate coefficient k_{OH^+} of the reaction of OH^+ with normal H_2 is shown in Figure 4. The reaction rate coefficients obtained from experiments with OH^+ injection (see Figure 2) and O^+ injection (see Figure 1) are compared in the figure. Both temperature dependencies are in very good agreement in the
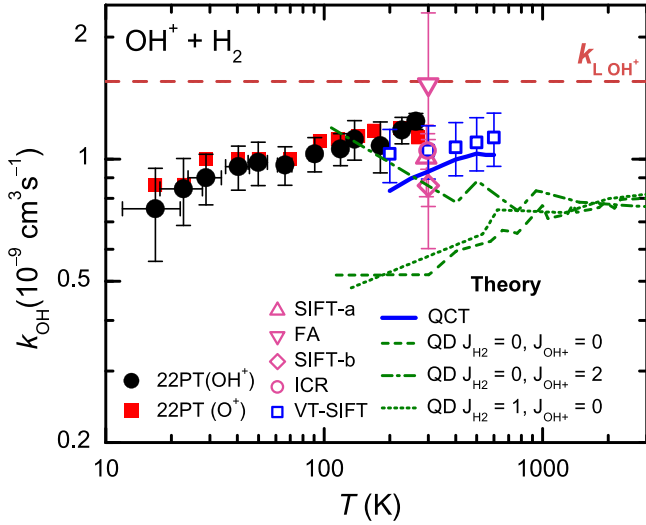
Figure 4. Temperature dependence of the rate coefficient k_{OH^+} of the reaction of OH^+ with normal hydrogen. The averaged data obtained in experiments with OH^+ and O^+ ions injected into the trap are indicated by full circles and squares, respectively. The systematic error due to pressure measurement is 20%. The dashed horizontal line ($k_{L\,OH^+}$) indicates the Langevin collisional rate coefficient. The previous results at 300 K are FA (Fehsenfeld et al. 1967), ICR (Kim et al. 1975), SIFT-a (Jones et al. 1981), and SIFT-b (Shul et al. 1988). The temperature dependencies of k_{OH^+} calculated (QCT) and measured (VT-SIFT) by Martinez et al. (2015) are indicated by the full line and open squares, respectively. The dashed, dotted, and dash-dotted lines represent the phenomenological rate coefficients ($v\sigma$) derived from the theoretical QD cross-sections (Song et al. 2016a) corresponding to different rotational states of reactants as indicated in the legend.

Figure 5. Temperature dependence of the reaction rate coefficient $k_{H_2O^+}$ of the reaction of H_2O^+ with normal hydrogen. The averaged data obtained in experiments with H_2O^+, OH^+, and O^+ ions injected into the trap are indicated by full circles, triangles, and squares, respectively. The systematic error due to pressure determination is 20%. The dashed horizontal line ($k_{L\,H_2O^+}$) indicates the Langevin collisional rate coefficient. The previous results at 300 K are FA (Fehsenfeld et al. 1967), ICR (Kim et al. 1975), FDT (Dotan et al. 1980), and SIFT (Jones et al. 1981). The values measured (VT-SIFT) and calculated (QCT) by Ard et al. (2014) are indicated by the open squares and by the full line (QCT), respectively. The dashed line and stars represent the phenomenological rate coefficients ($v\sigma$) derived from the theoretical QD, and experimental DQDO cross-sections (Song et al. 2016b). The uncertainty of the DQDO results is 50%.

whole covered temperature range, indicating that a possible excitation of the intermediate products does not influence the present experimental results. The error bars of our data with OH^+ injection indicate the statistical errors combined with the systematic uncertainty due to temperature measurement. The uncertainties of the data with O^+ injection are of similar size.

Figure 4 also shows k_{OH^+} measured in several previous experiments at 300 K (FA, Fehsenfeld et al. 1967; ICR, Kim et al. 1975; SIFT, Jones et al. 1981; SIFT, Shul et al. 1988), the temperature dependent data from the VT-SIFT experiment (Martinez et al. 2015), and the theoretical temperature dependence obtained using the quasiclassical trajectory method (QCT; Martinez et al. 2015). For qualitative comparison with our data, the cross-sections (σ) of Song et al. (2016a) obtained using quantum dynamics (QD) for OH^+ and H_2 in rotational states ($J_{H_2} = 0$, $J_{OH^+} = 0$); ($J_{H_2} = 0$, $J_{OH^+} = 2$); ($J_{H_2} = 1$; $J_{OH^+} = 0$) were converted to phenomenological rate coefficients by multiplying them with the relative velocity (v).

The agreement with the previously published values measured at 300 K is within the combined accuracy of the older and present values. The agreement of the present results with the experimental and theoretical dependencies obtained by Martinez et al. (2015) is good with a small systematic shift. The reaction rate coefficients calculated from the cross-sections of Song et al. (2016a) for ground state reactants are approximately by factor of 2 lower in comparison with present data, but also in comparison with the previous data measured at 300 K. The higher value of the thermal experimental rate coefficients is probably due to the thermal population of OH^+ rotational states. The $OH^+(J_{OH^+} = 2)$, which is still significantly populated at 100 K, has a theoretical reaction rate coefficient almost twice as large as the ground state $OH^+(J_{OH^+} = 0)$
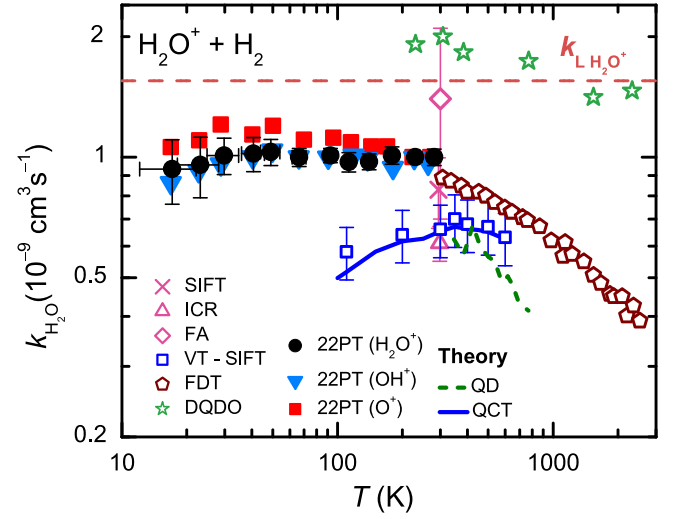
(Song et al. 2016a). The decrease of our measured reaction rate coefficient toward low temperatures may also be explained by the enhancement of the reaction rate coefficients via rotational excitation of OH^+, because about 90% of OH^+ is in the ground state at 15 K. The rotational excitation of H_2 has a much smaller effect according to the theory (Song et al. 2016a), even though it contains more energy. The influence of the H_2 rotational excitation will be further investigated by measuring with para-enriched hydrogen (Zymak et al. 2013).

The temperature dependencies of the reaction rate coefficient $k_{H_2O^+}$ measured in the experiments with the injection of O^+, OH^+, and H_2O^+ ions into the trap are shown in Figure 5. The experiments were carried out at nominal trap temperatures from 10 to 300 K. The results of experiments with the injection of O^+ and OH^+ ions are in agreement over the whole temperature range with the most reliable temperature dependence measured with the injection of H_2O^+ ions (see the example in Figure 3). Figure 5 also includes $k_{H_2O^+}$ measured in previous experiments at 300 K (FA, Fehsenfeld et al. 1967; ICR, Kim et al. 1975; FDT, Dotan et al. 1980; SIFT, Jones et al. 1981) and temperature dependent theoretical (QCT) and experimental (VT-SIFT) data between 100 and 600 K by Ard et al. (2014). The cross-sections of Song et al. (2016b) obtained theoretically using the QD method and experimentally using the double-quadrupole double-octopole (DQDO) apparatus are averaged over the thermal population of the H_2O^+ rotational states and represented by phenomenological rate coefficients.

The agreement with previous values obtained at 300 K is also within the combined accuracy of the old and present values. However, our results show that the rate coefficient is not decreasing with temperature as claimed by Ard et al. (2014). Their experimental and theoretical data are systematically lower than the present ion trap data and also the

previously published FDT results at higher temperatures (Dotan et al. 1980).

4. Conclusion and Outlook

We have reported results of experimental studies of the temperature dependencies of the rate coefficients for the $OH^+ + H_2$ and $H_2O^+ + H_2$ reactions using the cryogenic 22-pole RF ion trap with the electron impact storage ion source. The data cover a much wider temperature range (15–300 K) than previous experimental results. The agreement of previous and present data in the overlapping temperature range confirms the accuracy of our experimental methods and we recommend incorporating these new low-temperature data into astrophysical models. We are preparing further low-temperature studies of the reactions of O^+, OH^+, and H_2O^+ with D_2 and also with HD (deuterium hydride), and also studies of reactivity with H_2 in ortho and para nuclear spin configurations. The latter studies may reveal effects of the rotational state of H_2 that have been predicted.

Software: lmfit (Newville et al. 2014).

ORCID iDs

Thuy Dung Tran ⓘ https://orcid.org/0000-0002-9894-1647
Serhiy Rednyk ⓘ https://orcid.org/0000-0002-0408-0170
Artem Kovalenko ⓘ https://orcid.org/0000-0001-9521-6821
Štěpán Roučka ⓘ https://orcid.org/0000-0002-2419-946X
Petr Dohnal ⓘ https://orcid.org/0000-0003-0341-0382
Radek Plašil ⓘ https://orcid.org/0000-0001-8520-8983
Dieter Gerlich ⓘ https://orcid.org/0000-0002-3550-305X
Juraj Glosík ⓘ https://orcid.org/0000-0002-2638-9435

References

Ard, S. G., Li, A., Martinez, O., et al. 2014, JPCA, 118, 11485
Bulut, N., Castillo, J. F., Jambrina, P. G., et al. 2015, JPCA, 119, 11951
Chakrabarty, S., Holz, M., Campbell, E. K., et al. 2013, JPhCh Lett., 4, 4051
Chase, M. W. (ed.) 1998, NIST-JANAF Thermochemical Tables (Woodbury, NY: AIP)
Dotan, I., Lindinger, W., Rowe, B., et al. 1980, CPL, 72, 67
Endres, E. S., Egger, G., Lee, S., et al. 2017, JMoSp, 332, 134
Fehsenfeld, F. C., Schmeltekopf, A. L., & Ferguson, E. E. 1967, JChPh, 46, 2802
Gerin, M., De Luca, M., Black, J., et al. 2010, A&A, 518, L110
Gerin, M., Neufeld, D. A., & Goicoechea, J. R. 2016, ARA&A, 54, 181
Gerlich, D., Borodi, G., Luca, A., Mogo, C., & Smith, M. A. 2011, ZPC, 225, 475
Gerlich, D., Jusko, P., Roučka, Š., et al. 2012, ApJ, 749, 22
Gerlich, D., Plašil, R., Zymak, I., et al. 2013, JPCA, 117, 10068
Glosík, J., Plašil, R., Kotrík, T., et al. 2010, MolPh, 108, 2253
Gómez-Carrasco, S., Godard, B., Lique, F., et al. 2014, ApJ, 794, 33
Haney, M. A., & Franklin, J. L. 1969, JChPh, 50, 2028
Hejduk, M., Dohnal, P., Rubovič, P., et al. 2015, JChPh, 143, 044303
Hollenbach, D., Kaufman, M. J., Bergin, E. A., & Melnick, G. J. 2009, ApJ, 690, 1497
Hollenbach, D., Kaufman, M. J., Neufeld, D., Wolfire, M., & Goicoechea, J. R. 2012, ApJ, 754, 105
Indriolo, N., & McCall, B. J. 2013, Chem. Soc. Rev., 42, 7763
Indriolo, N., Neufeld, D. A., Gerin, M., et al. 2015, ApJ, 800, 40
Jones, J. D. C., Birkinshaw, K., & Twiddy, N. D. 1981, CPL, 77, 484
Jusko, P., Asvany, O., Wallerstein, A.-C., Brünken, S., & Schlemmer, S. 2014, PhRvL, 112, 253005
Kim, J. K., Theard, L. P., & Huntress, W. T. 1975, JChPh, 62, 45
Larsson, M., & Orel, A. E. 2008, Dissociative Recombination of Molecular Ions (Cambridge: Cambridge Univ. Press)
Lauzin, C., Jacovella, U., & Merkt, F. 2015, MolPh, 113, 3918
Li, X., Huang, Y.-L., Flesch, G. D., & Ng, C. Y. 1997, JChPh, 106, 564
Liu, J., Salumbides, E. J., Hollenstein, U., et al. 2009, JChPh, 130, 174306
Markus, C. R., Hodges, J. N., Perry, A. J., et al. 2016, ApJ, 817, 138
Martinez, O., Ard, S. G., Li, A., et al. 2015, JChPh, 143, 114310
Mulin, D., Roučka, Š., Jusko, P., et al. 2015, PCCP, 17, 8732
Muller, S., Müller, H. S. P., Black, J. H., et al. 2016, A&A, 595, A128
Neufeld, D. A., & Wolfire, M. G. 2016, ApJ, 826, 183
Neufeld, D. A., & Wolfire, M. G. 2017, ApJ, 845, 163
Newville, M., Stensitzki, T., Allen, D. B., & Ingargiola, A. 2014, LMFIT: Non-linear Least-Square Minimization and Curve-Fitting for Python, Tech. Rep., Zenodo, doi:10.5281/zenodo.11813
Ossenkopf, V., Müller, H. S. P., Lis, D. C., et al. 2010, A&A, 518, L111
Paul, W., Lücke, B., Schlemmer, S., & Gerlich, D. 1995, IJMSI, 149, 373
Pilbratt, G. L., Riedinger, J. R., Passvogel, T., et al. 2010, A&A, 518, L1
Plašil, R., Zymak, I., Jusko, P., et al. 2012, RSPTA, 370, 5066
Rakshit, A. B., & Warneck, P. 1980, J. Chem. Soc., Faraday Trans. 2, 76, 1084
Rakshit, A. B., & Warneck, P. 1981, JChPh, 74, 2853
Sansonetti, J. E., & Martin, W. C. 2005, JPCRD, 34, 1559
Shul, R. J., Passarella, R., DiFazio, L. T., Keesee, R. G., & Castleman, A. W. 1988, JPhCh, 92, 4947
Smith, D., Adams, N. G., & Miller, T. M. 1978, JChPh, 69, 308
Song, H., Li, A., & Guo, H. 2016a, JPCA, 120, 4742
Song, H., Li, A., Guo, H., et al. 2016b, PCCP, 18, 22509
Song, H., Li, A., Yang, M., & Guo, H. 2017, PCCP, 19, 17396
van Dishoeck, E. F., Bergin, E. A., Lis, D. C., & Lunine, J. I. 2014, Protostars and Planets VI (Tucson, AZ: Univ. Arizona Press), 835
van Dishoeck, E. F., Herbst, E., & Neufeld, D. A. 2013, ChRv, 113, 9043
Wiedmann, R. T., Tonkyn, R. G., White, M. G., Wang, K., & McKoy, V. 1992, JChPh, 97, 768
Wyrowski, F., van der Tak, F., Herpin, F., et al. 2010, A&A, 521, L34
Zymak, I., Hejduk, M., Mulin, D., et al. 2013, ApJ, 768, 86
Zymak, I., Jusko, P., Roučka, Š., et al. 2011, EPJAP, 56, 24010

Article IV: Effect of rotational excitation of H_2 on isotopic exchange reaction with OD$^-$ at low temperatures

Roučka, Š., Rednyk, S., Kovalenko, A., Tran, T. D., Plašil, R., Kálosi, Á., Dohnal, P., Gerlich, D., Glosík, J.

LETTER TO THE EDITOR

Effect of rotational excitation of H₂ on isotopic exchange reaction with OD⁻ at low temperatures

Š. Roučka, S. Rednyk, A. Kovalenko, T. D. Tran, R. Plašil, Á. Kálosi, P. Dohnal, D. Gerlich, and J. Glosík

Department of Surface and Plasma Science, Faculty of Mathematics and Physics, Charles University, V Holešovičkách 2, 180 00 Prague, Czech Republic
e-mail: stepan.roucka@mff.cuni.cz

ABSTRACT

Aims. This paper presents experimentally obtained rate coefficients for the weakly endothermic reaction $OD^- + H_2 \rightarrow OH^- + HD$ with ortho- and para-hydrogen at astrophysically relevant temperatures between 10 and 300 K.

Methods. The reaction was studied with normal and para-enriched (99.5% para-H_2) hydrogen in a 22-pole ion trap. The measured temperature dependencies of reaction rate coefficients are analyzed using a model which assumes that the rotational energies of the two reactants are equivalent to the translational energy in driving the reaction.

Results. At room temperature, the rate coefficients of reactions with both nuclear spin variants reach 7×10^{-11} cm³ s⁻¹, which is in good agreement with the previous results from ion trap and swarm experiments with normal hydrogen. Cooling down the trap slows down the reaction and leads, at a nominal trap temperature of 11 K, to a rate coefficient below 10^{-14} cm³ s⁻¹ for para-enriched hydrogen. The fitted reaction endothermicity of 25.3 ± 2.2 meV agrees well with the literature value calculated in the Born-Oppenheimer approximation, $\Delta H^0 = 24.0$ meV. A simpler evaluation procedure, fitting the data with Arrhenius functions, results in $^p k = 16.8 \times 10^{-11} \exp(-234\,\mathrm{K}/T)$ cm³ s⁻¹ for pure para-hydrogen and $^o k = 9.4 \times 10^{-11} \exp(-101\,\mathrm{K}/T)$ cm³ s⁻¹ for pure ortho-hydrogen.

Key words. astrochemistry – molecular data – molecular processes – methods: laboratory: molecular – ISM: molecules

1. Introduction

In the present study we investigate the weakly endothermic H/D exchange reaction

$$OD^- + H_2 \xrightarrow{k_1} OH^- + HD, \qquad \Delta H^0 = 24.0\,\mathrm{meV}. \qquad (1)$$

Isotope exchange between different molecules is always nearly thermoneutral; however, due to differences in zero-point energies of the reactants and the products, endothermicities or exothermicities of some tens of meV are obtained. Hence, rate coefficients for H/D exchange tend to be very sensitive to temperatures between 10 and 1000 K, which are typical for the interstellar medium. One consequence is that deuterated molecular species are important tracers for the physical conditions prevailing in the interstellar medium (Roberts & Millar 2000). For example, observations of deuteration have been used, in combination with chemical models, to explore the origin of solar-system molecules (Cleeves et al. 2014b), to constrain the ionization rates in protoplanetary disks (Miettinen et al. 2011; Cleeves et al. 2014a), or to measure the age of prestellar cores (Pagani et al. 2013). The observations of the H/D ratios in molecules are generally concentrating on cations or neutrals, while not much is known about deuteration of anions. Negatively charged ions have recently been observed in space (McCarthy et al. 2006; Cernicharo et al. 2007; Brünken et al. 2007), and their role is increasingly more frequently investigated using astrochemical networks (Walsh et al. 2009; McElroy et al. 2013). In

particular, UMIST-based models (McElroy et al. 2013) predict that OH⁻ ions are present in cold dark clouds in quantities comparable to its positive counterpart, OH⁺. While OH and OH⁺ are routinely observed (see, e.g., Gerin et al. 2010; Wampfler et al. 2010), OH⁻ is still just a candidate for detection in space (Cazzoli & Puzzarini 2006).

The importance of the OH⁻ ion is underlined by a number of recent laboratory and theoretical studies of its destruction (Hlavenka et al. 2009; Hauser et al. 2015a), formation (Jusko et al. 2015; Plašil et al. 2017), inelastic collisions (Hauser et al. 2015b), or its rotational spectrum (Cazzoli & Puzzarini 2006; Matsushima et al. 2006; Jusko et al. 2014; Lee et al. 2016). Additionally, the OH⁻ anion has become a tool for thermometry of ions in ion traps (Otto et al. 2013; Endres et al. 2017) and storage rings (DESIREE, Schmidt et al. 2017; CSR, Meyer et al. 2017), based on threshold photodetachment spectroscopy.

This work presents rate coefficients measured for reaction (1) with normal and para-enriched H_2 at trap temperatures ranging from 10 to 300 K. Previous studies, performed at room temperature (Grabowski et al. 1983) or in the ranges of 10–300 K (Mulin et al. 2015) and 300–508 K (Viggiano & Morris 1994), used only normal H_2. Experimental determination of state-specific rate coefficients for $J_{H_2} = 0$ and 1 is essential because the reactivity is highly sensitive to the internal excitation of the reactants. Moreover, the interstellar ortho-/para-H_2 population is often far from thermal equilibrium.
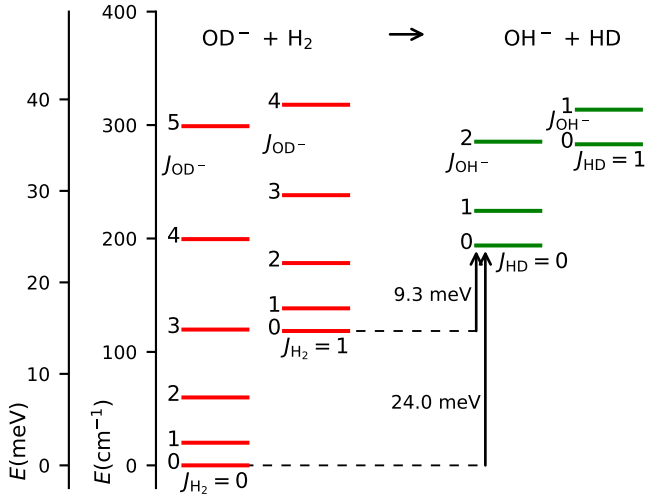
Fig. 1. Rotational energy levels of the reactants (left-hand side) and products (right-hand side) for reaction (1). The rotational constants for OD^-, OH^-, HD, and H_2 are taken from the literature (Huber & Herzberg 1979; Rehfuss et al. 1986; Matsushima et al. 2006). The two arrows indicate that 24.0 meV of translational energy are needed to reach the threshold at 0, while 9.3 meV are sufficient for reaction with ortho-H_2 ($J_{H_2} = 1$).

To compare internal excitation with the endothermicity, Fig. 1 shows the lowest rotational states of the involved diatomic molecules. The nuclear spin states $I = 0$ (para) and 1 (ortho) are linked to the even and odd rotational states, respectively. The 0 K reaction enthalpy of 24 meV was calculated in the Born-Oppenheimer approximation, as discussed in detail by Mulin et al. (2015). At meV accuracy, the energetics are influenced by isotopic electronic shifts of the potential energy surfaces of OD^- and OH^-, as shown for several other isotope exchange reactions with H_2 and D_2 (Kleinman & Wolfsberg 1973, 1974; Adohi-Krou et al. 2004). In particular, spectroscopic studies of OH and OD neutrals suggest that the isotopic shift of electronic ground-state potential energy surface in this system can be up to 2.5 meV (see note 78 in Ruscic et al. 2002). We here also derive an experimental value of the reaction endothermicity.

2. Experiment

The experiments have been carried out using the RF 22-pole ion trap machine described by Gerlich (1995, 2008) and Zymak et al. (2011). This instrument has been used to study isotope effects in anion–neutral reactions (Mulin et al. 2015; Roučka et al. 2015; Plašil et al. 2017), therefore we only recall a few specific details. The 22-pole trap was operated at an RF frequency of 17.4 MHz and at amplitudes up to 60 V. The nominal trap temperature (T_{22PT}) was varied from 300 K down to 10 K.

OD^- ions were produced in an electron impact storage ion source (SIS) using a mixture of N_2O and D_2 (Jusko et al. 2013, 2014). They were extracted from the source, mass selected by a quadrupole mass filter, and guided into the ion trap, where reactions with H_2 were followed as a function of time and H_2 number density. A He/H_2 gas mixture was introduced directly into the trap volume. After various well-defined trapping times, the trap was opened and ions were extracted, mass selected by a second quadrupole mass spectrometer, and counted by an MCP detector. The numbers of detected ions were proportional to the numbers of trapped ions, and minor differences in the overall

detection efficiency for OD^- and OH^- were accounted for in the data analysis.

The addition of helium buffer gas ensures that most of the ions are collisionally thermalized before reacting with H_2. Typically used He/H_2 mixtures result in ten collisions with He for every one collision with H_2 on average. Moreover, at low temperatures, H_2 molecules also act as a buffer gas because of the low probability for a reactive collision. Recent experiments in our apparatus (Plašil et al. 2012; Zymak et al. 2013) as well as in other 22-pole trap experiments (Hauser et al. 2015b; Endres et al. 2017) have confirmed that the collisional temperature is slightly higher than the temperature of the trap. In the present case we can safely assume that the collisional temperature in interaction of OD^- with H_2 does not exceed the trap temperature by more than 10 K. For simplicity of presentation, we define the collisional temperature as $T = T_{22PT} + 5$ K with an uncertainty of ± 5 K.

We used normal hydrogen ($^nH_2$) and para-enriched hydrogen ($^eH_2$) as reactants, with number densities varying from 10^{12} up to 10^{13} cm^{-3}. In normal H_2, the para/ortho ratio is 1/3, corresponding to the 300 thermal equilibrium. The para-enriched hydrogen, containing 99.5% of para-H_2, was produced using a para-hydrogen generator with paramagnetic catalyst (Hejduk et al. 2012; Dohnal et al. 2012; Zymak et al. 2013). The amount of ortho impurities was determined in situ using chemical probing with N^+ ions (Zymak et al. 2013). The nuclear spin-state-specific rate coefficients $^pk_1$ and $^ok_1$ for the reaction of OD^- with para- and ortho-H_2 were then calculated from the measured rate coefficients $^nk_1$ and $^ek_1$ for the reaction with $^nH_2$ and with $^eH_2$.

To evaluate the measured time dependencies, especially at low temperatures, we have to take into account reconversion of OH^- products back to OD^- via the fast exothermic reaction (Mulin et al. 2015)

$$OH^- + D_2 \xrightarrow{k_2} OD^- + HD, \qquad \Delta H^0 = -17.2 \text{ meV}. \qquad (2)$$

The D_2 traces in the trap originate from the ion source. Equilibrium between this backward reconversion reaction and reaction (1) is established at long enough trapping times.

3. Results and discussion

The change in numbers of detected OD^- and OH^- ions in the trap can be described with the balance equations

$$\frac{d N_{OD^-}}{d t} = -k_1 N_{OD^-} [H_2] + k_2 \xi N_{OH^-} [D_2], \qquad (3)$$

$$\frac{d N_{OH^-}}{d t} = -k_2 N_{OH^-} [D_2] + k_1 \frac{N_{OD^-}}{\xi} [H_2], \qquad (4)$$

where k_1 and k_2 are the rate coefficients of reactions (1) and (2), and [H_2] and [D_2] are the number densities of H_2 and D_2 in the trap, respectively. The factor ξ, which is close to 1, accounts for the detection efficiency of OD^- relative to OH^-. In the following, the additional index n and e is used, that is, ^nk_i and ^ek_i, to indicate reactions with $^nH_2$ and $^eH_2$, respectively. The reaction rate coefficients are determined by fitting the measured time dependencies of the numbers of detected ions, $N_{OD^-}(t)$ and $N_{OH^-}(t)$, with solution of Eqs. (3) and (4). Free parameters of the fit are the reaction rates $r_1 = k_1[H_2]$ and $r_2 = k_2[D_2]$, the initial numbers of detected ions, $N_{OD^-}(t = 0)$ and $N_{OH^-}(t = 0)$, and the relative detection efficiency ξ.
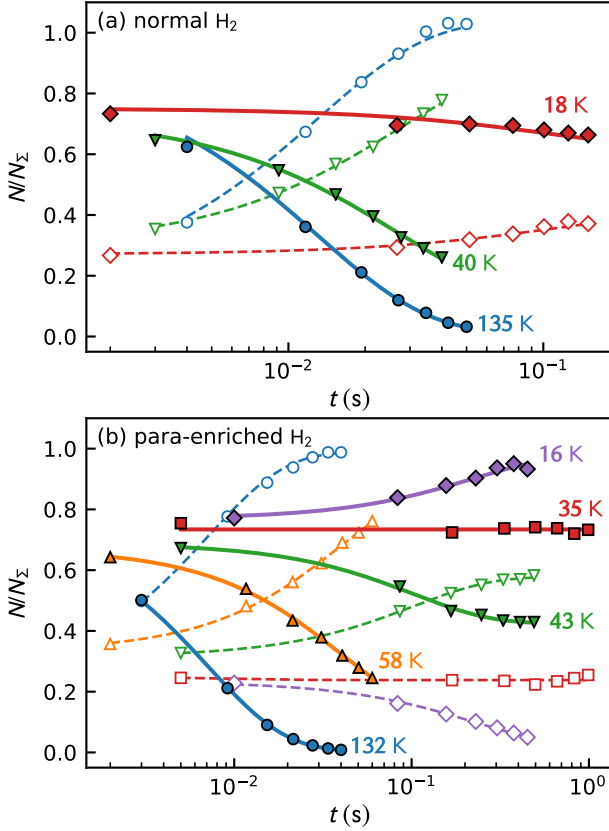
Fig. 2. Time dependencies of the normalized numbers of OD$^-$ (filled symbols) and OH$^-$ (open symbols), measured with ^{n}H$_2$ (*panel a*) and ^{e}H$_2$ (*panel b*). The collisional temperatures are indicated in the figure, and the densities of ^{n}H$_2$, ^{e}H$_2$, He, and D$_2$ are listed in Table 1.

Examples of measured and fitted time dependencies are plotted in Fig. 2. For clarity, the numbers are normalized by the total number of ions, N_Σ, measured directly after filling the trap. The upper panel of Fig. 2 shows data obtained with ^{n}H$_2$ as target gas, and the lower panel those for ^{e}H$_2$. The corresponding densities of ^{n}H$_2$, ^{e}H$_2$, He, and D$_2$ in the trap are listed in Table 1. The density of D$_2$ penetrating from the ion source is typically 1000 times lower than that of H$_2$. Nevertheless, the equilibrium numbers of OD$^-$ are comparable to or even higher than those of OH$^-$ at the lowest temperatures because of the very slow forward reaction and the fast backward reconversion reaction. The effect of backward reconversion is even more pronounced for a reaction with para-enriched H$_2$. The dependence of the reaction rate r_1 on the hydrogen number density was measured to be linear, confirming the binary character of reaction (1).

Figure 3 compares the rate coefficients, $^n k_1$ and $^e k_1$, measured between 15 and 300 with previous results for $^n k_1$ from the same experimental arrangement (Mulin et al. 2015; shown as a function of collisional temperature, $T = T_{22PT} + 5$ K). The agreement is very good (within a few percent). We also show results from the FDT experiment of Viggiano & Morris (1994) and the SIFT experiment of Grabowski et al. (1983). The data we present were simplified by binning the results of nearly 300 measurements into logarithmically spaced bins in temperature. The indicated uncertainties of the reaction rate coefficients take into account the estimated fit errors and the 5 uncertainty of the collisional temperature, which also influences the reactant number density. The uncertainty due to pressure measurement is 20%.

Table 1. Experimental conditions (collisional temperatures T, number densities of H$_2$, He, and D$_2$, and fractions of ortho-H$_2$) used to measure the data shown in Fig. 2.

$\frac{T}{K}$	$\frac{[H_2]}{10^{12}\,cm^{-3}}$	$\frac{[^oH_2]}{[H_2]}$	$\frac{[He]}{10^{12}\,cm^{-3}}$	$\frac{[D_2]}{10^9\,cm^{-3}}$
135	1.8	0.75	16	3.0
40	6.8	0.75	30	5.4
18	10.3	0.75	45	8.2
132	3.7	0.005	22	2.2
58	7.2	0.005	33	3.3
43	8.3	0.005	38	3.8
35	9.2	0.005	42	4.2
16	10.4	0.005	33	6.3

Notes. The H$_2$ and He gases are introduced to the trap volume via the inlet system, and D$_2$ is diffusing into the trap from the ion source. The uncertainties of the number densities are close to 20%.
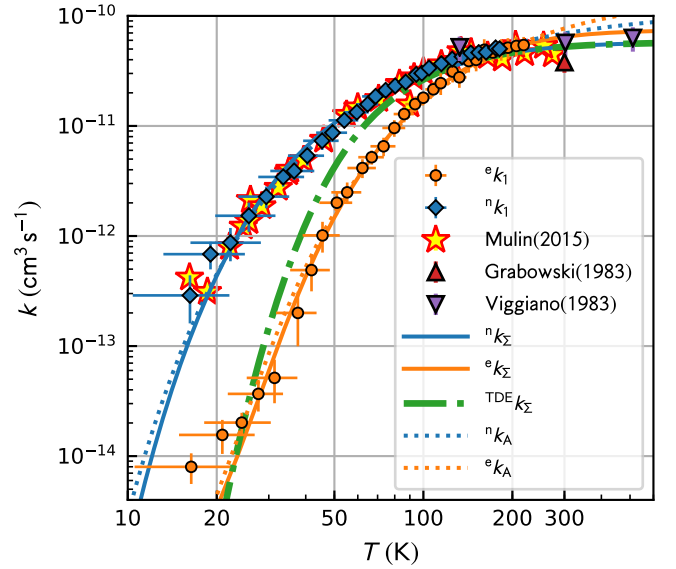

Fig. 3. Temperature dependencies of the rate coefficients, $^n k_1$ and $^e k_1$, measured for reaction (1) with ^{n}H$_2$ and with ^{e}H$_2$. We also plot data obtained in our previous experiments with ^{n}H$_2$ using the same experimental arrangement (Mulin et al. 2015), FDT data of Viggiano & Morris (1994), and SIFT data of Grabowski et al. (1983). The solid and dotted lines show the result of a state-specific model and an Arrhenius model, respectively. For details, see the text. The dash-dotted line indicates the thermal rate coefficient, i.e., the ortho/para ratio is also equilibrated to T.

The Arrhenius plot of the measured reaction rate coefficients shown in Fig. 4 reveals a nearly linear dependence of $^n k_1$ and $^e k_1$ over two and three orders of magnitude, respectively. The deviations from linearity for temperatures below 25 are smaller than the estimated temperature uncertainty of ±5 K.

We analyzed our data using the simple statistical model described by Mulin et al. (2015), which takes into account any non-equilibrium population of H$_2$ rotational states. Generally, the rate coefficient k_1 of reaction (1) can be expressed as a weighted sum k_Σ of state-specific rate coefficients $k_{J_{H_2} J_{OD^-}}$, averaged over the rotational states J_{H_2} and J_{OD^-} of H$_2$ and OD$^-$. In particular, we define rate coefficients $^n k_\Sigma$ and $^e k_\Sigma$ for reaction with normal and para-enriched H$_2$ as

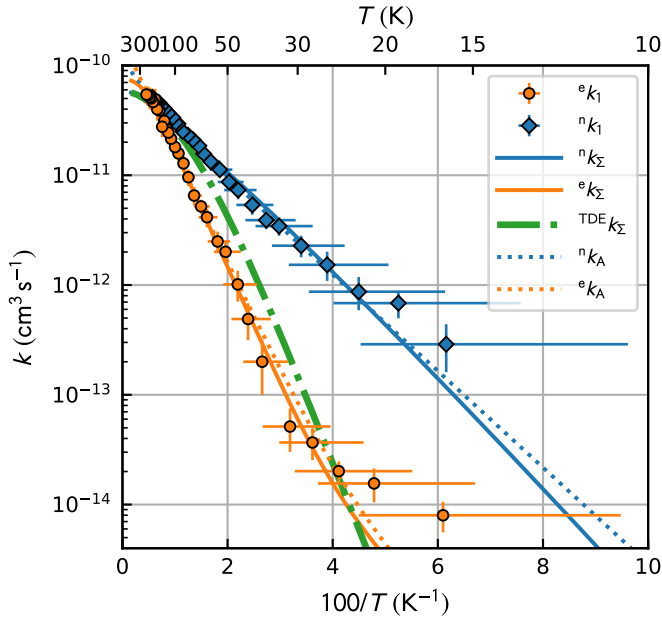$$^{n/e} k_\Sigma = \sum_{J_{H_2}, J_{OD^-}} {}^{n/e} P_{J_{H_2}} P_{J_{OD^-}} k_{J_{H_2} J_{OD^-}}, \quad (5)$$

Fig. 4. Arrhenius plot of $^{e}k_1$ and $^{n}k_1$ measured in experiments with $^{e}H_2$ and $^{n}H_2$. The solid and dotted lines show the results from a state-specific model and an Arrhenius model, respectively. The dash-dotted line shows the fully thermalized rate coefficients. For details, see the text.

where $^{n/e}P_{J_{H_2}}$ and $P_{J_{OD^-}}$ are the corresponding populations of rotational states. Our model uses the assumption that all state-specific rate coefficients follow the Arrhenius temperature dependence

$$k_{J_{H_2} J_{OD^-}} = {}^{p/o}k_0 \exp\left(-\frac{\Delta E_{J_{H_2} J_{OD^-}}}{k_B T}\right), \tag{6}$$

with the activation energy given by

$$\Delta E_{J_{H_2} J_{OD^-}} = \max\left\{0, \Delta H_{fit}^0 - E_{J_{H_2}} - E_{J_{OD^-}}\right\}. \tag{7}$$

The model assumes that both the rotational energy of $E_{J_{H_2}}$ and $E_{J_{OD^-}}$ and the translational energy are equivalent in driving the reaction. In Eq. (6) we also assume that there is a global pre-exponential factor $^{p}k_0$ for reactions with para-H_2 (J_{H_2} even) and $^{o}k_0$ for all reactions of ortho-H_2 (J_{H_2} odd). The only free parameters of the model are the reaction endoergicity ΔH_{fit}^0 and the pre-exponential factors $^{p}k_0$ and $^{o}k_0$. The model was fitted globally to both temperature dependencies of rate coefficients of reactions with ortho- and para-H_2, resulting in

$$\Delta H_{fit}^0 = 25.3_{-2.1}^{+2.4}\,\text{meV},$$

$$^{p}k_0 = 7.4_{-0.4}^{+0.7} \times 10^{-11}\,\text{cm}^3\,\text{s}^{-1}, \quad ^{o}k_0 = 5.2_{-1.3}^{+1.3} \times 10^{-11}\,\text{cm}^3\,\text{s}^{-1}.$$

These mean values were obtained from fits corresponding to the collisional temperature $T = T_{22PT} + 5\,\text{K}$. The quoted uncertainties include the statistical errors and the systematic errors due to temperature uncertainty, which were estimated by fitting the data with collisional temperatures defined as $T^- = T_{22PT}$ and $T^+ = T_{22PT} + 10\,\text{K}$. The pre-exponential factors $^{p}k_0$ and $^{o}k_0$ have additional uncertainty of 20% due to the uncertainty of the pressure. The fitted curves are included in Figs. 3 and 4.

The true thermal reaction rate coefficient $^{TDE}k_\Sigma$ plotted in Figs. 3 and 4 was derived from our model by inserting the equilibrium population of all H_2 rotational states, $^{TDE}P_{J_{H_2}}$, into Eq. (5), that is, also assuming equilibrium ortho/para population.

To facilitate the incorporation of our data into chemical models, we also fit our data with the simple Arrhenius model, described by the equation

$$^{n/e}k_A = (1 - {}^{n/e}f)\,^{p}k_A + {}^{n/e}f\,^{o}k_A, \tag{8}$$

where $^{n/e}f = [^{o}H_2]/[^{n/e}H_2]$ is the fraction of ortho-H_2 in the normal/para-enriched H_2 and

$$^{p/o}k_A = {}^{p/o}k_{A0} \exp(-{}^{p/o}E_A/(k_B T)). \tag{9}$$

The agreement of the fit with our data (Fig. 4) indicates that the linear combination of Arrhenius dependencies (8) is a good approximation. The resulting parameters are

$$^{o}E_A = 8.7_{-1.7}^{+2.1}\,\text{meV}, \qquad ^{o}k_{A0} = 9.4_{-2.2}^{+3.1} \times 10^{-11}\,\text{cm}^3\,\text{s}^{-1},$$
$$^{p}E_A = 20.1_{-2.3}^{+2.7}\,\text{meV}, \qquad ^{p}k_{A0} = 16.8_{-2.7}^{+3.6} \times 10^{-11}\,\text{cm}^3\,\text{s}^{-1}.$$

The errors were estimated by the same procedure as discussed above for the state-specific model parameters.

The fitted endothermicity ΔH_{fit}^0 is in good agreement with the value $\Delta H^0 = 24.0\,\text{meV}$ discussed in the Introduction. This confirms that the isotopic energy shifts are not significantly larger than our experimental accuracy ($\approx 2.5\,\text{meV}$). The discrepancy between the Arrhenius activation energy $^{p}E_A$ and the endothermicities ΔH_{fit}^0 and ΔH^0 is not surprising because $^{p}E_A$ is an empirical parameter that does not account for the internal excitation of the reactants. Nevertheless, the activation energy $^{o}E_A$ of the reaction with ortho-H_2 is in good agreement with the Born-Oppenheimer estimate of 9.3 meV. It is also in agreement with the activation energy of reaction with normal H_2, $E_{A\text{-exp}} = (7.9 \pm 0.3)\,\text{meV}$ determined by Mulin et al. (2015), which confirms that reaction with ortho-H_2 was the dominant process in that experiment.

4. Conclusions

We have extended our previous measurements (Mulin et al. 2015) of the isotope exchange reaction between OD$^-$ and H_2 using nearly pure para-hydrogen. The data allowed us to extract nuclear-spin specific rate coefficients at temperatures from 15 to 300 . As expected, the two results are equal at room temperature and agree well with previous data (Viggiano & Morris 1994; Grabowski et al. 1983). Over a wide range of temperatures, the rate coefficients fall with decreasing temperature in accordance with the Arrhenius formula. For astrochemical models, reactions with pure para- or ortho-H_2 can be simply characterized with Arrhenius functions $^{p}k = 16.8 \times 10^{-11} \exp(-234\,\text{K}/T)\,\text{cm}^3\,\text{s}^{-1}$ and $^{o}k = 9.4 \times 10^{-11} \exp(-101\,\text{K}/T)\,\text{cm}^3\,\text{s}^{-1}$, respectively.

References

Adohi-Krou, A., Martin, F., Ross, A. J., Linton, C., & Le Roy R. J. 2004, J. Chem. Phys., 121, 6309
Brünken, S., Gupta, H., Gottlieb, C. A., McCarthy, M. C., & Thaddeus, P. 2007, ApJ, 664, L43
Cazzoli, G., & Puzzarini, C. 2006, ApJ, 648, L79
Cernicharo, J., Guélin, M., Agúndez, M., et al. 2007, A&A, 467, L37
Cleeves, L. I., Bergin, E. A., & Adams, F. C. 2014a, ApJ, 794, 123
Cleeves, L. I., Bergin, E. A., Alexander, C. M. O., et al. 2014b, Science, 345, 1590

Dohnal, P., Hejduk, M., Varju, J., et al. 2012, Phil. Trans. R. Soc. A, 370, 5101

Endres, E. S., Egger, G., Lee, S., et al. 2017, J. Mol. Spectr., 332, 134

Gerin, M., De Luca, M., Black, J., et al. 2010, A&A, 518, L110

Gerlich, D. 1995, Phys. Scr., 1995, 256

Gerlich, D. 2008, Low Temperatures and Cold Molecules (London: Imperial College Press)

Grabowski, J. J., DePuy, C. H., & Bierbaum, V. M. 1983, J. Am. Chem. Soc., 105, 2565

Hauser, D., Lakhmanskaya, O., Lee, S., Roučka, Š., & Wester, R. 2015a, New J. Phys.

Hauser, D., Lee, S., Carelli, F., et al. 2015b, Nat. Phys., 11, 467

Hejduk, M., Dohnal, P., Varju, J., et al. 2012, Plasma Sources Sci. Technol., 21, 024002

Hlavenka, P., Otto, R., Trippel, S., et al. 2009, J. Chem. Phys., 130, 061105

Huber, K. P., & Herzberg, G. 1979, Molecular Spectra and Molecular Structure: Constants of Diatomic Molecules (New York: Van Nostrand Reinhold)

Jusko, P., Roučka, Š., Plašil, R., & Glosík, J. 2013, Int. J. Mass Spectrom., 352, 19

Jusko, P., Asvany, O., Wallerstein, A.-C., Brünken, S., & Schlemmer, S. 2014, Phys. Rev. Lett., 112, 253005

Jusko, P., Roučka, Š., Mulin, D., et al. 2015, J. Chem. Phys., 142, 014304

Kleinman, L. I., & Wolfsberg, M. 1973, J. Chem. Phys., 59, 2043

Kleinman, L. I., & Wolfsberg, M. 1974, J. Chem. Phys., 60, 4740

Lee, S., Hauser, D., Lakhmanskaya, O., et al. 2016, Phys. Rev. A, 93, 032513

Matsushima, F., Yonezu, T., Okabe, T., Tomaru, K., & Moriwaki, Y. 2006, J. Mol. Spectrosc., 235, 261

McCarthy, M. C., Gottlieb, C. A., Gupta, H., & Thaddeus, P. 2006, ApJ, 652, L141

McElroy, D., Walsh, C., Markwick, A. J., et al. 2013, A&A, 550, A36

Meyer, C., Becker, A., Blaum, K., et al. 2017, Phys. Rev. Lett., 119, 023202

Miettinen, O., Hennemann, M., & Linz, H. 2011, A&A, 534, A134

Mulin, D., Roučka, Š., Jusko, P., et al. 2015, Phys. Chem. Chem. Phys., 17, 8732

Otto, R., von Zastrow, A., Best, T., & Wester, R. 2013, Phys. Chem. Chem. Phys., 15, 612

Pagani, L., Lesaffre, P., Jorfi, M., et al. 2013, A&A, 551, A38

Plašil, R., Zymak, I., Jusko, P., et al. 2012, Phil. Trans. R. Soc. A, 370, 5066

Plašil, R., Tran, T. D., Roučka, Š., et al. 2017, Phys. Rev. A, 96, 062703

Rehfuss, B. D., Crofton, M. W., & Oka, T. 1986, J. Phys. Phys., 85, 1785

Roberts, H., & Millar, T. J. 2000, A&A, 361, 388

Roučka, Š., Mulin, D., Jusko, P., et al. 2015, J. Phys. Chem. Lett., 6, 4762

Ruscic, B., Wagner, A. F., Harding, L. B., et al. 2002, J. Phys. Chem. A, 106, 2727

Schmidt, H. T., Eklund, G., Chartkunchand, K. C., et al. 2017, Phys. Rev. Lett., 119, 073001

Viggiano, A. A., & Morris, R. A. 1994, J. Chem. Phys., 100, 2748

Walsh, C., Harada, N., Herbst, E., & Millar, T. J. 2009, ApJ, 700, 752

Wampfler, S. F., Herczeg, G. J., Bruderer, S., et al. 2010, A&A, 521, L36

Zymak, I., Jusko, P., Roučka, Š., et al. 2011, Eur. Phys. J. Appl. Phys., 56, 24010

Zymak, I., Hejduk, M., Mulin, D., et al. 2013, ApJ, 768, 86

Article V: Isotopic effects in the interaction of O^- with D_2 and H_2 at low temperatures

Plašil, R., Tran, T. D., Roučka, Š., Jusko, P., Mulin, D., Zymak, I., Rednyk, S., Kovalenko, A., Dohnal, P., Glosík, J., Houfek, K., Táborský, J., Čížek, M.

2017

Isotopic effects in the interaction of O⁻ with D₂ and H₂ at low temperatures

Radek Plašil,[*] Thuy Dung Tran, Štěpán Roučka, Pavol Jusko, Dmytro Mulin, Illia Zymak,
Serhiy Rednyk, Artem Kovalenko, Petr Dohnal, and Juraj Glosík

Department of Surface and Plasma Science, Faculty of Mathematics and Physics, Charles University, Prague, Czech Republic
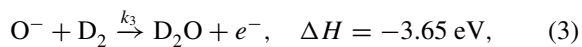
Karel Houfek, Jiří Táborský, and Martin Čížek

Institute of Theoretical Physics, Faculty of Mathematics and Physics, Charles University, Prague, Czech Republic

(Received 3 October 2017; published 7 December 2017)

The isotopic effects in reactions of O⁻ ions with H₂ and D₂ have been studied experimentally using a cryogenic 22-pole radio-frequency ion trap. The rate coefficients for associative detachment leading to $H_2O + e^-$ and to $D_2O + e^-$ and for atom transfer reactions leading to formation of OH^- and OD^- ions were determined at temperatures ranging from 15 to 300 K. The measured temperature dependencies of the rate coefficients for both channels of reactions of O⁻ with H₂ and D₂ are compared with the results of the classical trajectory Monte Carlo simulation of the O⁻ + H₂ and O⁻ + D₂ collisions using the newly calculated potential energy surfaces. The measured temperature dependencies of the reaction rate coefficients for associative detachment are in very good agreement with the calculated ones. Agreement between experimental and calculated temperature dependencies of the rate coefficients of atom transfer reactions is off at most by a factor of 3 and the isotope effect is reproduced.

I. INTRODUCTION

The reaction of O⁻ with H₂ or D₂ has two exothermic channels corresponding to associative detachment (AD) and hydrogen or deuterium atom transfer (AT) [channels (1) and (2) for hydrogen or (3) and (4) for deuterium]:

$$O^- + H_2 \xrightarrow{k_1} H_2O + e^-, \quad \Delta H = -3.57\,\text{eV}, \quad (1)$$

$$O^- + H_2 \xrightarrow{k_2} OH^- + H, \quad \Delta H = -0.30\,\text{eV}, \quad (2)$$

$$O^- + D_2 \xrightarrow{k_3} D_2O + e^-, \quad \Delta H = -3.65\,\text{eV}, \quad (3)$$

$$O^- + D_2 \xrightarrow{k_4} OD^- + D, \quad \Delta H = -0.28\,\text{eV}, \quad (4)$$

with the reaction rate coefficients k_1, k_2, k_3, and k_4, respectively. The reaction enthalpies at 0 K were calculated from bond dissociation energies [1,2] and electron affinities [3–5] and corrected for zero-point energy differences in case of the deuterated reactions [6–8]. The endothermic proton or deuteron transfer channel in which $H^- + OH$ or $D^- + OD$ is formed with $\Delta H = 0.77$ or 0.79 eV, respectively, does not play a role in the present low temperature experiments.

Since hydrogen and oxygen are among the most abundant elements in the Universe, the studied reactions are also astrochemically relevant. In particular, associative detachment contributes to formation of water in the interstellar medium [9], which is a fundamental problem in astrochemistry tightly related to the origin of terrestrial water [10–12]. Knowledge of gas-phase processes involving water [13] and especially those leading to isotopic fractionation [12,14] appears to be crucial for understanding water formation in space.

In low-energy collisions of reactants in the ground electronic states, $O^-(^2P) + D_2(X\,^1\Sigma_g^+)$, the collision system has three accessible electronic states $1^2A'$, $1^2A''$, and $2^2A'$ (as in collisions of O⁻ with H₂). For better orientation, one-dimensional cuts of the calculated potential energy surfaces (PES) of D_2O^- and D_2O along the minimum energy path going from $O^- + D_2$ to $OD^- + D$ on the $1^2A'$ PES are shown in Fig. 1. Plotted are also cuts through the PES calculated for $1^2A''$ and $2^2A'$ states along the same coordinate. Autodetachment towards $e^- + D_2O$ can occur in the region where the anionic curve is above the neutral one. For further details see also [15,16] where features of the PES including a local minimum on the $1^2A'$ surface were discussed.

The O⁻ ion can be present in two fine structure states $O^-(^2P_{\frac{1}{2}})$ and $O^-(^2P_{\frac{3}{2}})$ which are separated by 22 meV [17,18]. We assume that the ratio of population of the $O^-(^2P_{\frac{1}{2}})$ and $O^-(^2P_{\frac{3}{2}})$ states is 1:2, which corresponds to statistical probability of production in the ion source. We do not expect that this ratio will be changed in collisions with helium buffer gas, which is used to thermalize ions injected into the trap [19]. Collisions with H₂ or D₂ also cannot contribute to a change of the ratio, since at low temperature the reactions proceed with nearly collisional rate, i.e., almost every collision of O⁻ with H₂ or D₂ is reactive.

Molecules H₂ and D₂ can be in a para or ortho nuclear spin configuration. The ground state of H₂ is para-H₂ and the ground state of D₂ is ortho-D₂. In the present experiments we are using normal hydrogen and normal deuterium gases, where the populations of ortho and para states correspond to thermal equilibrium at 300 K, which is close to the statistical ratio 1/3 for para-H₂/ortho-H₂ and 1/2 for para-D₂/ortho-D₂. Our experiments have indicated that para- or ortho-H₂ populations do not change while passing the reactant gas from a reservoir into the trap volume [20,21] and we expect that the same will hold for D₂.

Experimental studies of the reactions (1), (2), (3), and (4) and the temperature dependencies of their rate coefficients have been carried out by other groups at room temperature
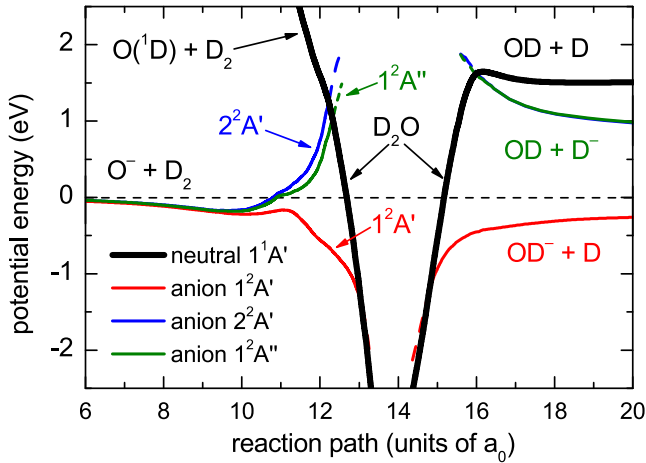
---

*radek.plasil@mff.cuni.cz

FIG. 1. The calculated potential energy surfaces (PES) of D_2O^- and D_2O along the minimum energy path going from $O^- + D_2$ to $OD^- + D$ on the $1\,^2A'$ PES. Plotted are also the PES corresponding to the $1\,^2A''$ and $2\,^2A'$ states, which are connected to the $OD + D^-$ asymptote. The PES of D_2O^- in the autodetachment region are indicated by dashed lines. For further details see also [15].

and above using flowing afterglow, drift tube, tandem mass spectrometry, and octopole ion trap instruments (see, e.g., Refs. [22,23] and references therein). A study at mean collision energies down to 0.02 eV has been carried out by Viggiano *et al.* [24] using a temperature variable flow-drift tube. The isotope effects on the product energy partitioning in the atom transfer reaction have been studied by Lee and Farrar [25]. The kinetic energy distribution of electrons produced in associative detachment has been studied by Mauer and Schulz [26], Esaulov *et al.* [27], and most recently by Jusko *et al.* [23]. All these studies of AD indicate production of low-energy electrons and high internal excitation of the produced H_2O or D_2O molecules.

The intermediate H_2O^- or D_2O^- complex has been studied theoretically [28,29] and experimentally [30–33] by means of dissociative electron attachment to the neutral H_2O or D_2O molecule at energies 6–12 eV. The detailed potential energy surfaces of the lowest H_2O and H_2O^- states have been calculated by Claydon *et al.* [34], Werner *et al.* [35], and newly by Houfek and Čížek [16].

To our knowledge, there are no measured rate coefficients of the reaction of O^- with D_2 for temperatures below 170 K, despite the fact that temperatures down to 10 K are typical for interstellar molecular clouds [12,13,36]. The rate coefficients of the reaction of O^- with H_2 were recently studied in our laboratory in the temperature range 10–300 K [15] and we measured the energy distribution of electrons produced in associative detachment of O^- with H_2 and D_2 [reactions (1) and (3)] at 300 K and the corresponding rate coefficients [23].

We present an extended study of the reaction of O^- with D_2 down to 15 K. We report the measured temperature dependencies of the rate coefficient of associative detachment [reaction (3)] and of deuterium atom transfer [reaction (4)]. Although this work is focused on the interaction of O^- with D_2, we also present newly measured rate coefficients of the

reactions (1) and (2) with significantly improved accuracy compared to those of Jusko *et al.* [15]. We also report the calculated rate coefficients of AD and AT in collisions of O^- with H_2 and D_2 and we discuss the observed isotope effect.

II. EXPERIMENT

The reaction of O^- ions with H_2 or D_2 was studied using the cryogenic 22-pole radio-frequency ion trap. As the detailed description of the instrument can be found elsewhere [37–41], only a very short description will be given here. Primary O^- ions were produced in the storage ion source by electron bombardment of N_2O. In the standard procedure the anions are extracted from the ionization chamber of the ion source, mass selected, and injected into the ion trap. The anions injected into the trap are thermalized in collisions with helium buffer gas and react with H_2 or D_2 reactant gas. The trap is cooled by a cryocooler reaching temperatures down to 10 K. Due to low H_2 or D_2 density in comparison with helium density (the ratios $[H_2]/[He]$ and $[D_2]/[He]$ are ≈ 0.01) we expect thermalization of kinetic energy of O^- prior to their reaction. The thermalization of trapped ions was studied in many experiments and in the present work it can be assumed that the kinetic temperature T of $O^- + H_2$ or D_2 collisions typically deviates from the nominal trap temperature T_{22PT} by +5 K, i.e., $T = T_{22PT} + (5 \pm 5)$ K (for more details see Refs. [21,40,42]). After preselected storage (reaction) time t the stored primary and product ions are extracted from the ion trap, mass selected by the second quadrupole mass spectrometer, and counted by the detector system with a microchannel plate. On the basis of the experimental data we assume that the number of detected ions is proportional to the number of trapped ions and that the detection efficiency is the same for O^-, OH^-, and OD^-. From measured dependencies of relative numbers of detected anions on the storage time, the reaction rate coefficient, and the branching ratio are determined.

In order to determine the pressure p_{22PT} in the trap, the pressure p_{SRG} measured using a calibrated spinning rotor gauge at room temperature T_{room} connected directly to the trap volume is corrected for thermal transpiration using the formula

$$p_{22PT} = p_{SRG}\sqrt{T_{gas}/T_{room}}. \quad (5)$$

The systematic uncertainty of the reactant gas number density due to accuracy of pressure reading, stability of leak valves, and temperature dependence of vacuum conductivity of the trap is below 20%. In addition, the uncertainty of the gas temperature also contributes to the uncertainty of number density due to thermal transpiration (5).

III. EXPERIMENTAL RESULTS

The measured time dependencies of numbers of trapped anions were analyzed by least-squares fitting with the following formulas obtained by integrating the kinetic equations. For the reaction with D_2 the formulas are

$$N_O(t) = N_O(0)\, e^{-(k_3+k_4)[D_2]t}, \quad (6)$$

$$N_{OD}(t) = N_{OD}(0) + N_O(0)\,(1 - e^{-(k_3+k_4)[D_2]t})\,\frac{k_4}{k_3+k_4}, \quad (7)$$
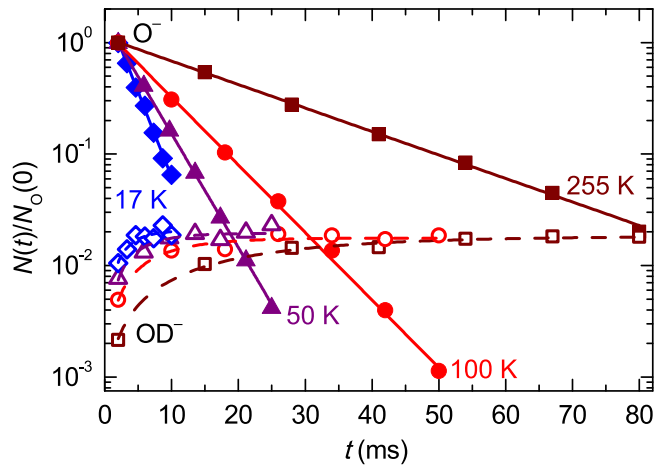
FIG. 2. Relative number of primary O^- ions $N_O(t)/N_O(0)$ (full symbols) and OD^- product ions $N_{OD}(t)/N_O(0)$ (empty symbols) at indicated trap temperatures as a function of storage time. The statistical error bars are smaller than the symbols. The fitted curves are indicated by lines. The D_2 number density is 3.1×10^{11} cm^{-3} at 17 K and it scales with $1/\sqrt{T}$ due to thermal transpiration.

where k_3 and k_4 are the respective reaction rate coefficients of the reactions (3) and (4), $N_O(t)$ and $N_{OD}(t)$ are numbers of the respective O^- and OD^- ions after storage time t, and $[D_2]$ is the deuterium number density in the trap volume. $N_O(0)$, $N_{OD}(0)$, k_3, and k_4 are free parameters of the fit. Good agreement of the fits with the measured data is illustrated in Fig. 2.

By varying the trap temperature, we were able to measure the reaction rate coefficients in the temperature range of 15–300 K. The loss of O^- ions in pure helium without added H_2 or D_2 was negligible in the whole temperature range.

The binary character of the studied reactions can be seen from the dependence of the loss rate r on the reactant gas number density. Examples of such dependencies for the reaction with deuterium are shown in Fig. 3. The linearity of these dependencies confirms that the loss of O^- ions in the trap
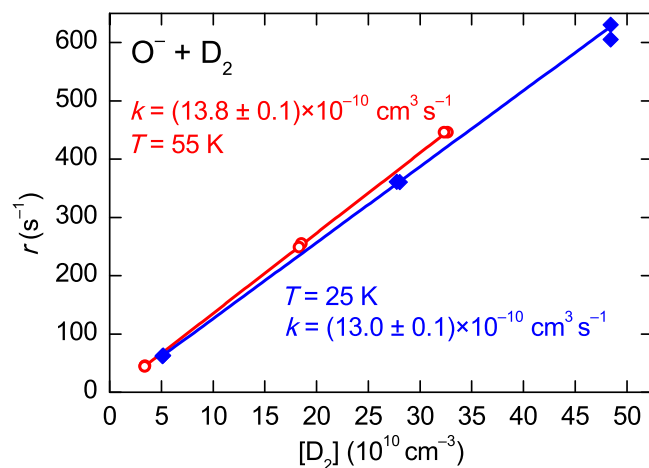

FIG. 3. The measured loss rate of O^- as a function of D_2 number density at 25 and 55 K. The overall reaction rate coefficients $k = k_3 + k_4$ are given by the slope of the fitted linear dependencies.
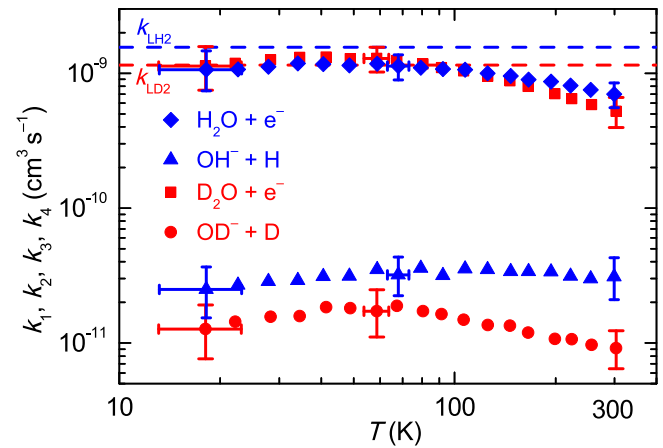

FIG. 4. Measured temperature dependencies of the rate coefficients of AD and AT reactions of O^- with H_2 and D_2. The dashed horizontal lines are the Langevin rate coefficients k_{LH2} and k_{LD2} for the $O^- + H_2$ and $O^- + D_2$ collisions, respectively. The overall uncertainty is indicated for a few representative points by the error bars with caps.

is caused by the binary ion-molecule reaction with D_2, i.e., the rate can be expressed by the formula $r = (k_3 + k_4) [D_2]$.

The measured temperature dependencies of the rate coefficients k_1, k_2, k_3, and k_4 of the reactions (1), (2), (3), and (4) are shown in Fig. 4. We have to note that the rate coefficients for reactions with H_2 are approximately 40% lower in comparison with our previous low temperature experiment [15]. The difference between present and previous [15] data is higher than the estimated systematic uncertainties, which are 20% in both cases. As we found out, the systematic uncertainty in the previous work was underestimated, since it did not account for the nonlinearity of the ionization gauge in the trap vacuum chamber, which was calibrated using a spinning rotor gauge at moderate pressures ($\gtrsim 10^{-7}$ mbar) and used for measurement of pressure of the reactant gas ($\approx 10^{-8}$ mbar). Our recent experiments show that the nonlinearity in the relevant pressure range indeed reaches up to 40%. In order to eliminate this source of error in the present work, we have measured the reactant gas pressure using the spinning rotor gauge which is connected directly to the trap envelope. We have also checked that other experiments in our laboratory, which were using the same procedure for calibration of H_2 pressure [21,42], were not operated in the problematic pressure range of the ionization gauge and we have reproduced their results in experiments with direct measurement of reactant pressure.

In the covered range of temperatures, the measured temperature dependencies of the rate coefficients of reactions with D_2 (k_3 and k_4) are similar to those of reactions with H_2 (k_1 and k_2). To show possible influence of the difference in the mass of H_2 and D_2 on the reaction rate coefficients, we plotted in Fig. 5 the measured reaction rate coefficients k_1, k_2, k_3, and k_4 normalized to the corresponding Langevin collisional rate coefficients 1.56×10^{-9} cm^3 s^{-1} for $O^- + H_2$ and 1.15×10^{-9} cm^3 s^{-1} for $O^- + D_2$. From the plots in Fig. 5 it is clear that the difference in the Langevin collisional rate coefficients cannot simply explain the measured differences
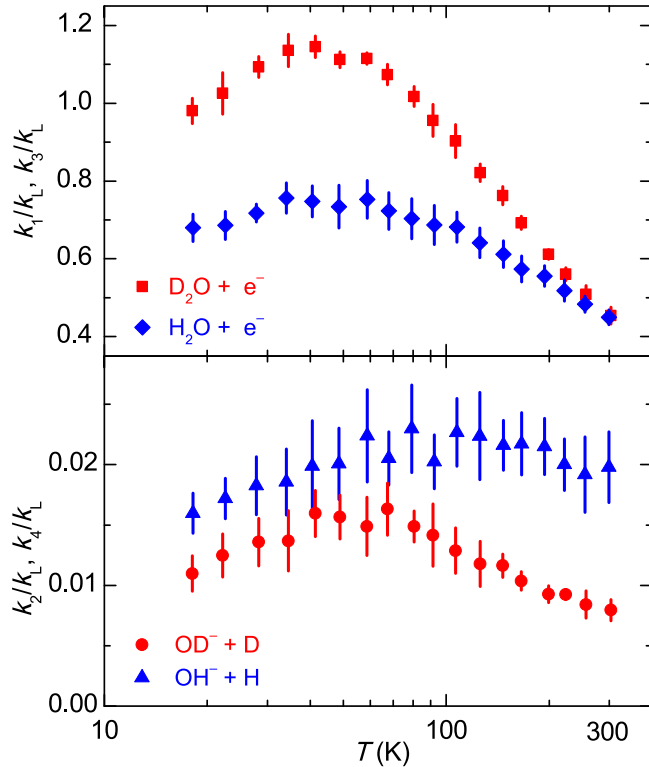
FIG. 5. Measured rate coefficients for the reaction of O^- with D_2 and H_2 normalized to the corresponding Langevin collisional rate coefficients k_L. Upper panel: Normalized reaction rate coefficients k_1 and k_3 for associative detachment (1) and (3), respectively. Lower panel: Normalized reaction rate coefficients k_2 and k_4 for atom transfer (2) and (4), respectively. Statistical error bars, which are relevant for relative comparison, are indicated.

in the temperature dependencies of the rate coefficients of the reactions of O^- with H_2 and D_2. The difference of the reaction rate coefficients k_2 and k_4 for the atom transfer reactions with H_2 [reaction (2)] and D_2 [reaction (4)] is very pronounced. To highlight the difference between the rate coefficients k_2 and k_4 of the atom transfer reactions (2) and (4) the temperature dependencies of the corresponding branching ratios (k_2/k_1 and k_4/k_3) for the reaction channels leading to OH^- or OD^- are shown in Fig. 6. Note that in the temperature range 15–300 K the measured branching ratio for production of OH^- is higher at least by a factor of 2 than the measured branching ratio for production of OD^-.

IV. THEORY AND RESULTS OF CALCULATIONS

In order to understand the experimental results we performed the classical trajectory Monte Carlo simulation of the $O^- + H_2$ and $O^- + D_2$ collisions. We used the potential energy surfaces calculated previously using the multireference configuration interaction method [15]. We considered only the lowest electronic $1^2 A'$ state, which connects the initial $O^- + H_2$ and the final $OH^- + H$ channels through the electron autodetachment region where neutral H_2O can be formed (see Fig. 1 for the $O^- + D_2$ reaction). As discussed in detail in Refs. [15,16,35] there are other two states $1^2 A''$, $2^2 A'$
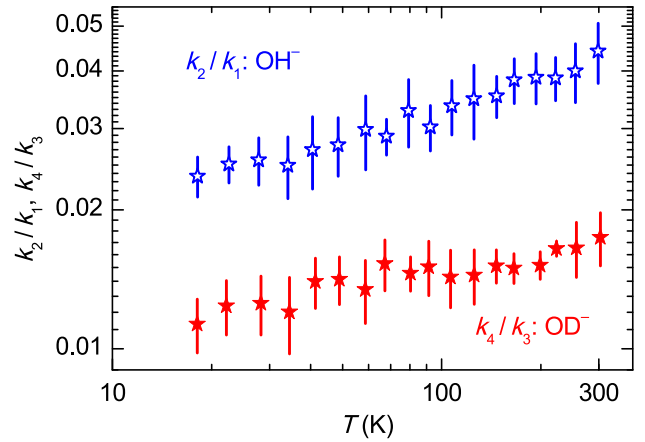

FIG. 6. Temperature dependencies of the branching ratios for the formation of OH^- and OD^- in the reaction of O^- with H_2 or D_2, respectively. Statistical error bars are indicated.

connected to the $O^- + H_2$ asymptote, however these two states cannot directly contribute neither to associative detachment nor to the $OH^- + H$ channel at low energies. There is nevertheless strong evidence (see [15] for detailed explanation) that the initial flux in those two states is transferred to the lowest state through a conical intersection near linear molecular configurations. The potential energy surface of the $1^2 A'$ state was fitted with a sum of a large number of Gaussian functions, so that the error of the final fit does not exceed 10 meV in the regions energetically accessible in the $O^- + H_2$ collision at energies below 0.2 eV [43]. The autodetachment region was localized as a coordinate domain, where the calculated ground state of the neutral H_2O molecule is located below the $1^2 A'$ state of the anion. The resulting region was then fitted to an ellipsoid in the space of mutual atomic separations R_{HH}, R_{OH1}, and R_{OH2} with semiaxes $a_{OH} = 0.85\,a_0$ and $a_{HH} = 1.65\,a_0$ (a_0 being the Bohr radius) [43].

To perform the classical trajectory Monte Carlo simulation we followed the procedure suggested by Karplus *et al.* [44]. Each trajectory was started in the asymptotic region of the $O^- + H_2$ channel with typical separation of colliding species of 30 a_0. The energy of the classical vibrational motion of the H_2 molecule was selected as the ground state of quantized motion. For each impact parameter b the orientation and the vibrational phase of the H_2 molecule was selected randomly. For low temperatures studied in this work we assume that the H_2 molecule has initially zero angular momentum, but all degrees of freedom are included in classical dynamics. The classical trajectory was followed numerically with the fourth-order Runge-Kutta method until the trajectory was terminated in the autodetachment region (we assume that all these trajectories contribute to the associative detachment process) or the asymptote of either the $O^- + H_2$ or the $OH^- + H$ channel was reached. The same procedure was repeated for 10^3–10^4 trajectories yielding the Monte Carlo estimate of reaction probability for each impact parameter b. We checked that the statistical error of Monte Carlo averaging is below 5%. The probability $P(E,b)$ of a certain process for a given energy E and impact parameter b is determined as a
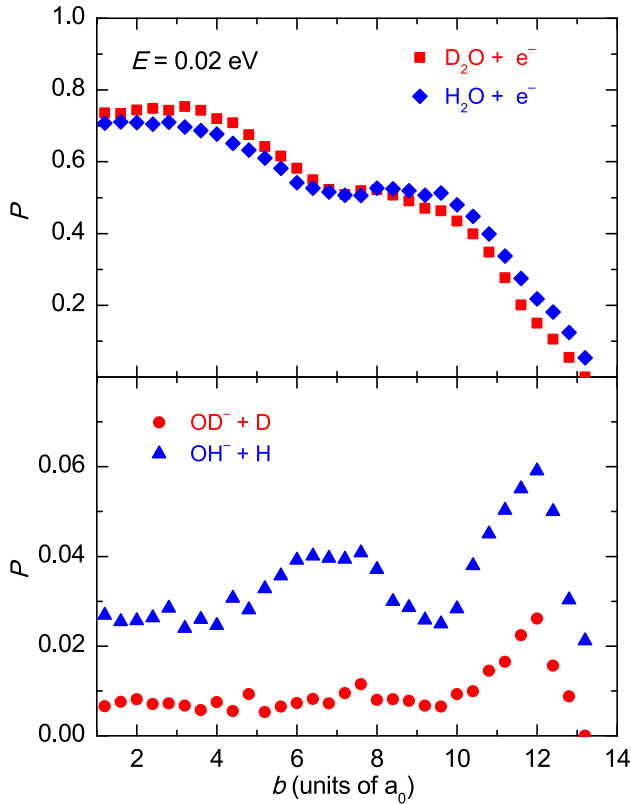
FIG. 7. Probabilities of associative detachment (upper panel) and atom transfer (lower panel) for the reactions of O^- with H_2 and D_2 calculated as functions of the impact parameter b at the collision energy $E = 20$ meV. The equivalent temperature $2E/3k_B$ is 155 K.

FIG. 8. Calculated energy dependencies of the cross sections for both channels of reactions of O^- with H_2 and D_2. The energy scale of this plot corresponds to equivalent temperatures $2E/3k_B$ in the range of 23–15 500 K. Upper panel: The cross sections for associative detachment forming H_2O and D_2O. The dashed straight line indicates the Langevin collisional cross section for $O^- + D_2$ (which differs from that of $O^- + H_2$ by about 1% due to differences in polarizabilities [45]). Lower panel: The cross sections for atom transfer leading to $OH^- + H$ and $OD^- + D$.

ratio of the number of trajectories ending in the corresponding channel to the number of all trajectories. The cross section $\sigma(E)$ as a function of energy of relative motion of O^- and H_2 for each reaction is then obtained by integration of the respective probability

$$\sigma(E) = 2\pi \int_0^{b_{max}} P(E, b)\, b\, db, \qquad (8)$$

where b_{max} is the impact parameter where the reactions vanish and only the elastic $O^- + H_2$ channel remains. Note that zero-point energy of H_2 vibrations is not included in E and adds to the total energy. Finally we calculated the reaction rate coefficients by averaging a product of velocity and cross section over the Maxwell-Boltzmann distribution of collision velocities. The same procedure was repeated for the $O^- + D_2$ system.

The typical results of our Monte Carlo simulations for $O^- + H_2$ and for $O^- + D_2$ are shown in Fig. 7 for the collision energy 20 meV. The graphs contain the dependence of the associative detachment and AT reaction probabilities on the impact parameter b, showing the relative number of trajectories ending in the autodetachment or OH^- (or OD^-) regions. We can observe a typical decrease of the associative detachment probability with increasing b, while the reaction probability of AT increases before the final drop to zero. This is consistent with 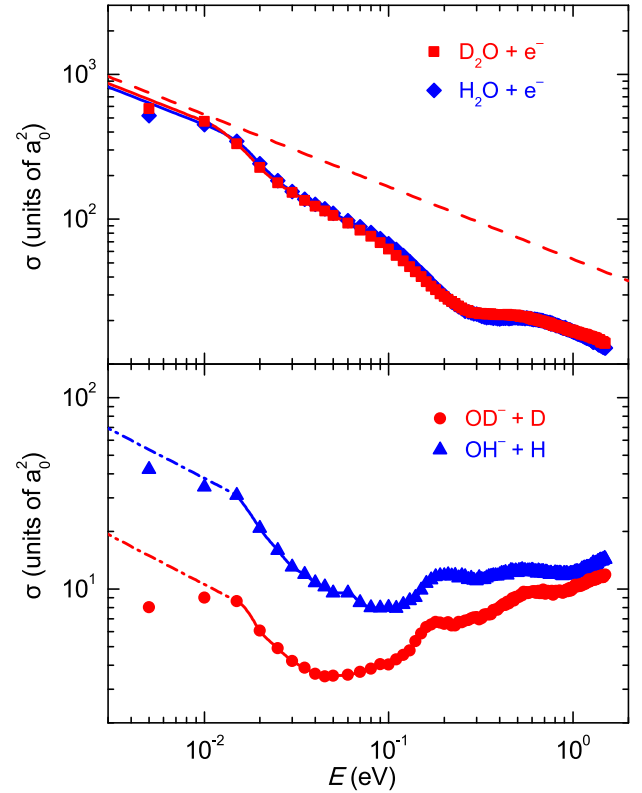the assumption that the trajectories leading to the reaction have to squeeze in a narrow space between the central autodetachment and classically forbidden regions.

The calculated cross sections (8) for both processes in the reactions of $O^- + H_2$ and $O^- + D_2$ are plotted in Fig. 8. Although the cross sections are calculated for collisional energies up to 1.5 eV to calculate the rate coefficients at higher temperatures, we suspect that the detailed dynamics of nonadiabatic transitions in the conical intersection among all three $1^2A'$, $1^2A''$, and $2^2A'$ electronic states starts to play a role already at energies higher than 0.2 eV [15]. First few points of the cross section curve are considerably influenced by low accuracy of the potential energy fit. The error of the fit is approximately 10 meV which corresponds to abrupt change of behavior of the cross sections at this energy. Therefore we do not use the points below 15 meV in the calculation of the rates but we use the Langevin behavior $\sigma(E) \sim 1/\sqrt{E}$ to extrapolate the data as indicated by dash-dotted lines in Fig. 8. The dashed straight line in the upper panel indicates the Langevin cross section for the reaction of $O^- + D_2$.

The resulting rate coefficients for both channels of the reactions $O^- + H_2$ and $O^- + D_2$ are shown in Fig. 9 together with the present and some previous [22–24] experimental data.
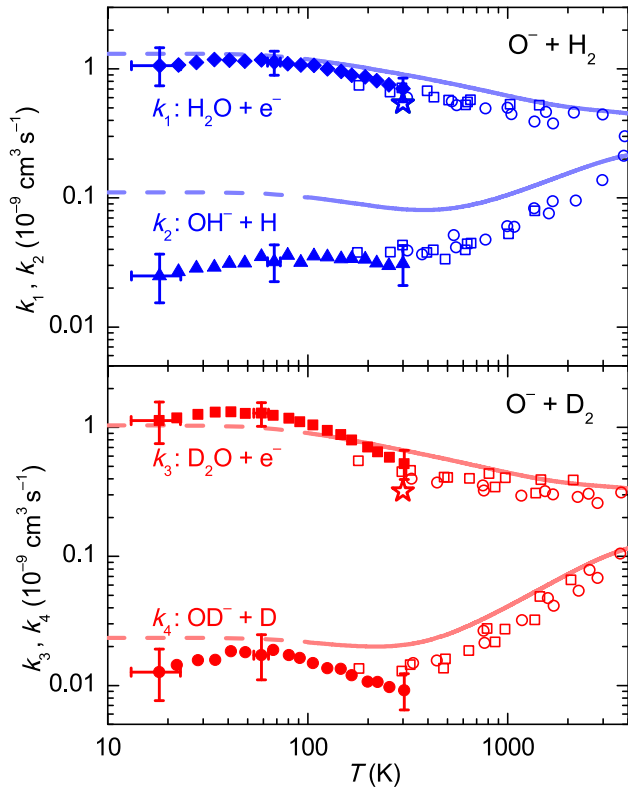
FIG. 9. Calculated and measured temperature dependencies of the reaction rate coefficients for both channels of the reactions of O^- with H_2 and D_2. The experimental data points from the 22-pole instrument (full symbols) are compared with the results from the Monte Carlo simulations (lines) for both the hydrogenated (upper panel) and deuterated (lower panel) system. Open symbols indicate the experimental data of Viggiano *et al.* [24] (squares), McFarland *et al.* [22] (circles), and Jusko *et al.* [23] (stars). The part of the theoretical curve strongly dependent on the extrapolation of the calculated data is shown with dashed lines. The error bars with caps indicate the overall uncertainty for a few representative points.

The data that are influenced significantly by the cross section extrapolation below 10 meV are marked by dashed curves. Comparing the calculated and experimental rate coefficients in this figure, we see good qualitative agreement both in isotopic ratios of the AD and AT reaction processes and also in temperature dependencies. The absolute magnitude of the rate coefficients is off at most by a factor of 3, which is satisfactory considering the crudeness of the current model. First of all, it is a classical model and quantum effects may play an important role for such low energies, especially for the lighter H_2 molecule, which could explain why agreement of the computed rate k_2 with experiment is worse than for k_4. The crudeness of the model is also more pronounced for the AT reaction rates than for the AD rates because the AT rates are much smaller. Second, the nonadiabatic coupling near the conical intersection and the spin-orbit coupling are not taken into account. We plan to include these effects in future calculations. Moreover, we are currently using a crude model of the electron autodetachment. The local complex potential approximation could be implemented in the semiclassical procedure, however we do not have the data for the autodetachment widths at

the moment. It has also been shown that the local complex potential model can be inappropriate [46], especially for polar molecules [47,48].

V. CONCLUSIONS AND OUTLOOK

We measured the rate coefficients of associative detachment and H or D atom transfer in the reaction of O^- with H_2 or D_2 at temperatures between 15 and 300 K (Fig. 4). At temperatures below 80 K the associative detachment rate coefficients for H_2 and D_2 are nearly identical, close to 1.2×10^{-9} cm^3 s^{-1}. On the other hand, at 300 K, their values decrease below $\approx 50\%$ of the respective Langevin collisional rate coefficients (Fig. 5). The measured atom transfer rate coefficients k_2 and k_4 are 2%–4% and 1%–2% of the corresponding overall reaction rate coefficients, respectively (see the branching ratios in Fig. 6). Comparison of the atom transfer data for the reactions with H_2 and D_2 normalized to the corresponding Langevin collisional rate coefficients (Fig. 5) indicates large difference between the temperature dependencies of the rate coefficients. The branching ratio (k_2/k_1) for the reaction with H_2 is by a factor of 2 higher than the branching ratio (k_4/k_3) for the reaction with D_2 (Fig. 6).

In order to understand the observed isotope effect, we carried out the classical trajectory Monte Carlo simulations of the $O^- + H_2$ and $O^- + D_2$ interactions using the newly calculated PES. From the calculated probabilities for both channels of both reactions as functions of the impact parameter b and collision energy, we calculated the corresponding reaction cross sections (Fig. 8) and the rate coefficients for temperatures from 10 up to 4000 K (Fig. 9). Comparison of the calculated rate coefficients with the experimental data (Fig. 9) reveals good agreement in branching ratios, in the isotope effect, and in the shape of the temperature dependencies of the respective reaction rate coefficients.

The qualitative picture that emerges from the current classical trajectory simulation and from the shape of the potential energy landscape is following. At low energies the trajectories follow the initial channel potential valley, which is the most attractive along linear geometry alignment of $O^- + H_2$ or D_2. At short distances a barrier emerges in the linear geometry and $O^- + H_2$ or D_2 has to tilt in order to reach the autodetachment region through a saddle point. After passing the saddle point the autodetachment region represents a large obstacle in the path towards the atom transfer reaction channel. It is easier to reach the atom transfer channel for the H_2 molecule, which is lighter than D_2 and can tilt its orientation more easily. The reaction is also more probable for larger energies when the classically allowed region around the autodetachment ellipsoid becomes more voluminous. This enhances the reactivity of H_2, which has larger zero-point energy of vibrational motion than D_2. We checked that the difference in zero-point energy of the initial state of H_2 or D_2 is responsible for 50%–75% (depending on collision energy) of the isotopic effect.

It is interesting to note that the behavior of the temperature dependencies of the rate coefficients changes at temperatures around 300 K. This was not so clearly visible on the basis of

data from previous high temperature (drift tube) experiments. Only combination of drift tube data, our low temperature data and data obtained in our calculations give a better idea about the details of the O$^-$ + H$_2$ and O$^-$ + D$_2$ reactions. Further experimental and theoretical studies are needed. We are planning to study the differences in reactivity between ortho and para nuclear spin configurations of H$_2$ by means of the 22-pole trap combined with a para-hydrogen generator. For better understanding of these fundamental processes we are preparing studies of the reaction of O$^-$ with HD. We also plan to deepen our theoretical understanding of the studied reactions by taking into account the nonadiabatic coupling near the conical intersection and the spin-orbit coupling. Calculation of the autodetachment widths and implementation of the local complex potential approximation in the semiclassical procedure will be a subject of our future work.

[1] J. Liu, D. Sprecher, C. Jungen, W. Ubachs, and F. Merkt, J. Chem. Phys. **132**, 154301 (2010).

[2] P. Maksyutenko, T. R. Rizzo, and O. V. Boyarkin, J. Chem. Phys. **125**, 181101 (2006).

[3] J. R. Smith, J. B. Kim, and W. C. Lineberger, Phys. Rev. A **55**, 2036 (1997).

[4] C. Blondel, W. Chaibi, C. Delsart, C. Drag, F. Goldfarb, and S. Kröger, Eur. Phys. J. D **33**, 335 (2005).

[5] K. R. Lykke, K. K. Murray, and W. C. Lineberger, Phys. Rev. A **43**, 6104 (1991).

[6] K. Huber and G. Herzberg, *Molecular Spectra And Molecular Structure: Constants Of Diatomic Molecules*, Molecular Spectra and Molecular Structure, Vol. IV (Van Nostrand Reinhold, New York, 1979).

[7] D. S. Eisenberg and W. Kauzmann, *The Structure and Properties of Water* (Oxford University Press, Oxford, 1969).

[8] K. K. Irikura, J. Phys. Chem. Ref. Data **36**, 389 (2007).

[9] A. Dalgarno and R. A. McCray, Astrophys. J. **181**, 95 (1973).

[10] B. Marty, Earth Planet. Sci. Lett. **313–314**, 56 (2012).

[11] E. A. Bergin and E. F. van Dishoeck, Phil. Trans. R. Soc. London Sect. A **370**, 2778 (2012).

[12] L. I. Cleeves, E. A. Bergin, C. M. O. Alexander, F. Du, D. Graninger, K. I. Öberg, and T. J. Harries, Science **345**, 1590 (2014).

[13] D. Hollenbach, M. J. Kaufman, E. A. Bergin, and G. J. Melnick, Astrophys. J. **690**, 1497 (2009).

[14] H. Roberts and T. J. Millar, Astron. Astrophys. **361**, 388 (2000).

[15] P. Jusko, Š. Roučka, D. Mulin, I. Zymak, R. Plašil, D. Gerlich, M. Čížek, K. Houfek, and J. Glosík, J. Chem. Phys. **142**, 014304 (2015).

[16] K. Houfek and M. Čížek, Eur. Phys. J. D **70**, 107 (2016).

[17] D. M. Neumark, K. R. Lykke, T. Andersen, and W. C. Lineberger, Phys. Rev. A **32**, 1890 (1985).

[18] C. Blondel, C. Delsart, C. Valli, S. Yiou, M. R. Godefroid, and S. Van Eck, Phys. Rev. A **64**, 052504 (2001).

[19] L. A. Viehland, R. Webb, E. P. F. Lee, and T. G. Wright, J. Chem. Phys. **122**, 114302 (2005).

[20] M. Hejduk, P. Dohnal, J. Varju, P. Rubovič, R. Plašil, and J. Glosík, Plasma Sources Sci. Technol. **21**, 024002 (2012).

[21] I. Zymak, M. Hejduk, D. Mulin, R. Plašil, J. Glosík, and D. Gerlich, Astrophys. J. **768**, 86 (2013).

[22] M. McFarland, D. L. Albritton, F. C. Fehsenfeld, E. E. Ferguson, and A. L. Schmeltekopf, J. Chem. Phys. **59**, 6629 (1973).

[23] P. Jusko, Š. Roučka, R. Plašil, and J. Glosík, Int. J. Mass Spectrom. **352**, 19 (2013).

[24] A. A. Viggiano, R. A. Morris, C. A. Deakyne, F. Dale, and J. F. Paulson, J. Phys. Chem. **95**, 3644 (1991).

[25] S. T. Lee and J. M. Farrar, J. Chem. Phys. **111**, 7348 (1999).

[26] J. L. Mauer and G. J. Schulz, Phys. Rev. A **7**, 593 (1973).

[27] V. A. Esaulov, R. L. Champion, J. P. Grouard, R. I. Hall, J. L. Montmagnon, and F. Penent, J. Chem. Phys. **92**, 2305 (1990).

[28] D. J. Haxton, C. W. McCurdy, and T. N. Rescigno, Phys. Rev. A **75**, 012710 (2007).

[29] D. J. Haxton, T. N. Rescigno, and C. W. McCurdy, Phys. Rev. A **75**, 012711 (2007).

[30] H. Adaniya, B. Rudek, T. Osipov, D. J. Haxton, T. Weber, T. N. Rescigno, C. W. McCurdy, and A. Belkacem, Phys. Rev. Lett. **103**, 233201 (2009).

[31] D. J. Haxton, H. Adaniya, D. S. Slaughter, B. Rudek, T. Osipov, T. Weber, T. N. Rescigno, C. W. McCurdy, and A. Belkacem, Phys. Rev. A **84**, 030701 (2011).

[32] N. B. Ram, V. S. Prabhudesai, and E. Krishnakumar, J. Chem. Sci. **124**, 271 (2012).

[33] J. Fedor, P. Cicman, B. Coupier, S. Feil, M. Winkler, K. Głuch, J. Husarik, D. Jaksch, B. Farizon, N. J. Mason, P Scheier, and T. D. Märk, J. Phys. B: At. Mol. Opt. Phys. **39**, 3935 (2006).

[34] C. R. Claydon, G. A. Segal, and H. S. Taylor, J. Chem. Phys. **54**, 3799 (1971).

[35] H. J. Werner, U. Manz, and P. Rosmus, J. Chem. Phys. **87**, 2913 (1987).

[36] T. J. Millar, Plasma Sources Sci. Tech. **24**, 043001 (2015).

[37] D. Gerlich and G. Borodi, Faraday Discuss. **142**, 57 (2009).

[38] I. Zymak, P. Jusko, Š. Roučka, R. Plašil, P. Rubovič, D. Gerlich, and J. Glosík, Eur. Phys. J. Appl. Phys. **56**, 24010 (2011).

[39] D. Gerlich, P. Jusko, Š. Roučka, I. Zymak, R. Plašil, and J. Glosík, Astrophys. J. **749**, 22 (2012).

[40] R. Plašil, I. Zymak, P. Jusko, D. Mulin, D. Gerlich, and J. Glosík, Philos. Trans. R. Soc. London Ser. A **370**, 5066 (2012).

[41] D. Gerlich, R. Plašil, I. Zymak, M. Hejduk, P. Jusko, D. Mulin, and J. Glosík, J. Phys. Chem. A **117**, 10068 (2013).

[42] D. Mulin, Š. Roučka, P. Jusko, I. Zymak, R. Plašil, D. Gerlich, R. Wester, and J. Glosík, Phys. Chem. Chem. Phys. **17**, 8732 (2015).

[43] J. Táborský, Master thesis, Charles University, Faculty of Mathematics and Physics, Prague, 2016 .

[44] M. Karplus, R. N. Porter, and R. D. Sharma, J. Chem. Phys. **43**, 3259 (1965).

[45] Y. Y. Milenko, L. V. Karnatsevich, and V. S. Kogan, Physica **60**, 90 (1972).

[46] R. J. Beiniek, J. Phys. B: At. Mol. Phys. **13**, 4405 (1980).

[47] S. Živanov, M. Allan, M. Čížek, J. Horáček, F. A. U. Thiel, and H. Hotop, Phys. Rev. Lett. **89**, 073201 (2002).

[48] S. Živanov, M. Čížek, J. Horáček, and M. Allan, J. Phys. B: At. Mol. Opt. Phys. **36**, 3513 (2003).